Discharge patterns of retinal ganglion cells in rodent models of degenerative retinal diseases

Dissertation zur Erlangung des Doktorgrades

der Naturwissenschaften

der Fakultät für Biologie

der Ludwigs-Maximilians-Universität

München

vorgelegt von

Jacob Menzler

München

15.15.2012

Erstgutachter: Prof. Dr. Christian Leibold
Zweitgutachter: Prof. Dr. Alexander Borst

Tag der mündlichen Prüfung: 12.03.2012

Contents

Contents

List of Figures

List of Tables

Abbreviations

AC   amacrine cell

ACh   acetylcholine

AP   action potential

AMPA   2-amino-3-(5-methyl-3-oxo-1,2- oxazol-4-yl)propanoic acid

BC   bipolar cells

CBC   cone bipolar cell

CBX   Carbenoxolone

CC   Cross-Correlation

cGMP   cyclic-Guanosin-monophosphat

CNS   Central Nervous System

GABA   γ-Aminobutyric-acid

GCL   ganglion cell layer

GluR   Glutamate receptor

DNQX   6,7-dinitroquinoxaline-2,3-dione

ERG   electro-retinogram

HC   horizontal cell

INL   inner nuclear layer

IOP   intra-ocular-pressure

IPL   inner plexiform layer

LGN   lateral geniculate nucleus

LFP   Local Field potential

MEA	Multi-electrode-array
MFA	Meclofenamic acid
MTA	Multi-Transistor-Array
NBQX	2,3-dihydroxy-6-nitro-7-sulfamoyl-benzo[f]quinoxaline-2,3-dione
NMDA	*N*-Methyl-D-aspartic acid
NTG	Normal tension glaucoma
OS	outer segments
ONC	optic nerve crush
ONL	outer nuclear layer
OPL	outer plexiform layer
ONS	optic nerve section
ONS	optic nerve section
PDE	phosphodiesterase
PND	postnatal day
PNS	peripheral nervous system
POD	postoperative day
PSTH	peri stimulus time histogram
RBC	rod bipolar cell
rd	retinal degeneration
RGC	retinal ganglion cell
RP	retinitis pigmentosa
RPE	retinal pigment epithelium
SC	superior colliculus

STA   spike triggered average

TTX   Tetrodotoxin

VEP   Visual evoked potential

wt   wild-type

Summary

The present study investigates the influence of two severe ophthalmologic diseases on the activity of retinal ganglion cells (RGCs). Action potentials were recorded extracellular, using a high density Multi-Transistor-Array with 16384 sensors on a $1mm^2$ array surface. Using spike triggered average analysis single RGC axonal action potentials propagating were visualized for the first time in rodent retinas.

In the first series of experiments the spontaneous RGC activity in *rd1* mice was analyzed. In *rd1,* a nonsense mutation of the phosphodiesterase 6 β gene causes rapid photoreceptor degeneration. The majority of *rd1* RGCs exhibited rhythmic bursting at a fundamental frequency of 7-10 Hz. In the present work is shown, that large proportions of the cells were correlated and additionally a Local Field Potential was detected, that oscillates with the same frequency. RGC spiking and the LFP were separated applying TTX. RGC spiking was locked to the LFP minimum and the LFP depolarized or hyperpolarized large areas of the retinal tissue recorded.

The LFPs propagated over the recorded tissue with velocity rates faster than known from retinal waves which rely on transmission of chemical synapses.

Cells that were located in areas of the same LFP phase, fired in synchrony and block of inhibitory synapses increased the LFP's spatial extension, but did not affect the activity otherwise. The LFP signal depended on glutamatergic transmission, what makes it likely to be produced by bipolar cells. Blocking glutamatergic synapses inhibited the LFP and most of the spiking. This revealed that a larger proportion of RGCs in *rd1* is electrically coupled than in *wt*. Gap junction blockers were most effective in blocking the complete retinal activity.

It can be concluded that increased bipolar cell activity and enhanced gap junction coupling between amacrine cells and bipolar cells are the cause of the *rd1* phenotype.

Based on these results, further experiments were designed to test if loss of the photoreceptor dark current leads to an imbalance of excitation and inhibition, that causes rhythmic activity.

The dark current generated by photoreceptors was blocked in C57BL/6 mouse retinas by constant bleaching, that induced elevated firing rates in ON- and OFF-RGCs. After long bleaching intervals half of the cells showed a spontaneous ~ 5 Hz

bursting pattern. Most cells did not fire in synchrony. When a mixture of blockers for inhibitory synapses was applied during bleaching, the majority of cells initiated rhythmic bursting, that was accompanied by a static Local Field potential. The same experiments conducted with rats revealed that firing rates were increased during bleaching, but the OFF-RGC initiated a ~3 Hz oscillation only after blockage of inhibitory synapses. A LFP was not detected.

RGC activity in *rd1* mouse retinas reflects presynaptic degeneration. In other forms of rd and in glaucoma, the RGCs themselves degenerate.

I established a surgical model of rapid RGC degeneration, injuring the optic nerve in wistar rats. The rats were then examined 4, 8 and 14 days postoperative to investigate axon and RGC function. The axonal conduction velocity was reduced 4 days postoperative to 70% of the control level and did not change significantly further. Changes in OFF-RGC function were concomitant, as maintained OFF-RGCs activity was diminished at day 4 and responses latency increased. ON-cell response latency and maintained activity was unaffected until eight days after surgery. The average firing rate of the light response decreased at day 4 for both cell types. Operated RGCs had diminished responses to grating stimuli with increasing spatial frequency, indicating changes in dendritic structure.

After optic nerve injury in rats, axonal malfunction and functional RGC degeneration are in close temporal proximity.

It is shown here that RGCs suffering from *rd1* display rhythmic population activity, while RGCs that are directly injured maintain reduced function probably until apoptosis.

1. Introduction

Perception of the external environment is a prerequisite of guided motion and behavior. Receptor molecules for electromagnetic or mechanical cues developed early in evolution. As mobility and perception are interdependent, in all species coordination of movement in space depends on one or two cardinal senses that represent the outside world and are related to self-perception.

Which senses are used depend on the environmental requirements but in primates the ear and mainly the eye are the source of information about the outside world.

Vision is realized by the reception of scattered photons that trigger a change in the membrane potential of the receptor cell. Adjacent cells layers read this information out, minimize noise, analyze features of the percept and transmit the information to the brain.

Losing this source of information is a handicap for normal participation in life.

In general two defects are the cause of blindness: the inability to detect photons or the impossibility to transmit the information to the brain.

The present work wants to shed light on the physiologic consequences of both defects. As this work aims to contribute to the understanding of degenerative diseases of the human retina, the eye (*section 1.1*) and the cellular assembly of the retina (*sect. 1.2*), will be introduced.

In the present work action potentials of retinal ganglion cells are recorded extracellular to analyze retinal functions. The generation of action potentials in RGCs is caused and regulated by presynaptic input. Function and physiology of retinal circuits and cell types will be characterized (*sect. 1.3*), before I focus on the retinal diseases studied and the animal models used (*sect. 1.4*). At last, extracellular recording with a Multi-Transistor-Array is introduced (*sect. 1.5*).

.

1.1 The mammalian eye

The architecture of the mammalian eye (**Fig. 1.1**) is a variation of the eye plan common to all vertebrates. In contrast to cephalopods where all parts of the eye develop from dermal ectoderm, the sensory tissue of the vertebrate retina is derived from the neural tube. An optic vesicle is formed that later invaginates, the inner layer becomes the retina and the outer layer the retinal pigment epithelium.

Both eyes are located in orbits, i.e. cavities in the skull lateral to the nasal bone. The eye is connected to the orbit by six muscles that control its movements. The sclera (**Fig.1.1, grey**) encloses the eyeball and the RGC axons that leave towards the LGN and form the Optic nerve. Light enters the eye through the transparent cornea (**Fig.1.1, white**) that is adjacent to the sclera. At the transition zone sclera and cornea are connected to the conjunctiva that shelters the orbit from outside.
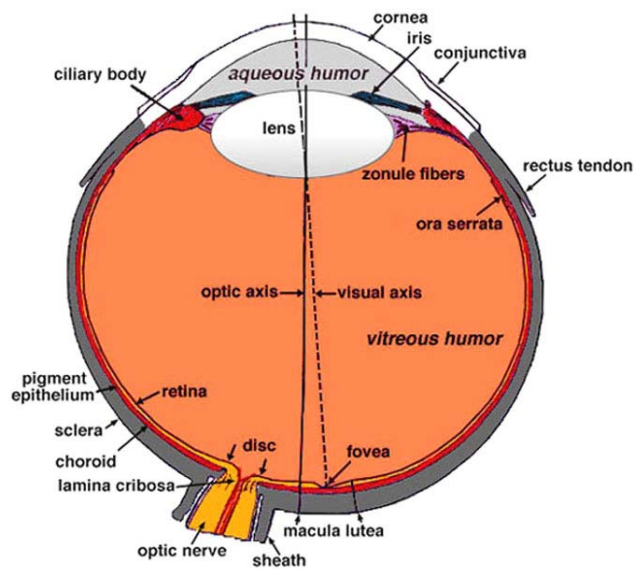
Figure 1.1: Horizontal sagittal section of the eye. (Kolb et al. 1995) see text for details

Behind the cornea is (**Fig. 1.1, white ellipsoid**) the first eye chamber, filled with aqueous humor and then the lens. Cornea, aqueous humor and lens are the refractive elements of the eye that focus the light onto the retina. While the refractive effect of cornea and aqueous humor is fixed, lens refraction is adjustable.

The refraction of the lens increases with its diameter. Connected by the zonule fibers (**Fig.1.1, purple**) with the ciliary muscle (**Fig. 1.1, red**), its contraction or relaxation leads to a round or flat shape of the lens allowing focusing on nearby or far objects.

The amount of light that can pass through the lens is controlled by the iris (**Fig. 1.1, blue**), consisting of the Iris pigment epithelium and muscles. The iris pigment epithelium passes over to the retinal pigment epithelium inside the eye.

Beneath the outer layer of the sclera are two more layers, the choroidea (**Fig.1.1, red**) and the retina (**Fig.1.1, yellow**). The choroid contains the blood vessels that originate at the ophthalmic artery and enters the eye via the optic disc. The retina has a high metabolic rate and changes in vascularization are involved in a variety of degenerative disorders. In the rostral region the choroid forms the ciliary body, which secrets the aequeous humor.

The retina is the most inner layer of the eye and the retinal ganglion cells project with their axon to the Central nervous system and form the optic nerve. The optic disc contains no photoreceptors and marks the entrance of the blood vessels and the exit of the Optic Nerve.

Both pass the bony structure of the lamina cribrosa an opening of the neurocranium. From the choroid the retina is isolated by Bruchs membrane and from the vitreous body by the inner limiting membrane. The vitreous body fills the eyeball between retina and lens and maintains the intra ocular pressure together with the aqueous humor (IOP) that gives the eye its round shape.

In rodents the lens is much larger than indicated in **Fig.1.1** and fills nearly the complete eye ball.

1.2 The retina

So far, about 50 distinct cell types are identified within the retina (Masland, 2001), that belong to the cell classes of photoreceptors, horizontal cells, bipolar cells, amacrine cells and ganglion cells.

The retina is adjacent to the Retinal pigment epithelium (**Fig. 1.2**, on the top of the photoreceptors) that recycles the chromophores, maintains the photoreceptor (PR) metabolism and constitutes the retina-blood barrier. Below are the outer segments of the PRs, whose cell bodies are located in the outer nuclear layer (ONL). PRs synapse with horizontal cells (HCs) and bipolar cells (BCs) in the outer plexiform layer (OPL).
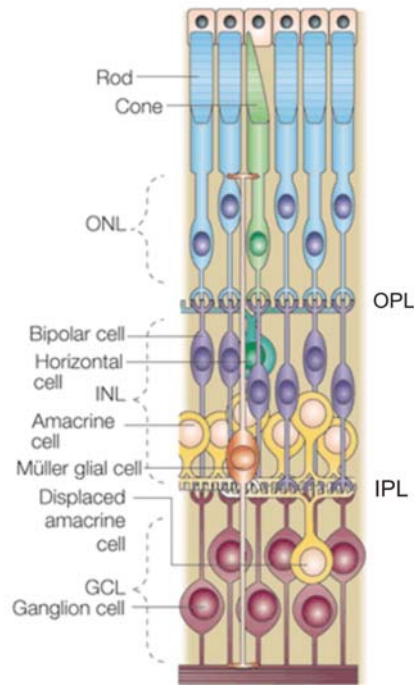
Figure 1.2: Scheme of cell types and layers in the retina. (*from* Dyer & Cepko, 2001).

The somas of BCs and HCs are also apart from the synaptic contacts and form together with the amacrine cells the inner nuclear layer (INL). The synapses of bipolar cells with amacrine cells (ACs) and with retinal ganglion cells constitute the inner plexiform layer (IPL). The last layer is the ganglion cell layer (GCL) that is

separated from the vitreous by the inner limiting membrane. In the GCL also cell bodies of ACs are located, the so called 'displaced' ACs.

The RGC axon form the Optic nerve which is not myelinated intra-retinal in rodents. In between the other cells the glia cells are located. In the retina, three types of glia cells exist, the Müller cells, the astrocytes and the microglia. The Müller cells especially maintain ion homeostasis, support cell metabolism and recycle and synthesize the neurotransmitter precursors. Müller cells are transparent and play a role in guiding photons to the photoreceptors (Franze et al. 2007).

1.3 Physiology and pathways of the retina

The photoreceptors in the retina generate a continuous dark current. In the outer segment cGMP gated cation channels are open and sodium and calcium ions flux in during the absence of photons. The membrane potential is thereby depolarized and causes a sustained release of glutamate at the ribbon synapse of the photoreceptors (**Fig. 1.3 A)**. Excess sodium and calcium ions are removed at the base (ellipsoid region) of the outer segment by a sodium potassium antiporter, that hydrolyzed ATP.
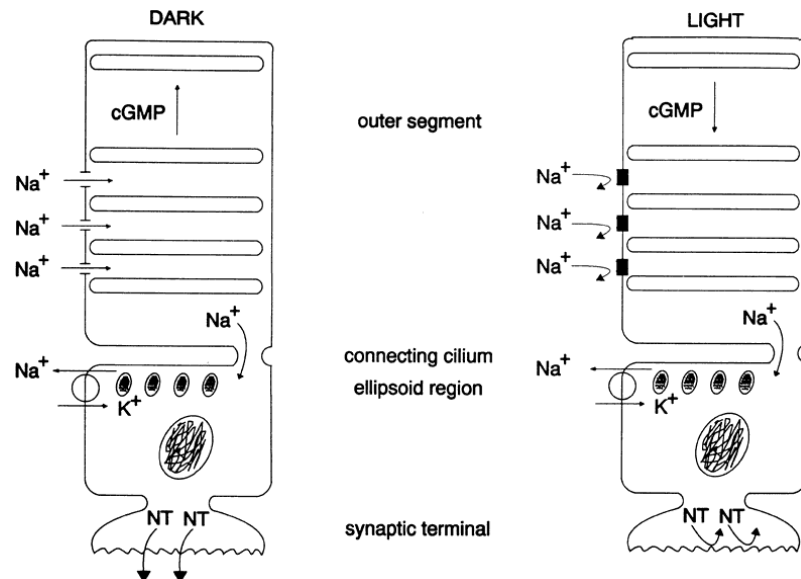
Figure 1.3: Photoreceptor dark current (*from* Tasman & Jaeger, 2006)
  (A) illustrates the ion flux in a photoreceptor when photons are absent. High levels von cGMP keep cation channels in the outer segment open. Sodium accumulates in the outer segment and diffuses in the ellipsoid region, where an ATP driven antiporter extrudes excess sodium. The depolarization of the membrane potential causes sustained glutamate release.
  (B) When photons change the conformation of the rhodopsin chromophore retinal from 11-cis to all-trans, G-proteins activate the Phosphodiesterases (PDE). The PDEs hydrolyse cGMP and its decrease in concentration closes the cation channels. Sodium is still extruded, the membrane potential hyperpolarizes and glutamate release stops.

Activation of the rod rhodopsine or cone photopsine photopigment leads to the hydrolysis of cGMP by the G-protein activated phosphodiesterase (PDE). Decrease of cGMP closes the cation channels and hyperpolarizes the cell (**Fig. 1.3 B**). This stops the glutamate release on bipolar- and horizontal cells (Fain, 2001)

Photoreceptors are homo- and heterotypic interconnected by gap junctions and their synaptic glutamate release is regulated by horicontal cells (HCs) that are excited by glutamate and provide inhibitory feedback to large clusters of photoreceptors. Glutamate is the cardinal excitatory neurotransmitter in the retina. Two classes of glutamate receptors (GluR) are known: the ionotrophic GluR to which belong AMPA, Kainate and NMDA receptors and the metabotrophic GluRs.

Which class of glutamate receptors a cone bipolar cell (CBC) expresses at the photoreceptor synapse defines its light response polarity as ON- or OFF-cell. OFF CBCs are equipped with ionotropic AMPA and kainate glutamate receptors (GluR) and directly depolarized by glutamate release (sign conserving synapse, see **Fig. 1.4**). ON type CBCs express metabotropic, L-AP4 sensitive glutamate receptors and depolarize when the dark current stops. The family of L-AP4 sensitive mGluRs regulates the intracellular cGMP level, but the exact mechanism of membrane depolarization is still unknown. CBCs synapse directly onto RGCs. Beside encoding the contrast quality (ON, OFF or ON-OFF), CBCs mediate information about the wavelength or colour of a stimulus and so far nine types of cone BCs are known in mammals (Gosh et al., 2004).

ON and OFF CBC cells have a distinct morphologic feature: the stratification of their axons within the IPL (Nelson et al., 1978; **Fig. 1.4**), which is complemented by the stratification of the RGCs dendritic tree in this layer. The CBC axons meet the RGC dendrites in the IPL, which is divided in two major sublaminae: in the caudal sublamina a, where the axons of OFF-CBCs terminate while in the rostral part of the IPL, the sublamina b, the ON-CBCs synapse (cf. **Fig. 1.4)**. ON-OFF CBCs make synapses in both sublaminae.
In contrast to the variety of CBCs, only one type of rod bipolar cell (RBC) exists (Sharpe & Stockmann, 1999; Wässle, 2004). It expresses a metabotropic glutamate receptor (mGluR 6) and is therefore of ON-type. Separate ON and OFF channels for this pathway are generated by the AII amacrine cell (AC), which is the postsynaptic target of the RBC (Daw et al. 2003). The AII AC depolarizes upon RBC glutamate release and is also of ON-polarity. Via a gap junction the excitation is mediated to ON-CBCs, concomitantly they release glycine onto OFF-CBCs and OFF-RGCs (**Fig. 1.4**).
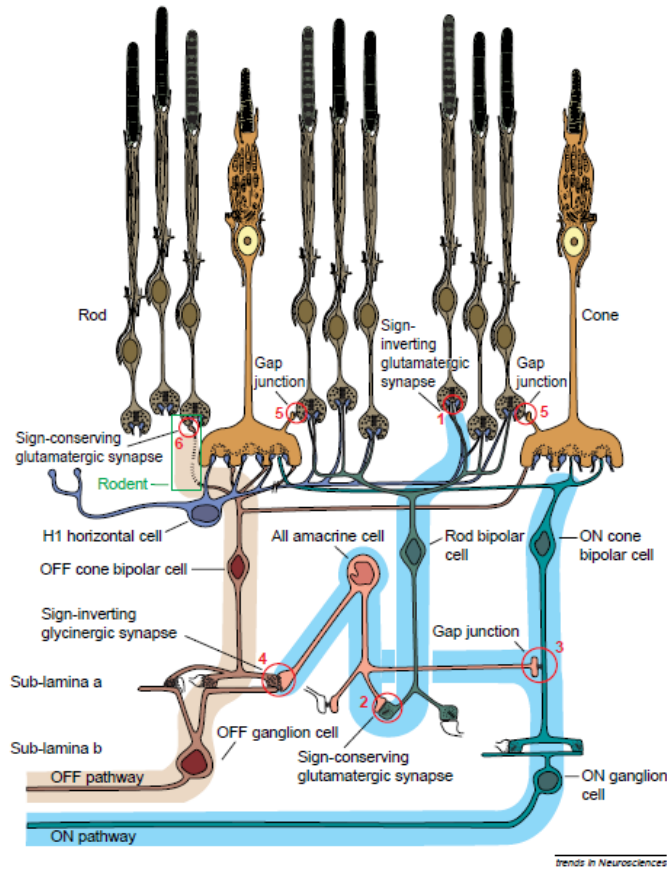
Figure 1.4: ON- and OFF-pathways in the retina. (Sharpe & Stockmann, 1999)
Cones release glutamate onto two types of Cone Bipolar cells (CBCs): ON-CBCs depolarize when glutamate release decreases due to metabotropic glutamate receptors. OFF-CBCs hyperpolarize when glutamate release decreases. OFF-CBCs synapse on OFF-type retinal ganglion cells (RGCs) and ON-CBCs on ON-RGCs. OFF-RGCs make their synapses more distal to the ganglion cells than ON-cells. RGC axons transmit the information to the Lateral Geniculate Nucleus. Rod photoreceptors release glutamate on rod bipolar cells which depolarize when less glutamate is present. Split of the information into an ON- and OFF-channel is done by the AII-amacrine cell. This cell is electrically coupled to On-CBCs and releases glycine on the OFF-CBC synapse with OFF-RGCs.

Mice and rats are nocturnal animals. Mice have 27x more rods than cones, while in rats about 100 times more rods exist than cones (Tsukamoto et al, 2001; Euler & Wässle, 2004). This is not reflected by the organization of the bipolar cell layer: In rats as well as in mice, CBC constitute about the half of the bipolar cell population.

The information processed by ACs and BCs converges onto retinal ganglion cells.

The degree of convergence varies between species and within a species. Ecologic needs promoted the evolution of different retinal organization types, e.g. a foveal organization of cones, BCs and RGCs, which demands less convergence.

RGCs sum the presynaptic information up and generate action potentials that are transmitted to the brain. As recent studies show, RGCs are not the only cell class capable of generating action potentials (amacrine cells: Heflin & Cook, 2007; bipolar cells: Dreosti et al., 2011) However, the RGC action potential is the most pronounced signal in the retina.

RGCs display two types of activity. When a visual stimulus activates the photoreceptors, RGCs generate action potentials that signal the presence of visual features. The most simple response types to light increment or decrement are the ON-, OFF- and ON-OFF response, which are used for functional classification and correspond to a distinct stratification pattern in the IPL.

Additional to this quite simple responses a variety of specialized RGCs are known that perform together with the BCs and ACs within their receptive field complex feature detection (Gollisch & Meister, 2010; Borst & Euler, 2011).

Besides stimulus evoked spiking, it was early recognized that RGCs fire spontaneous in the absence of visual stimuli (Kuffler 1957, Rodieck 1967).

One of the interesting features of spontaneous activity is that some cells fire correlated.

RGCs fire correlated upon visual stimulation. A light ON stimulus leads to positive correlations within the ON- or OFF-cell groups and to a negative correlation between ON and OFF-cells (**Fig. 1.5 a**). In the absence of a visual stimulus, cells tend to fire randomly, but a subset of cells may correlate because they share synaptic input from the same presynaptic cells or have a direct synaptic connection. The shape of the cross correlogram (CC) of two cells is an indicator for the synaptic input they share (Mastronarde, 1989). Combining cross-correlation analysis with pharmacology the type of the synaptic connection can be revealed (Brivanlou et al., 1998). In **Fig. 1.5 b** three types of CCs and the synaptic connection causing them are depicted.
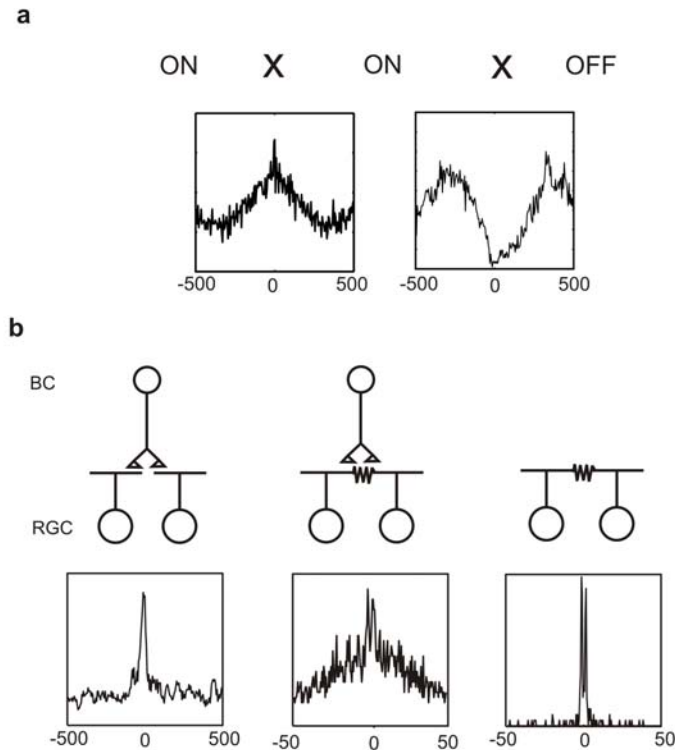
Figure 1.5: Cross correlation patterns found in the rat and mouse retina.

In (**a**) the cross correlation (CC) of the responses to a light flash of two ON- and one OFF-cell are shown. While ON-cells display a positive correlation, ON- and OFF-cell correlations are negative. The synchronous firing is triggered by the light stimulus and the cells may not correlate without stimulation (CCs with 5 ms bin size)

In (**b**) correlation patterns occurring during spontaneous activity in darkness are shown (bottom) and above the hypothetical circuit causing this correlation (after Mastronarde 1989). Two cells fire in synchrony when they share synaptic input from one cell. The CC pattern has a positive peak at zero (left panel, bin size 5ms). If both cells are additionally connected via gap junctions (middle panel) a double peak will appear on the top of the correlation peak. To detect such double peaks binning has to be refined (bin size 0.5ms). If two cells are connected only by a gap junction only a double peak will appear (right panel). The x-axis indicates milliseconds, the y-axis percent of correlated spikes.

Cells that share input from the same presynaptic cell, from a bipolar cell as depicted in **Fig. 1.5b** or an amacrine cell, show a central peak at zero time lag in the correlogram. The width of the central peak can vary depending on the precision of the presynaptic input. If two RGCs are connected via an electrical synapse additionally to presynaptic input, a double peak will be visible on the top of a broader peak (**Fig. 1.5 b**, second panel). If there is only an electrical connection between the RGCs., a sharp double peak will appear in the correlogram (**Fig. 1.5b**, third panel).

CC pattern help to identify types of synaptic inputs cells receive and thereby to clarify features of the underlying circuit.

1.4 Diseases of the retina

In the present work, animal models of two major retinal diseases will be studied. The first part of the work focuses on retinitis pigmentosa, an inherited loss of photorecetors and the second part on glaucoma, an age related loss of RGCs. Loss of RGCs (or neurons in general) is also characteristic for other degenerative diseases.

1.4.1 Retinitis pigmentosa and retinal degeneration

Retinitis pigmentosa (RP) in human patients is characterized by progressive photoreceptor loss (Jones & Marc 2005). Starting with rod degeneration from retinal periphery, patients first loose night vision and due to subsequent cone loss patients become complete blind. Depending on the gene defect, retinal degeneration takes place during adolescence or in the fourth life decade. About 34 gene defects are known to cause RP and are inherited autosomal dominant (7 genes), recessive (25 genes) or X chromosome linked (2 genes). The variety of genetic defects complicates a proper treatment of the disease but the resulting phenotype is similar in all cases (Bird 1995). In general, the known mutations affect the visual cycle or the phototransduction pathway in rods. The defects in signal transduction subsequently lead to rod photoreceptor death (Cottet & Schorderet 2009). The mechanism that links cone photoreceptor degeneration with rod photoreceptors apoptosis needs further investigation, but nutritional defects and insulin signaling seem to play a key role (Punzo et al. 2009).

The first mouse retina lacking photoreceptors was discovered 1924 by Keeler (Keeler, 1924) and initially used for genetic studies. From his stock the C3H mouse strain was derived that is still widely used to investigate the consequences of RP in animals (Keeler, 1966). In **Fig. 1.6** an original drawing from Keeler 1924 is shown, that illustrates the key feature of all animal models of retinitis pigmentosa: the complete loss of photoreceptor outer segments and their nuclei (**Fig. 1.6**, right). In *rd1* mice, opposite to human patients, photoreceptor degeneration starts in the central retina and progresses to the periphery (Jimenez et al. 1996).

The mentioned C3H mice as well as the FVB mice belong to the rd1 type (Both strains were used here). Beside the *rd1* mouse a variety of other animal models for inherited retinal degeneration is known (for review see Jones & Marc 2005).
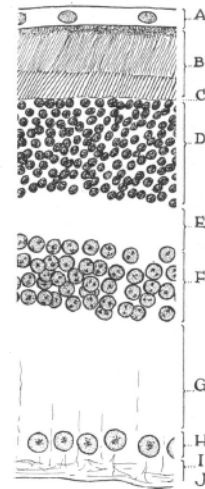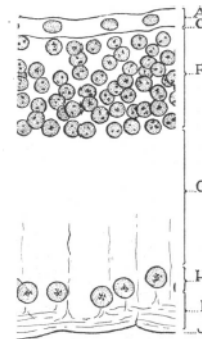
Figure 1.6: The PDE6b missense mutation causes loss of the outer segments and the outer nuclear layer (*from* Keeler 1924)
On the left a normal retina is sketched with Outer segments (B&C),Outer nuclear layer (D) and outer plexiform layer (F) visible. The schematic sketch on the left illustrates the consequences of retinal degeneration, only the inner nuclear, inner plexiform and RGC layer are left (F-J).

The *rd1* animals carry a nonsense mutation of the phosophodiesterase 6 β subunit, that causes high cGMP levels in rod outer segments and leads to the apoptosis of all rod photoreceptors around postnatal day (PND) 17 (Carter-Dawson et al., 1978). Mutations in the *PDE6B* gene occur also in human patients and are responsible for up to 4 % of all cases of Retinitis pigmentosa (Dryja et al., 1999).

The rod degeneration includes the loss of rod outer segments and rod nuclei.

Different to this complete loss of rod photoreceptors is the degeneration of cones, which are not primarily affected. Cone outer segments degenerate prior to cone somata and are undetectable around PND 28. Remaining cone nuclei are still found around PND 100 (Lin et al. 2010).

So far the functionality of the residual cone somata is unknown. Recent findings indicate that the remaining cone somata are still able to generate a dark current and can be reactivated using vector based expression of light sensitive ion channels (Busskamp et al. 2010).

Loss of the presynaptic photoreceptors affects the cells in the inner retina. Concomitant with the onset of degeneration mGluR6 expression in rod bipolar cells is down regulated and residual proteins are mislocalized, as a consequence glutamate sensitivity in bipolar cells decreases (Puthussery et al. 2010). In *rd1* mice horizontal cells start sprouting upon photoreceptor degeneration to regain new synaptic contact, while rod bipolar cells retract their dendrites (Strettoi et al. 2002). Within the first 100 postnatal days around 20% of HCs and rod BCs die in *rd1* mice (Strettoi, 2000).

In later stages of RP a general remodeling of the cellular organization in the retina is reported, but this is not seen in *rd1* mice earlier than PND 600 (Marc et al. 2005).

Other models of retinal degeneration show additionally to photoreceptor loss secondary degeneration of RGCs leading to complete RGC loss at late stages (Villegas-Perez et al. 1998; Kolomiets et al., 2010)

The first investigation of visual activity in *rd1* mice was undertaken by Hubel and Dräger (Hubel & Dräger, 1978), who recorded rhythmic bursting cells in the visual cortex of anesthetized animals.

After a long period of silence, in recent times three studies were published about electrophysiological changes in the retina of *rd1* mice.

The first study (Stasheff, 2008) recorded C3H mice RGCs during development and in maturity with a MEA and found an increase of spontaneous activity that he termed 'hyperactivity'. In this exciting study the idea, that the cells are rhythmic is indicated, but not further investigated.

In the same year a patch-clamp study on *rd1* mouse RGCs was published (Margolis & Detwiler 2008). ON and OFF cells were identified by morphological features and it was shown that this cells spike in a stable 10 Hz rhythm. As the sample was much smaller than in Stasheffs MEA study it remained unclear in which proportion of cells this may take place and which role the different neurotransmitter systems play.

The third study on C3H mice also used a MEA but analyzed only low-pass filtered data (Ye & Goo, 2007) of C3H mice younger than PND 30. In the low pass filtered data they found a "slow wave" component which had a frequency of 10 Hz.

From these studies only one indicates that RGCs in *rd1* exhibit rhythmic spiking (Margolis et al. 2008), but confirms this only for a small sample of cells.

In the present study will be analyzed which proportion of *rd1* cells is indeed rhythmic and how this affects their correlation pattern. Additionally low frequent voltage deflections were analyzed to understand their temporal and spatial pattern and their relation to RGC activity. The aberrant activity seen in *rd1* mice relies on presynaptic input (Margolis et al., 2008). Therefore the effects of a variety of neurotransmitter antagonists and synaptic blockers will be investigated. The analysis will reveal the major components that generate the aberrant electrical phenotype seen in *rd1*.

Based on the data available so far it was recently proposed (Margolis & Detwiler, 2011) that loss of inhibition may be the trigger of rhythmic hyperactivity in *rd1* mice. It was also claimed claimed that it should be possible to induce the *rd1* phenotype in *wt* mice using appropriate blocking substances that create an imbalance between excitation and inhibition.

However, blocking inhibition in *wt* retina induces regular bursting in RGCs at a fundamental frequency less than 1 Hz and leaves firing rates unaffected (Margolis & Detwiler, 2011). This result was confirmed in recordings of bipolar cells under the same condition (Borowska et al., 2011) It can therefore be concluded that blocking inhibitory synapse alone is not sufficient to generate a *rd1* like phenotype.

My study focuses on the critical role of the dark current in spontaneous activity of RGCs in *rd1* and *wt* mice. Absence of light causes the dark current and the permanent release of glutamate onto bipolar cells. ON-bipolar cells interpret the presence of glutamate as "darkness". After photoreceptor loss, no glutamate is released and this may trigger hyperactivity of bipolar cells.

Considering the role of light and light activation in the retina gave rise to the "equivalent light" hypothesis (Fain & Lismann, 1993). In many forms of *rd*, but not in *rd1*, the mutation in rod photoreceptors closes the cGMP gated channels constantly, which is also the case when photons activate the opsines/rhodopsines. Therefore Fain & Lissmann related the loss of photoreceptors to known effects of light damages, which also trigger photoreceptor degeneration (Marc et al., 2008). In *rd1*, the loss of photoreceptors may also be an "equivalent light".

In the present study the role of the dark current in maintaining normal retinal activity will be studied and it will be shown that loss of the dark current is sufficient to induce rhythmic spiking in RGCs of *wt* mice.

1.4.2 RGC degeneration and glaucoma

In the *rd1* mouse used here, the RGCs only receive altered synaptic input due to photoreceptor degeneration.

But in other *rd* mice (Wang et al., 2000) a progressive loss of RGCs was shown. More obviously is RGC degeneration in different rat models of *rd* (Sekirnjak et al., 2011; Kolomiets et al, 2010; Villegaz-Perez et al., 1998).

Loss of RGCs progresses very slow in these animals and for the analysis of RGC activity it is critical to differentiate between the effects of presynaptic degeneration and degenerative changes of the RGC itself.

Therefore RGC degeneration can be better studied in animals suffering from glaucomatous diseases.

Like RP, glaucoma is a leading cause of blindness in the world. It is characterized by progressive loss of RGCs and degeneration of the optic nerve. Similar to RP, glaucoma affects initially the peripheral retina. The pathophysiology of glaucoma is not yet fully understood. Glaucoma is clinically related to elevate Intra-Ocular-Pressure (IOP) that crushes the RGC axons behind the optic disc and thereby initiates RGC degeneration. Responsible for high IOP is often the decreased drainage of aqueous humor, which fills the posterior and anterior eye chambers and is secreted by processes of the ciliary body (Quigley 2011). But cases of glaucoma are known that are not related to elevated IOP or hypertension and therefore termed Normal tension glaucoma (NTG) (Sowka 2005). Glaucoma is divided into Open angle glaucoma that progresses slowly and closed angle glaucoma with sudden onset.

Suffering from glaucoma is related to ageing and has no clear genetic basis and known risk factors for glaucoma are of more general kind (Quigley 2011).

By now glaucoma treatment depends on early detection of the disease which is followed by surgical intervention, which slows the progression. Lost visual function cannot be restored.

Curing later stages of glaucoma faces the same general problems that are related to axonal regeneration in neuronal tissues (Luo & Leary 2005, Raff et al. 2002).

Therefore glaucoma research is intermingled with research for axonal regeneration strategies (Heiduschka & Thanos 2000).

Investigating glaucoma, a variety of animal models is available (Levkovich-Verbin 2003). As mentioned, glaucoma lacks a clear genetic cause and therefore most animal models rely on physical intervention.

Just recently a mouse strain was identified that carries a gene mutation leading to elevated IOP, the DBA/2J mice strain (Moon et al. 2005).

In this study the role of the IOP is neglectable and to study RGC loss I established a surgical model of glaucoma, where the optic nerve of rats is either crushed or sectioned within the orbit.

By the lesion the axon contact with its target is weakened (crush) or disrupted (section). Neurons receive neurotrophic factors from their target synapses which are retrograde transported (Thoenen 1987, Krishnamoorty et al. 2001). Additionally, axons lack a metabolic system and are maintained by anterograde transport (Colemann 2011)

These transport mechanism collapse upon injury and in case of complete axon disruption transport vesicles accumulate at the end of the axon stump (Moore & Thanos, 1996; Griffin et al. 1995).

Axonal section causes a type of degeneration termed "Wallerian", where after a short period the somatic and axonal cytoskeleton break down and the cells are degraded (Thanos & Thiel 1991, Luo & O'Leary, 2005). In contrast to this rapid apoptosis, a slow and cell compartment specific degeneration occurs when the axon is intact but under physical stress or affected by a chronic disease. In this case the axon is "dying back" over a longer period while the cell soma is left intact. This compartment specific degeneration resembles developmental events of synapse reduction where specific axon branches are degraded (Raff et al., 2002)

A variety of studies investigated the time course of RGc degeneration for different species after surgical treatments (Berkelaar et al. 1997, Germain 2007, Kanamori 2010, Watanabe 2002). For rats and rabbits a relatively slow rate of RGC apoptosis within the first week was shown, which accelerated in the second week after treatment (Berkelaar 1997, Germain 2007). It was mentioned that RGCs with larger somata survive longest after optic Nerve injury (Mey & Thanos 1993).

RGC whose axons were left intact undergo secondary degeneration and initiate apoptosis upon the loss of their neighboring cells (Levkovich-Verbin et al. 2010).

In animals suffering from experimental glaucoma, it was shown that the shrinkage of the dendritic tree is the first sign of glaucomatous degeneration in monkey and mouse (Weber et al. 1998, Leung et al. 2011).

While degenerative processes are well studied on the levels of morphology and molecular biology only one study investigated the impact of Optic nerve lesion on single RGC functionality (Takao et al. 2002).

Furthermore it is not known, how the loss of RGCs is related to axonal function.

Functional studies at the single cell level are necessary to investigate if the surviving RGCs after optic nerve lesion remain intact or change their response properties. As the surviving neurons are the primary target of any treatment for glaucoma and optic nerve neuropathies, the functional state of these cells and the time course of their degeneration are of special interest.

Most experiments aiming to prevent RGC loss apply the promoting substances

before or during the optic nerve lesion (Hellstrom et al., 2011; Almasieh et al. 2010; Heiduschka et al. 2005). In clinical cases a treatment will be applied after a severe damage was diagnosed, therefore treatment strategies rely on the condition of the surviving neurons.

1.5 Extracellular recording of retinal Ganglion cells

In this study the electrical Retinal Ganglion cell activity was recorded extracellular using a Multi-Transistor-Array (MTA).

Here the Complementary Metal Oxide Semiconductor (CMOS)-based Neurochip G1183 (Lambacher et al., 2010) was used (**Fig. 1.7 A**), which has an active sensor area of 1 mm^2 comprising 16384 recording transistors (**Fig. 1.7 B**). The distance between two neighboring sensors is 7.4 μm. In **Fig. 1.7 C** the major compartments are illustrated. The cell (depicted as RC element) is capacitive coupled to the capacitive surface of the transistor. Coupling depends on the resistivity of the medium and the "gap" between tissue and the insulating oxide of the chip. Changes in the extracellular potential caused by action potentials modulate voltage across the oxide and thereby the source-drain current in the transistor.
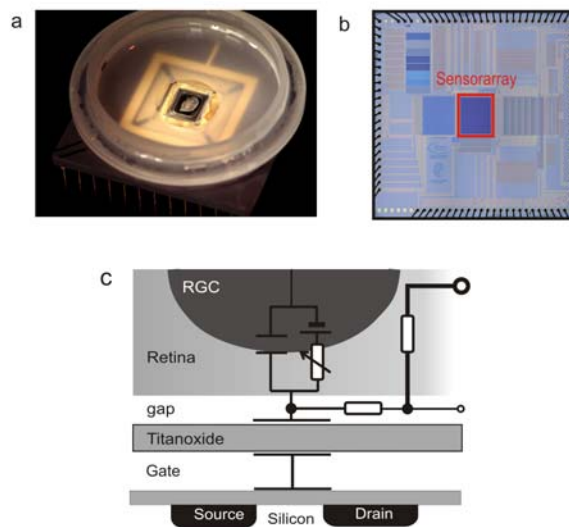
Figure 1.7: The G1183 Neurochip
(a) *The G1183 Neurochip with a Perspex chamber mounted on a ceramic socket. The chamber allows perfusion of the tissue. On the chip a piece of mouse retina is adhered.*
(b) *Picture of the Chip with Sensor array and Stimulation array indicated*
(c) *Major components of the capacitive retina-chip coupling can be simplified by electronic parts. Recording principle of the G1183 chip: Changes in extracellular ion concentration due to RGC activity modulate the Source-Drain current of the underlying recording transistor.*

.

Each neuron has a negative membrane potential - or resting potential - caused by asymmetric distribution of ions as expressed in the Nernst equation. These gradients are actively maintained by specific ion pumps.

Neurotransmitter receptors, mainly located at the dendrites, open specific ion channels and due to the initial gradient and the electric charge of the ions the membrane potential will be altered.

Influx of chloride ions due to GABA or Glycin receptor activation will hyperpolarize the cell, while sodium and calcium influx after glutamate or acetylcholine receptor activation depolarizes the cell.

Given the activation of depolarizing ion channels, the membrane potential will be elevated to the threshold of voltage gated sodium channels. These channels enable massive sodium influx and depolarize the membrane potential to positive values. Voltage gated potassium channels open during depolarization and an increasing potassium efflux leads to a hyperpolarization of the cell. This picture of a neurons action potential is based on the intracellular recordings of Hodgkin and Huxley (Hodgkin & Huxley 1952; **Fig. 1.8**).

Extracellular recordings depend on the electric field produced by the ionic current crossing the cell membrane during an action potential. Changes in the extracellular electric field can be measured when an electrode is placed nearby.

According to Ohm's law the electric field (E) is the product of resistivity (ρ) and current density (j):

$$(1) \qquad E = \rho * j$$

For recording the distance between the electrode and the neuron is a critical parameter. The voltage V recorded by an electrode depends on its distance *r* to the point source of the circular electric field, the total current *I* and the resistivity ρ, which is a matter constant.

$$(2) \qquad V = \rho I / 4\pi r$$

For the retina on a MTA Chip the tissue resistivity was estimated to be $\rho = 1000\ \Omega cm$ (Zeitler, Fromherz, Zeck *to submit*). The total current *I* for a model cell of 100 pF capacitance that changes its membrane potential for 100 mV is:

$$(3) \qquad I = 100\ pF *\ 100\ mV/\ 1\ ms = 10^{-8}\ A$$

Therefore, for an extracellular electrode, 20 μm apart from the cell body, the recorded voltage is:

$$(4) \qquad V = 10^{-8}\,A * 1000\ \Omega cm/(4\,\pi * 20 * 10^{-6}m) = 400\ \mu V$$

The action potential amplitudes recorded in mouse and rat retina (compare **Fig. 1.9**) are in the range of 100 – 500 μV.

The series of events during an action potential sketched above determine the form of the recorded signal. Somatic APs are biphasic with a negative peak indicating sodium influx and a small positive overshoot produced by potassium currents.
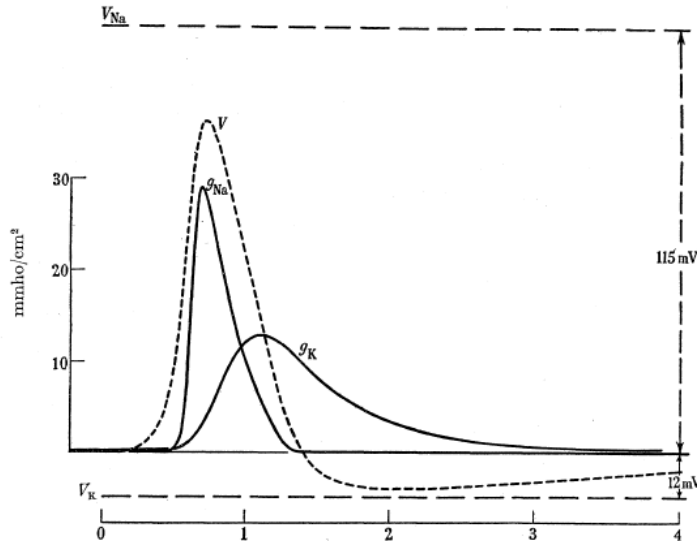
Figure 1.8: The action potential is shaped by the kinetic of voltage gated sodium and potassium channels (Hodgkin & Huxley 1952).
The graph shows the changes in sodium (gNa) and potassium conductance (gK) when a cell is depolarized to spike threshold. Changes of the membrane potential (V) are indicated by the dashed line, after a strong depolarization, the voltage decreases exponentially to values below the initial resting potential. In extracellular recordings algebraic signs are inverted compared to intracellular recordings, e.g. depolarization has negative voltage.

In extracellular recordings not only somatic APs are obtained but also axonal APs.

Action potentials in axons have to propagate over long distances and signal decrement has to be minimized. Axonal action potentials are triphasic (Plonsey & Barr, 2007), with two hyperpolarizing phases in front and behind the depolarized region. Nevertheless, axonal APs recorded here were biphasic and only near the axon hillock a stationary third phase was seen (**Fig. 1.9 c**). As intra-retinal axons are

not myelinated, the depolarization propagates continuously along the axons at a cell specific propagation velocity.

In rabbit single axonal action potentials can be recorded, while in rat and mouse retina the signal is hidden in the transistor noise. The ratio of somatic to axonal spike amplitude was estimated 1:10 in the rabbit. Comparing the average spike amplitudes of rabbits with mouse and rats (**Fig. 1.9 a**), this makes the detection of a single axonal action potential unlikely (**Fig. 1.9 b**; voltage map of 1 ms raw data activity).
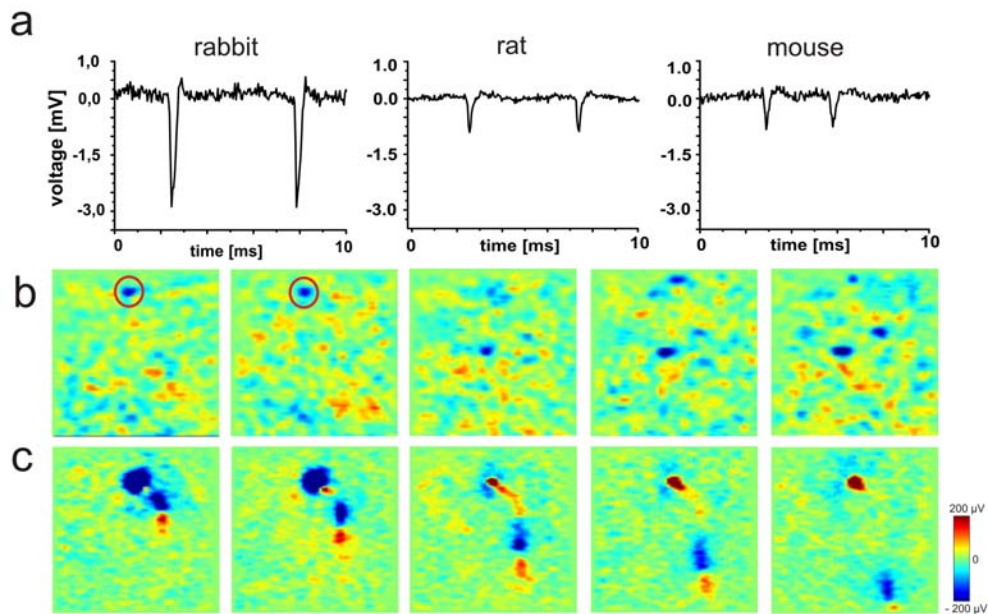
Figure 1.9: Detection of axonal action potentials by spike triggered average
- **(a)** The average spike amplitude of rabbits is five times higher than in rat and mouse. Given a ratio of somatic to axonal spikes of ~ 1:10 detection of single axonal APs is unlikely in rat and mouse
- **(b)** Colour coded voltage map of the spiking of a cell (red circle) and the activity during the next millisecond. No axonal AP is visible, but other spiking cells (blue)
- **(c)** Averaging the voltage maps of the first millisecond after each somatic spike of one cell (red circle in **(b)**) enhances the axonal AP and visualizes the path of its propagation. Each square represents $1mm^2$ retinal surface.

Averaging the voltage values of every transistor after a somatic action potential using a spike-triggered-average algorithm enhances the signal and enables the visualization of axons in rat and mouse (**Fig. 1.9c**).

In summary, extracellular electrodes detect voltage changes in single axons and single cells if they can be placed in close proximity.

Additionally, extracellular electrodes can record cell population signals. When large cell populations are active at once, e.g. during heart muscle activity, epilepsy or in the retina perceiving a light flash, the single signals sum up and constitute a population signal (Buzsaki, 2006).

Such signals can be recorded even at extra corporal sites as in EEG (Electro-encephalogram, ERG (Electro-retinogram) and similar methods (Plonsey & Barr, 2007).
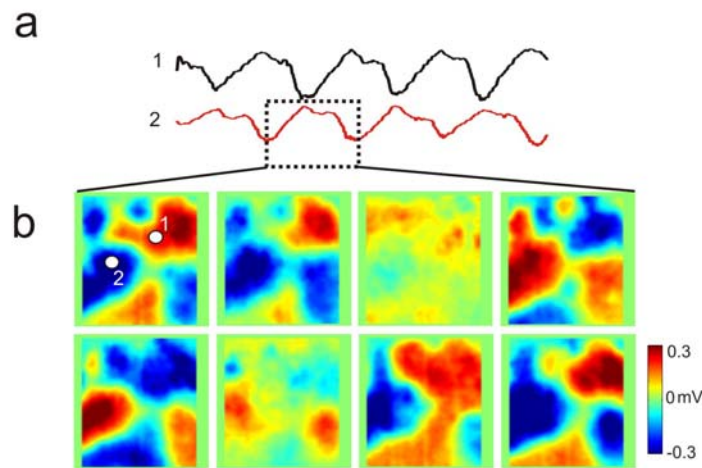
Figure 1.10: Extracellular recorded Local Field Potential in the mouse retina
In (**a**) the low pass filtered voltage traces of two sensors are shown. The location
of the sensors is indicated by white dots in (**b**), where the spatial properties of the LFP are
illustrated. The dots have the size of the average area on which the activity of a single cell is
seen (**Fig. 1.22 b**)

Population signals restricted to smaller cell populations can be recorded by an ectracellular electrode in the tissue. These signals are termed Local Field potentials as the cell population act as a single point source generating a large electric field change. (**Fig. 1.10**, compare to single cell activity in **Fig. 1.19 b**)

The physical explanation of LFPs is still under discussion, but the phenomenon relies on the fact that low frequent waves (< 150 Hz) can travel over large distances in tissues and sum up, while high frequent waves like action potentials (> 1 kHz) do not (Bedard et al., 2008, Mitzdorf , 1985) as tissues act as low-pass filters.

In this study local field potentials of the retina were recorded extracellular (**Fig. 1.10**).

LFPs cannot be assigned to single cells, while Action potentials have to.

The extracellular recording of APs constitutes a challenge of proper detection and spike assignment.

In intracellular recordings each spike of a cell can be interpreted as response to its condition. In this configuration each spike is a more or less meaningful signal of the known cell.

In extracellular recordings the set of action potentials recorded has to be assigned to one or more cells. In the following some fundamental outlines of a spike sorting process will be discussed.

Using a single electrode two fundamental facts facilitate spike sorting:

a) Each AP is followed by a refractory period of 1 ms where no AP can be elicited

b) Due to the decrease of the recorded voltage over distance, APs of two cells that are not equidistant differ in amplitude

Application of both principles is limited by the fact that spike trains of two cells may be time shifted so that the majority of spikes does not violate the refractory period of the other cell.

Furthermore even cells that are not equidistant may have spikes of similar amplitude. A step further is to consider the shape of the signal, i.e. the slope of the recorded action potential (Gerstein and Clarck 1964) what requires high temporal resolution (> 20 kHz). A variety of other features of the spike shape can be extracted and used by Principal component analysis to build clusters of spikes (Glaser & Marks 1968). All these algorithms rely on arbitrarily chosen spike features and need supervision.

These approaches work on data from a single electrode and spike sorting was enhanced using Multi-Electrodes. In the classic case, spikes were recorded by a tetrode (Gray et al. 1995) and depending on the distance to the electrodes the spike shape varies and facilitates cluster analysis.

In this study, spikes were sorted in three steps (A more detailed analysis is presented in: Lambacher et al. 2010):

First, threshold crossings were detected using custom software (Labview) in the voltage trace of each transistor. A threshold crossing was defined as events that

exceed the root mean square of the transistor noise at least three times. This is a minimum requirement and as even arbitrary events may be of that size additionally every threshold crossing has to be detected by three sensors.

(1) A multitude of sensors due to the high sensor density will record each threshold crossing. From this results a list of {x1…xn} threshold crossings for each sensor, each threshold crossing has a temporal identity: sensor xy = { t1, t2….tn}.

(2) The threshold crossings which occur a) simultaneously and b) on adjacent sensors are merged into an action potential. In other words, the list is reorganized to a sequences of temporal events which are enumerated in the order of their appearance (AP#1, AP#2…AP#n) and to each AP a set of sensors is assigned (AP#1 = sensor 2,3,4,5).

(3) In the last step the sensor sets of all action potentials are analyzed for overlap respectively identical transistors. For example AP#1 is recorded by 2,3,4,5, AP#2 by 3,4,6,7. Each cell's APs are assumed to be recorded by a specific set of transistors. This feature is mainly used to assign action potentials to the corresponding cell. In addition inter spike intervals are used with regard to the refractory period violation.

At the end all these APs are assigned to one cell. This is of course a mechanistic process afterwards all created cells have to be supervised manually.

Aim of this study

The present study is aimed to understand the electric activity in two models of degenerating retina. Degeneration of the retina leads to blindness that actually cannot be cured.

First, a mouse model of *rd1* will be analyzed. In rd1 photoreceptors largely disappear but the other layers are left intact and continue to signal. Their spontaneous activity and the effect of different synaptic blockers will be investigated to reveal the underlying circuitry (**sect. 3.1**).

Based on this results, the *rd1* phenotype will be induced in normal C57Bl6 mice to produce a "fast" *rd1* model that sheds light on the origin of the aberrant activity seen in *rd1* (**sect. 3.2**). The same protocol will be applied to wistar rat retinas (**sect. 3.3**).

Loss of RGCs is a feature of late *rd* but also of other retinal diseases like glaucoma. Glaucoma is an age related degeneration of RGCs that can be mimicked by surgical injuries of the optic nerve. The consequences of axonal lesion on the propagation velocity of axonal APs will be studied in rat retinas as well as alterations in spontaneous and light evoked activity. (**sect. 3.4**) At least the effect of optic nerve lesion on the correlated firing of rat RGCs will be shown (**sect. 3.5**).

2 Materials & Methods

2.1 Materials

The following table lists all chemicals used in this study. Chemicals were dissolved in aqua bidest or in acetate buffer (TTX) to obtain stock solutions. Stock solutions were dissolved in AMES Medium to get the final concentrations used.

Substance	**Supplier**
Ames Medium	Sigma
D-(-)-2-Amino-7-phosphonoheptanoic acid (AP-7)	Tocris
DL-2-Amino-4-phosphonobutyric acid sodium salt (AP-4)	Tocris
(3β,20β)-3-(3-Carboxy-1-oxopropoxy)-11-oxoolean-12-en-29-oic acid disodium (Carbenoxolone)	Tocris
6,7-Dinitroquinoxaline-2,3(1H,4H)-dione (DNQX)	Sigma
Ketamine hydrochlorid	WDT
2-[(2,6-Dichloro-3-methylphenyl)amino]benzoic acid sodium salt (MFA)	Sigma
Rhodamine B isothiocyanate–Dextran	Sigma
(*S*)-1-Aminopropane-1,3-dicarboxylic acid (glutamate)	Sigma
2-(3-Carboxypropyl)-3-amino-6-(4 methoxyphenyl)pyridazinium bromide (Gabazine or SR 95531)	Sigma
Sodium bicarbonate	Sigma
Strychnidin-10-one hydrochloride	Tocris
Tetrodotoxin	Sigma
Xylazine hydrochloride	Bayer

Table 1: Chemicals used in the experiments

2.2   Animals

a) Mice

All experiments were performed in accordance to the animal use committee of the Max Planck Institutes. In this study retinas from male *rd1* mice were investigated between postnatal days P 35 –P 300, when their retinas are no longer responsive to light. All experiments on *rd1* retinas were first performed using the local colony of the FVB/NCrlMPI strain that is homozygous for the *Pde6b^{rd1}* mutation (Taketo et al., 1991). After the pharmacological protocols had been established, the experiments were repeated with *rd1* retinas from C3H/HeNCrl mice (Charles River, Sulzfeld, Germany) that are homozygous for the *Pde6b^{rd1}* mutation. Control experiments were performed on *wt* retinas from the local colony of C57/Bl6NMPI male mice. To rule out possible interference from different genetic backgrounds, I additionally obtained C3H *wt* male mice from F. Paquet-Durand (Tübingen). This mouse strain was initially created in the lab of S. Sanyal (Sanyal and Bal, 1973) by substituting the mutated *Pde6b* gene with the normal allele, and is maintained in various labs ever since. All animals were housed in temperature-regulated facilities on a 12 h light/dark cycle and fed *ad libitum*. All animals were dark adapted (1h) prior to the retina preparation.

b) Wistar rats

All experimental procedures were carried out in compliance with the institutional guidelines of the Max Planck Society and the local government (Regierung von Oberbayern; Statement of Compliance #A5132-01 Tierversuchsnummer: 55.2-1-54-2531-95-08). All animals are sacrificed prior to the removal of organs in accordance with the European Commission Recommendations for the euthanasia of experimental animals (Part1 and Part 2).
Female wistar rats (WR, local colony at the Max Planck Institute of Neurobiology) weighting 80-100 g were used for this study. Efforts were made to minimize the number of animals used as well as their suffering.

2.3   Surgical procedure for rats

Animals were anesthetized by i.p injection of 0.85 ml/kg of 5% ketamine hydrochloride solution (WDT, Garbsen, Germany) and 0.35 ml/kg of 2% xylazine hydrochloride solution (Rompun, Bayer, Germany).

All surgical procedures were performed unilateral. The eye lid was retracted using tweezers, and then a short incision was made in the conjunctiva. The conjunctiva was retracted and fixated with threads. This procedure exposed a 5 mm section of the optic nerve.

Optic nerve crush (ONC): The optic nerve was crushed behind the ophthalmic artery pressing with forceps for 10 sec.

Optic nerve section (ONS): A 5 μl Hamilton (Hamilton, Reno Nevada) syringe was used to puncture the optic nerve behind the ophthalmic artery. The enveloping nerve sheet was left intact. In some animals 3 μl Rhodamine dextrane was injected to monitor RGC loss.

Retinas of WR were used 4, 8 and 14 days after surgery. As controls animals of same sex, weight and age were used. Rodent retinas showed diminished light responses when stored in Ames solution longer than 1 hr prior to recording. Therefore the other eye could not be used as control.

2.4   Staining and cell count in rat retinas

After MTA-chip recordings the Ames medium was carefully removed from the chip and the retina was briefly dried to allow imaging through the inner retinal layers. Rhodamine-dextrane labeled cells were imaged using fluorescence light microscopy with an excitation and an emission frequency of 535 nm and 571 nm, respectively. Once the retinal layers became translucent the retina was imaged using a 20x objective. All stained cells within the recording array were photographed.

The resulting images were combined to create an overview of the whole recording area.

The position of electrically recorded cells was determined plotting the number of spikes recorded by each transistor. The resulting image was used to create outlines of the different areas of maximal spike count and these outlines were merged with the fluorescent microscope pictures. Thereby I was able to assign areas of high spike counts to cells.

Stained cells on the micrographs were counted using the image software Fiji. The threshold of the images was manually set to minimize background. The image was then transformed into a binary image. The particles on the image were counted using the "analyze particles" function, if their size was between 20-2000 pixels in case of 20x magnification. The counted particles were drawn as ellipses. Original picture and counted particles picture were combined, to allow manual supervision of the count.

2.5   Preparation of the retina and mounting on the multi-transistor-array

The preparation of the retina was performed under dim red illumination (640 nm LED, Roithner Lasertechnik), that also illuminated the room during the experiment. Mice were anesthetized with isoflurane (CP Pharma, Burgdorf, Germany) and killed by cervical dislocation. Their eyes were removed, bathed in room temperature-oxygenated Ames' medium (pH 7.4) and hemisected. Next, the lens and vitreous were removed from the eyecup and finally the retina gently peeled off the pigment epithelium. The retina was mounted ganglion cell side down on a poly-L-lysine (150 kDa MW, Sigma) coated multi-transistor array (MTA). The MTA itself was glued on a ceramic package (CPGA, Spectrum, San Jose, CA). The bond wires are shielded with a custom made Perspex chamber with an inner area of 12 mm^2. During the recording, retinal tissue on the MTA was continuously perfused with oxygenated Ames' medium (33-36°C) at a rate of 7 ml/min. For all experiments only freshly prepared retinas were used.

2.6   Electrical recording with multi-transistor arrays

The electrical response of the retina was measured using an array of 128 x 128 equally spaced sensor transistors covering an area of 1 mm^2. For the default configuration I measured every second column (128 x 64 sensors) with a sampling frequency of 12 kHz for each sensor. In each experiment sensor transistors were calibrated by applying an AC voltage (frequency: 70 Hz; amplitude: 3 mV peak-to-peak) to the bath electrode (Eversmann et al., 2003; Lambacher et al., 2004). The calibration voltage changes the electrical potential at the surface of the chip. The local change of electrical potential couples through the insulating chip oxide to the

gate of the sensor transistor and proportionally modulates the source-drain current therein. During the experiment, ion currents through excited retinal ganglion membranes change the local extracellular voltage with respect to the bath electrode. The response of each sensor transistor is solely determined by the potential above the insulating $TiZrO_2$ layer, averaged over the diameter (6.3 μm) of the top contact. The insulating $TiZrO_2$ layer had a thickness of $\sim$ 30 nm. The chip read-out pattern was optimized to avoid cross-talk of transistor signals on the chip (Eversmann et al., 2003; Lambacher et al., 2004) . During the recording, the columns of the sensor array were sequentially connected to 128 line amplifiers. After a settling time of 720 nanoseconds, the output of these line amplifiers was multiplexed over another 640 ns into 16-output channels. The read-out time of 128 x 64 sensor array was therefore $\sim$ (1.36 x 64) μs. Within each sensor column, an 8:1 multiplexer selects 16 sensors (sensor spacing 125 μm) that are read out within $\sim$ 640/8 ns.

2.7 Identification of action potentials and assignment to the corresponding ganglion cell

The method for identifying action potentials and assignment to corresponding neurons has been described in a recent report (Lambacher et al. 2011). Briefly, the analysis is done in three steps: (a) Identification of threshold crossings of a signal vector V calculated from neighbouring extracellular voltages, (b) Assignment of threshold crossings to one action potential and (c) Assignment of action potentials to corresponding neurons.

For the identification of threshold crossings, I first apply a band-pass filter to the calibrated data (0.1 – 3 kHz). As the sensor distance (7.4μm) is smaller than the ganglion cell soma size, each extracellular signal is picked up by more than one sensor. The duration of the somatic extracellular signal is longer than the time interval between consecutive data points. Therefore, for each recorded data point the length of a signal vector V is calculated:

$$V = \sqrt{\sum_{i=1}^{27} \frac{V_i^2}{\sigma_i^2}} \tag{1}$$

with V_i representing the signal amplitude of data point i in neighbourhood, σ_i: root mean square (*rms)* noise of transistor in neighbourhood. The sum runs over a 3x3x3 neighbourhood (3 sensor rows, 3 sensor columns, 3 time points) surrounding the data point under consideration. The data point itself is part of the neighbourhood. If V exceeds a threshold of 15 the data point is saved and considered part of the extracellular waveform that represents the action potential. Assuming equal noise on each of the nine neighbouring sensors and homogenous coupling on these sensors the threshold value of 15 means that those extracellular voltages exceeding $15/\sqrt{27}$ x *rms* of the corresponding sensor are detected. This threshold value is close to that of previous studies using metal electrode arrays (Zeck and Masland, 2007; Stasheff, 2008) but slightly higher than the value of $11.7/\sqrt{27}$ x *rms* used in the study of Lambacher et al. (2010).

In a second step threshold crossings are combined to action potentials. All threshold crossings that are spatially adjacent at the same time point are merged into a 'cluster'. Next, I consider the spatial overlap of time-consecutive 'clusters'.

Two such clusters are part of the same action potential if they share at least one sensor. All 'clusters' that belong to an action potential are combined and the data point (time stamp and sensor location) with the highest amplitude is chosen as a representative for the action potential.

Finally, action potentials are assigned to the corresponding ganglion cells. Action potentials recorded on one sensor may belong to different cells. I again take advantage of the high spatial sampling and align the centres of gravity of two action potentials in time. For each action potential I consider the extracellular voltages surrounding the centre of gravity. The cross correlation between the neighbourhoods of action potentials i and j is calculated as:

$$c_{ij} = (\sum_k V_{i,k} V_{j,k})/(N_i N_j) \tag{2}$$

with $N_i = \sum_l V_{i,l}^2$ as the normalization factor for action potential i. The index k ranges over all peaks that are common to both action potentials i and j while the index l ranges over all voltages that constitute the action potential. The following analysis separates action potentials that originate from different neurons. For a number of M overlapping action potentials a symmetric matrix of cross correlation values c_{ij} (i,j = 1:M) is obtained. This matrix is rearranged to minimize the c_{ij} differences between adjacent rows. If all action potentials under consideration belong to one neuron I obtain little variation within the correlation matrix. If action potentials from several neurons are compared separate clusters are visible in the crosscorrelation matrix. This matrix is then split and the action potentials within each cluster are assigned to a different neuron. The sorting of action potentials is comparable to the supervised algorithm used in a previous study, although there a different algorithm (k-means clustering) was used (Zeck and Masland, 2007). The spike sorting and splitting is done offline and semi- automated. The final spike trains are tested to obey a refractory period of at least 1 millisecond. No action potentials with interspike intervals shorter 1 ms were assigned to one neuron using the described method. Results were supervised by the experimentator.

2.8 Spike train analysis

Data were analyzed using custom software written in Matlab (Mathworks, Natick,WA). The average firing rate for each spontaneously active RGC was computed as the total number of spikes divided by the length of the recording period. The recording consists of 1-10 second concatenated segments of continuous voltage traces (0.1- 12 kHz sampling frequency). The fundamental spiking frequencies were estimated from the autocorrelation functions.

Cross-correlation (CC) functions were computed for cell pairs after spike trains had been assigned to particular cells. Normalized CCs were calculated using the Matlab routine *xcorr*. This routine calculates the dot product of two <u>normalized vectors</u> representing the RGCs spike trains. The spike trains were binned with either 4 or 0.4 ms time resolution. The correlation coefficient (Pearson's correlation) presented here represents the zeroth lag of the correlation function. It represents the percentage of spikes from one spike train that occurs in the same time bin in the correlated spike train, and therefore represents an estimate of the coupling strength between two RGCs. The length of correlated spike trains ($\sim$ 5 minutes in 4 ms time bins) sets the statistical significance of the correlation coefficient below 0.01.

2.9 Local field potentials and propagation velocity

Extracellular voltage changes characterized by negative deflections ($\sim$20 ms long) followed by slower repolarization ($\sim$ 100 ms), have been reported as a slow-wave component in a recent *rd1* study using multielectrode arrays with large electrode distances (Ye and Goo, 2007; Ryu et al., 2010). Voltage modulations that occur in phase across neighbouring sensors - but not across the whole sensor array (1mm^2) - reflect spatially confined local field potentials. Negative deflections in the extracellular potential are caused by the depletion of positive ions or by the accumulation of negative ions in the extracellular space, and reflect membrane depolarisations of neurons in the ganglion cell layer.

The LFP fundamental frequency was estimated from the power spectral density functions computed from long (10 seconds) calibrated voltage traces. The

fundamental frequency was measured as the first peak power in the range 3–100 Hz.

The calculation of LFP propagation velocity is performed in analogy to the velocity calculation of developmental calcium waves (Blankenship et al., 2009). The method requires accurate definition of the LFP boundary. Therefore, each voltage map (1mm^2) recorded by the sensor array at one time-point was first spatially filtered (Gaussian filter, σ = 10 μm). Time-consecutive voltage maps were averaged within a window of 2 ms. In each such averaged voltage map, we identified those sensor areas that measured voltages smaller than – 100 μV as a 'region of interest (ROI)'. Contiguous regions were considered to be part of one LFP. The next ROI was calculated after a delay of 10 ms. LFP propagation velocity was computed if consecutive ROIs covered at least half of the sensor array (1mm^2) and lasted longer than 50 milliseconds. The border of each ROI represents an isotemporal continuous line of the LFP wavefront. The furthest distance traveled during the last time interval was used as an ending point of the propagation path. Points along the propagation path were selected by finding the shortest distance between the point at time *t (in ms)* and the isotemporal line at time *t-Δt*. Velocity was calculated by averaging the distance between consecutive time points *Δt*. To clarify that the velocity values did not depend on the threshold (-100 μV) or the time steps *Δt* we calculated velocities for a subset of waves using a threshold of -50 μV and time steps between 7 and 15 ms respectively. We obtained qualitative similar results.

2.10 Identification of axonal signals

In rat and mouse retinas, extracellular recorded single axonal action potentials are not detected in the raw data as it is possible in recordings of rabbit RGCs (Zeck et al., 2011.) Somatic action potentials recorded with the MTA chip are typically smaller than 1 mV in mouse and rat retina (see **Fig. 1.11**) and probably hidden in the sensor noise (rms: 70 μV). Therefore a methodology recently described by Petrusca et al. (2007) who identified axons in primate retinas, was adapted.

Therefore the spike triggered average $\overline{v}_{ij}(t_k)$ is defined for any sensor (row: i; column: j) determined by the spiketrain $t_1,...,t_n$ of a RGC soma (located at a specific row i' and column j') as

$$\overline{v}_{ij}(t_k) = \frac{1}{n}\sum_{l=1}^{n} v_{ij}(t_{l+k}), \ \forall i, j, k \tag{3}$$

with:

n : the total number of spikes in the spike train;

t_l : time of occurrence of spike l;

$v_{ij}(t_{l+k})$: voltage at sensor row i, column j and time t_{l+k}.

Note that the above expression is valid for all i, j and k. If all i and j at a given k are evaluated, a two-dimensional voltage map at the temporal offset t_k to the somatic spike is obtained. Negative k values allow to view into the (average) history of the spikes, positive k values into the (average) future which may contain an axonal signal. With a constant propagation velocity and a fixed spatial path, axonal action potentials become visible as the (spatiotemporally) uncorrelated noise is suppressed by the averaging procedure.

I used about 1000 spikes to construct the spike triggered average for a single cell. An example is given in **Fig. 1.9 b & c**. With this approach only axons originating from a cell body within the recording area are detected. Axonal signals from axons of passage are not identified as no temporal reference signal (somatic spike) is available.

2.11 Evaluation of the intra-retinal conduction velocity

Voltage maps of consecutive time frames containing the average axonal activity were exported. In order to calculate the velocity of a single propagating action potential, spatial locations of its biphasic peak were determined by respective extremum values within each time frame. The axon's path was assumed to be linear (intra-retinal axons run nearly parallel) between consecutive time frames. For the entire axon path covering the array, linear pieces were concatenated. We corrected

for temporal gradients introduced by the readout scheme of the chip across different sensor columns (typical value: $(11.5 kHz \cdot 64)^{-1} \approx 1.4 \mu s$ per column). Gradients across different sensor rows can be neglected.

2.12 Statistical Analysis

I could not rigorously test if the distributions of the various parameters (firing rate; correlation coefficients; LFP velocity; maxima of the power spectral density) follow a normal distribution. To test for statistical significance, I therefore compared median values using the Wilcoxon-Mann-Whitney U test. For the firing rate and correlation coefficient I present mean values, as they are not different from the median.

2.13 Visual stimulation

Visual stimuli were presented on a monochrome OLED (organic light emitting diode) microdisplay (eMagin, Bellevue, Washington; 800 x 600 pixels; 60 Hz refresh rate) and designed using Visionworks Software (Vision Research Graphics, Durham, NH).

The display was connected to the photo output of an upright microscope (BXW50; Olympus Optical, Tokyo, Japan) in order to illuminate the back focal plane of a 5x objective (LMPlan Fl; Olympus Optical, Tokyo, Japan).

Stimulus presentation was triggered by the measurement system and temporally related to the timescale of recorded transients with millisecond precision. This was realized by comparing the timing of TTL-pulses of stimulus and measurement onsets respectively. Luminance values were determined at the focus plane of the retina (Optical Meter 1835-C, Newport Spectra-Physics, Darmstadt, Germany).

To characterize the RGC population responsiveness, full field flashes (spot diameter > 1mm at the retina, 400 ms length) were focused onto the retina. In order to selectively stimulate ON-cells I presented a bright spot (66.82 mW/m^2, I_{Stim}) on a dark background (1.38 mW/m^2, I_{BG}) and vice versa for OFF-cells. The stimulus contrast was calculated as the ratio $|I_{Stim} - I_{BG}| / (I_{Stim} + I_{BG})$ (Michelson contrast) and hence is the same (96%) for both protocols.

Spike trains of responding RGCs were convoluted with a Gaussian kernel of 5 ms standard deviation (Bolz et al., 1982) in order to classify cells into ON and OFF cells. To determine the response latency, the delay between stimulus onset and the first spike of the burst response was calculated.

Moving grating stimuli were presented to rat retinas with increasing spatial frequency to asses visual acuity.

Grating cycles had the following dimensions: 1000 µm, 500 µm, 300 µm, 250 µm, 200 µm and 150 µm. Based on the rat eye dimensions (Hughes & Wässle, 1979) this is converted to cycle/degree (c/d) units: 0.05 c/d, 0.1 c/d, 0.2 c/d, 0.22 c/d, 0.3 c/d and 0.38 c/d respectively. The temporal frequency of the grating was held constant at 2 Hz.

The same contrast as for full field flashes was used (96%). The stimulus was presented 2 min for each parameter configuration.

To quantify the grating response, a Fast Fourier Transformation was calculated for the spike trains of all cells for the presented spatial frequencies. The relevant measure of the response was the spectral amplitude at the temporal frequency of the stimulus presented. Only cells that responded to the lowest spatial frequency were taken into account. Spectral peak amplitudes for the presented frequencies were averaged over all cells in the respective group and normalized to the control response (Pu et al., 2006).

In the experiments with constant illumination a light spot of 2 mm diameter was projected onto the retina with intensities between 40 and 80 mW/m^2 .

2.14 Application of pharmacologic agents

In all experiments, stock solutions of the blockers were dissolved in Ames Medium to obtain the concentration indicated in the text. Variable volumes were then constantly washed in the recording chamber for approximately 10 minutes. The solutions were warmed (35-37°C)and bubbled with oxygen as the normal Ames.

Only in the experiments with constant illumination the Ames & Strychnine/Gabazine solution was not constantly washed in, as C57Bl/6 become inactive when higher strychnine concentrations last for longer than 1 minute. As

Strychnine/Gabazine solutions act fast and need long time to be washed out, the warmed and bubbled solution was pipetted into the recording chamber and after 30 sec, the normal perfusion (Ames) was started. When the effects of Strychnine/Gabazine became weaker the procedure was repeated.

This way of pharmacologic administration was tested in *rd1* mice, were no difference in the effect was seen. Chemicals were typically washed in for about 10 minutes.

3. Results

3.1 Characterization of the electrical RGC phenotype in *rd1* mice

The results of this chapter were published in Menzler, J., & Zeck, G. (2011). Network Oscillations in Rod-Degenerated Mouse Retinas. J.Neurosci., 31 (6), 2280-2291.

3.1.1 Retinal ganglion cells in *rd1* retinas exhibit rhythmic activity

I recorded spontaneous activity from two r*d1* mouse strains (C3H and FVB, aged P40-70) and obtained spike trains of ~1400 RGCs in 32 retinas. The majority (85 %) of the recorded cells spiked rhythmic at a fundamental frequency of 9.2 ± 1.8 Hz (mean ± std) with an average firing rate of 26 ± 13 Hz (mean ± std). The average firing rate was significantly higher (p < 0.01) than that of *wt* RGCs of the same age , which spiked at 12 ±6 Hz (n= 456 RGCs, n= 13 retinas, age P 35 – P 60). The frequency of the rhythmic bursting seems to depend on the mouse strain, FVB mice show 7-8 Hz oscillations while C3H mice burst in the range of ~ 10 Hz.

The rhythmic activity is not a transient period during degeneration.

RGCs in older retinas (C3H/HeNCrl, P 160 - P200, n=110 RGCs in 3 retinas) display rhythmic activity with an average fundamental frequency that is not significantly different from the values calculated for the younger retinas (8.8 ± 1.3 Hz, mean ± std, p= 0.22). The percentage of rhythmic RGCs declined slightly in older retinas (75 % of RGCs in P160-P200).

The spontaneous activity of twenty selected RGCs, recorded simultaneously in one retinal portion, is shown in **Fig 3.1 a**. The presented RGCs display a rhythmic bursting activity visible in the autocorrelation function (**Fig 3.1 b**). In contrast, the 20 wt RGCs shown in **Fig. 3.1 c**, display lower firing rates and the autocorrelation (**Fig. 3.1d**) reveals no specific firing pattern.
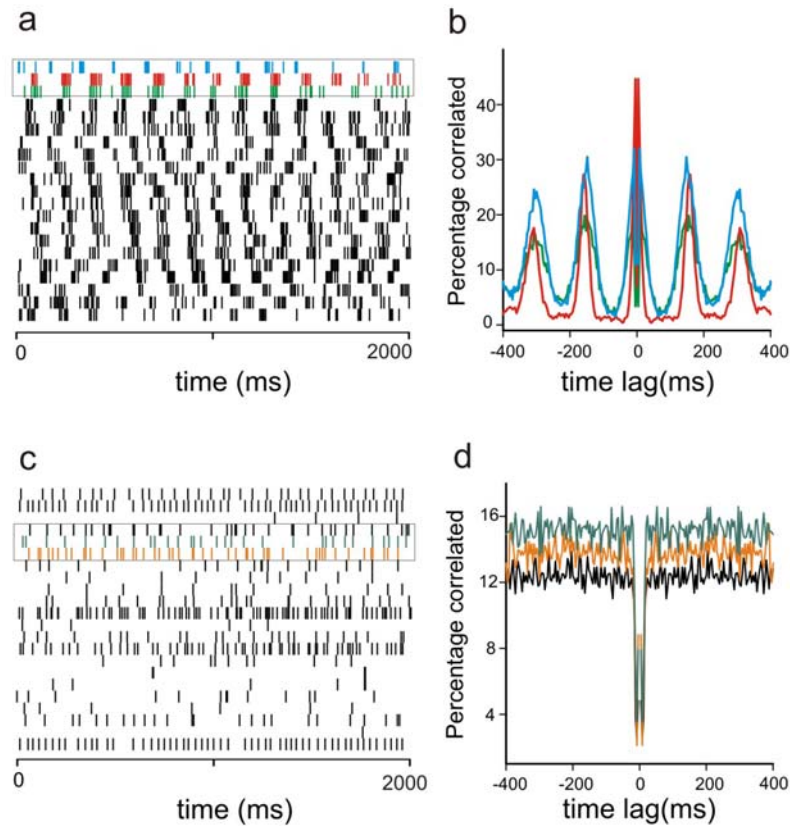
Figure 3.1: The majority of r**etinal ganglion cells (RGCs) in the *rd1* mouse retina exhibit rhythmic spiking**
(a &b) Spike train properties of retinal ganglion cells (RGCs) recorded in a 1 mm² portion of an rd1 retina.
(a) Spiking activity from 20 selected RGCs. Each tick represents the occurrence of one action potential. The three RGC spike trains in the upper row are further evaluated.
(b) Autocorrelation functions of the three selected rd1 RGCs reveal rhythmic activity with an average interval of ∼ 150 milliseconds. The peak at zero time lag is omitted.
(c &d) RGC spike train properties in wt retinas.
(c) Raster plot of spontaneous activity. **(d)** Autocorrelation function of three selected RGCs.
(*adapted from* Menzler & Zeck, 2011)

High-pass filtered (0.1 – 3 kHz) calibrated voltage traces of selected RGCs (Fig**. 3.1 a)** show the firing pattern of cells with a stable rhythm (**Fig. 3.2b).** In each retina some of the RGCs do not burst continuously (**Fig. 3.2c**), but their autocorrelation functions remain rhythmic (not shown). Their firing pattern is still locked to an underlying 7 - 10Hz rhythm.
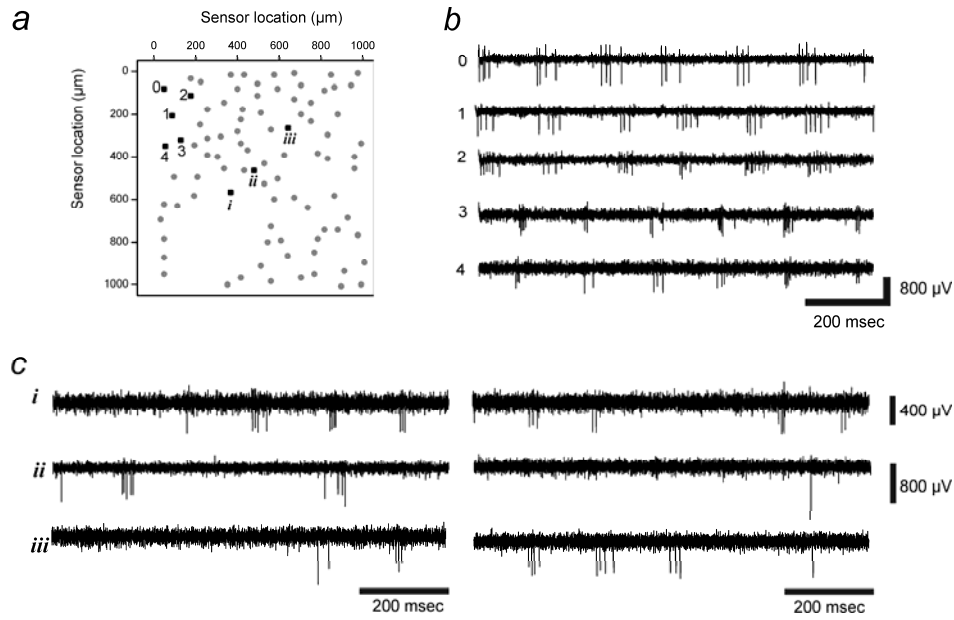
Figure 3.2: Stability of the rhythmic firing pattern in *rd1* RGCs
In **(a)** a schematic sensor array is shown. Grey dots indicate recorded RGCs (of which 20 are shown in **Fig. 3.1a**). For the cells labelled with numbers 0-4 a raw trace of 1 s is shown in **(b)**. These cells displayed a stable rhythmic firing pattern. For the cells labelled i-iii corresponding traces are shown in **(c)**. All three cells exhibited instable rhythmic firing pattern and missed bursts. However the burst of these cells were still locked to the fundamental spiking frequency. (*adapted from* Menzler & Zeck, 2011)

The cross- correlograms (CCs) between pairs of *rd1* RGC spike trains display multiple peaks (**Fig. 3.1 b**) separated by 100 -150 msecs. About 24 % of the CCs showed a peak at zero lag indicating synchronous firing of two cells (**Fig. 3.4 b**).

When cells pairs correlating with zero lag are correlated with smaller time bins (0.4 ms), several 'peaked' CCs displayed two sub-peaks around zero time lag (**Fig 3.3 b).** The two maxima were located on average at -1.4 ± 0.2 ms and 1.3 ± 0.3 ms respectively (n=40 pairs in 3 retinas). These peaks are a strong indicator of reciprocal electrical coupling between RGCs, where the spike in one cell depolarizes the coupled cell above spiking threshold.
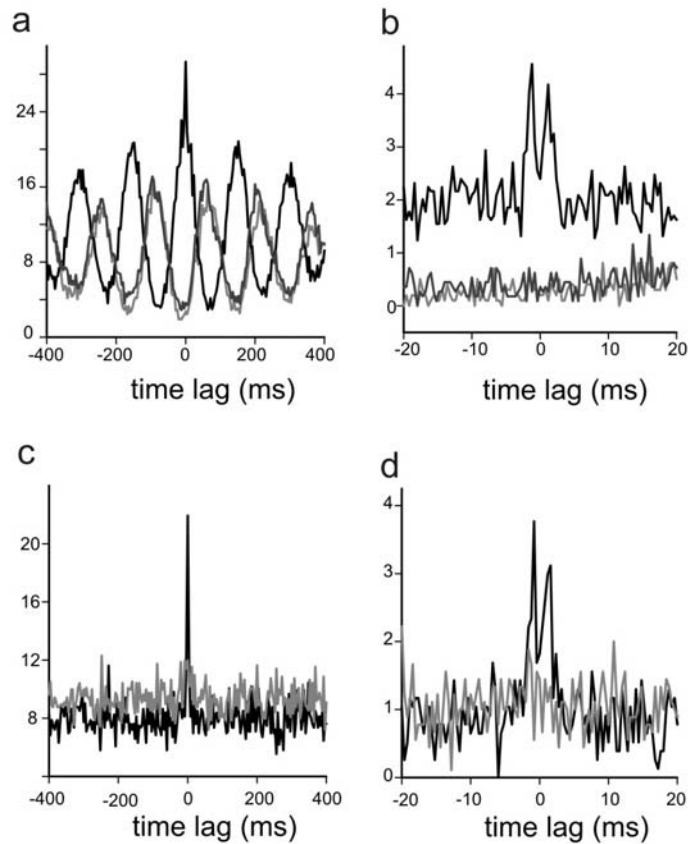
Figure 3.3: Correlated spiking in *rd1* and *wt* RGCs

(a) The spike train cross-correlations (CC) between three selected *rd1* RGCs (**3.1 a**) reveal strong oscillations. For two cell pair the activity is phase-shifted. One RGC pair fires in synchrony revealed by the central peak at zero time lag. Bin size 4 ms.
(b) The same CCs as shown in **(a)**, computed at higher resolution (Bin size 0.4 ms). A double-peak in one CC at zero time lag indicates electrical coupling between the two RGCs.
 (c) Spike train cross correlations between the three selected *wt* RGCs shown in **(3.1 c)**. Synchronous activity is detected in one cell pair. Bin size 4 ms. **(d)** The same CCs shown in **(c)**, computed at higher resolution reveal a double-peak in one CC around origin, similar to the result in the *rd1* retina (panel **b**). Bin size 0.4 ms. (*adapted from* Menzler & Zeck, 2011)

Comparable double-peaked synchronization patterns have been described in electrically coupled RGCs in healthy mammalian retinas (Mastronarde, 1989; Hu and Bloomfield, 2003). The average distance between electrically coupled *rd1* RGCs is 120 ± 30 µm. This indicates that only nearby RGCs are electrically coupled. The average correlation strength of these pairs is: 0.20 ± 0.05 (mean ± std, bin width: 4 ms). The correlation strength does not vary over the distance mentioned above.

In the average 25 % of the CCs between simultaneously recorded *rd1* peak at zero lag, while in *wt mice* rarely 5 % of the CCs have a peak at all. The CCs of two wt cell

pairs are shown in **Fig. 3.3 c**, where one cell pair fires correlated. In CCs calculated from *wt* RGC spike trains also 'peaked' CCs (n=15 in 7 retinas) were detected that display two sub-peaks around zero time lag (**Fig 3.3 d).** The CC maxima were located on average at -1.8 ± 0.4 ms and 1.7 ± 0.3 ms respectively while the spacing between cells was 133 ± 40 μm (range 66 – 224 μm). The average correlation strength of these pairs is: 0.10 ± 0.04 (mean ± std, bin width: 4 ms). The correlation coefficients in *wt* RGCs are statistically different (p<0.001) from those measured for *rd1* RGCs. I conclude that the subpopulation of electrically coupled RGCs in *rd1* and *wt* retinas have similar properties, except for the stronger electrical coupling strength between *rd1* RGCs.

3.1.2   The majority of rhythmic *rd1* RGCs display phase-shifted activity

The majority of spike train CCs (range 60 – 86%, n = 5 retinas) have their most central peak shifted with respect to zero time lag (**Fig.3.3a**). We therefore tested if there was any preferred phase shift between RGC spiking and if the phase shift depends on the RGC separation. As the fundamental RGC spiking frequency differs among retinas (range: 7 -10 Hz), we calculate for each retina an average rhythm. We then normalize each CC time lag to the retina specific rhythm. A time lag of 50 ms between two RGCs spiking at a fundamental frequency of 10 Hz corresponds to a relative shift of *period/2*, whereas the same absolute time shift gives a smaller relative shift for RGCs spiking at 7 Hz. First, the probability to measure a shifted CC peak is close to chance level for any value within one period, with the exception of zero time lag (**Fig.3.4 a,b;** n = 5 retinas).The average probability varies little if either half of the recording session is evaluated (**Fig.3.4 a)**, although for individual CCs a small shift of the central peak is observed (*data not shown*). Second, for all RGCs separated by less than 500 μm the median value of the central CC peaks increases from 8 ms (RGC separation < 50 μm) to 25 ms (RGC separation 500 μm, **Fig. 3.4 c)**. For separation distances larger 500 μm the peak time lags occur at any value with nearly equal probability (**Fig.3.4 d)**. These findings point toward a local driving force of the rhythmic spiking of *rd1* RGCs. In the next paragraph we therefore investigate whether this driving force is caused by independent, 'pacemaker-like' cells, as might be inferred from **Figure 3.4 a, b** or whether spatial interactions (suggested by **Fig 3.4 c, d**) shape the oscillatory behaviour.
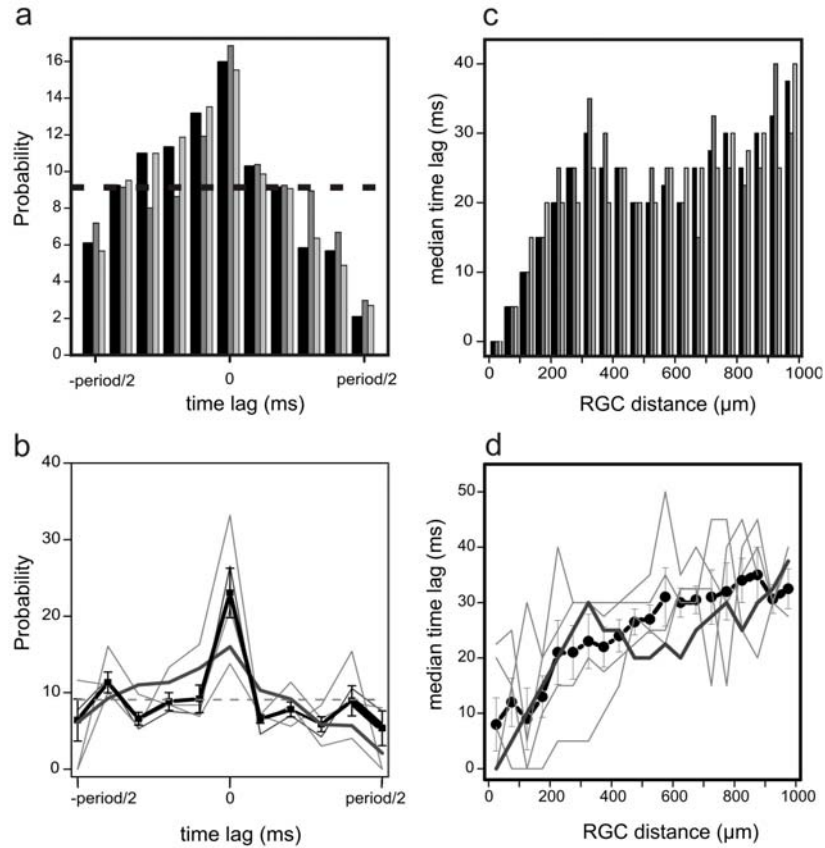
Figure 3.4: Nearby RGCs in *rd1* retinas oscillate with little time lag.

(a) Histogram of the time lags of the central CC peaks of RGC spike trains calculated within one *rd1* retina (two CCs were presented in **Fig 3.1c**). The dashed line marks chance level. Dark gray bars mark the result obtained if the first half of recording is considered, light gray bars the results obtained from the second half of recorded data. Bin size: 10 ms. Each CC time lag is normalized to the average rhythm period.
(b) Average of five CC histograms calculated as in **(a)**. With the exception of zero time lag, there is no preference for any phase shift of the central CC peak. Each gray line represents the result from one retina. Thick gray line represents the data shown in **(a)**. Black symbols mark the mean values for a given time lag. Dashed line represents uniform distribution.
(c) Dependence of the peak CC time lag on the distance between RGCs. The analysis was performed on the same dataset shown in **(a).** Up to separation distance of $\sim$ 300 µm, the median time lag increases with increasing distance. Black bars denote the median values obtained for the whole recording session. Dark gray bars mark the result obtained if the first half of recording is considered, light gray bars the results obtained from the second half of recorded data. No significant changes are measured. Bin size: 50 µm.
(d) Average of five histograms of median time lags calculated as in **(c)**. The same dataset of the five retinas evaluated in **(b)** was used. Thick gray line represents the data shown in **(c).** Black symbols mark the median time lag for a given RGC distance. The tendency of short time lags for RGC separations smaller 500 µm is preserved across retinas. (*adapted from* Menzler & Zeck, 2011)

3.1.3 The rhythmic spiking of rd1 RGCs correlates with local field potential minima

All sensors recording rhythmic *rd1* RGC spiking display a modulation of the extracellular voltage in the low frequency (1-60 Hz) range (**Fig. 3.5 a**). Voltage modulations that occur in phase across nearby sensors reflect spatially confined local field potentials (**Fig. 3.5 b**). Negative deflections in the extracellular potential are caused by the depletion of positive ions or the accumulation of negative ions in the extracellular space, as reported in other neural tissues (Mitzdorf, 1985) . LFPs were never found in *wt* retinas under the same recording conditions. LFPs are initiated at several locations across the *rd1* retina. During the recording time (1 -3 hours) the entire portion of the imaged ganglion cell layer was part of a LFP. Continuous (10sec) readout of the sensors was used for power spectral density (PSD) analysis indicating a fundamental LFP frequency of 7 – 10 Hz (**Table 2**). To investigate whether LFPs are responsible for rhythmic RGC spiking, we correlated the spike trains of individual RGCs with the timing of LFP minima recorded in the vicinity of the ganglion cells. Different temporal filters for action potential (0.1 – 3 kHz) and LFP (0 – 60 Hz) identification, and a distance of 32 μm between the RGC recording sensor and the LFP recording sensor guarantees that RGC spikes do not influence the LFP minima. The cross-correlation of three selected LFP-RGC pairs revealed an oscillatory function peaked around zero lag (**Fig. 3.5 c**). The analysis of 188 LFP-RGC pairings in three retinas reflects that most CC peaks occur in the interval around zero lag. The majority (75 %) of the CC peaks occur at a time lag between -12 and 2 ms (**Fig. 3.5 d**).
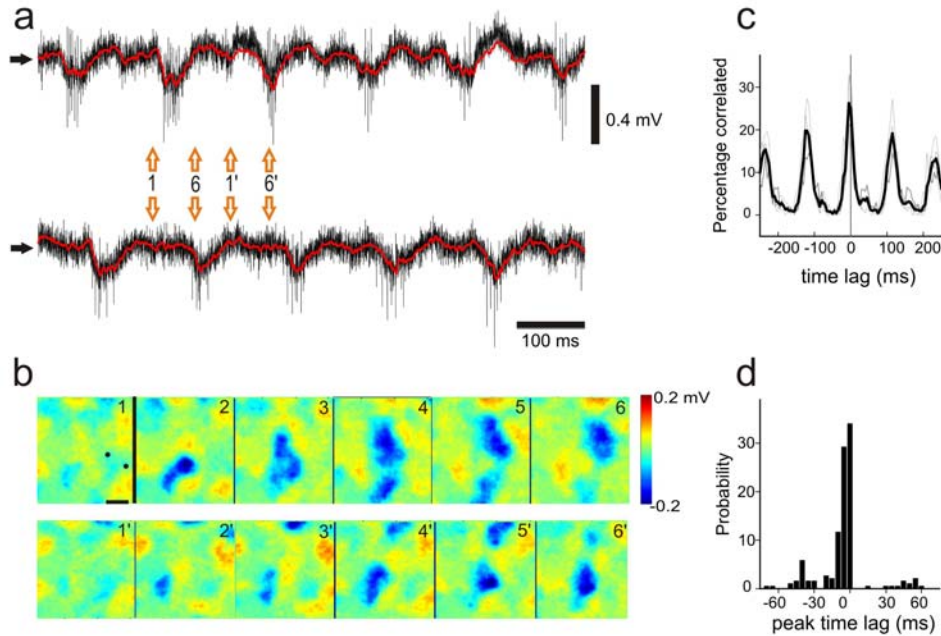
Figure 3.5: RGC spiking and local field potential minima coincide in *rd1* retinas.

(a) Extracellular voltage recordings from two sensor electrodes separated by ~ 300 µm.
The filter settings of 1 Hz – 3 kHz reveal single spikes and a slow oscillatory extracellular potential. The sensor locations are marked in subplot (b1).
Red trace: Low-pass filtered (1-60Hz) signals reveal rhythmic local field potentials (LFPs). The horizontal arrow marks zero extracellular potential. Open green arrows mark the start point and end point of a six frame series of extracellular voltage maps, shown in **(b)**.
(b) Extracellular voltage maps ('electrical images') recorded at a spatial resolution of 8 x 16 µm. Each image represents the average extracellular voltage over 2 ms. Separation between images is 10 ms. Scale bar: 200 µm.
(c) Cross correlation of three spike trains with LFP minima revealing central peaks with minimal time lag (gray). The average of the three traces is shown as a thick black line. LFP minima were evaluated for sensors separated by 32 µm from the RGC recoding sensor.
(d) Distribution of peak CC time lags for RGCs and nearby recorded LFPs in two retinas.
The recordings presented here were from a different *rd1* retina as shown in **Fig 3.1**.
(*adapted from* Menzler & Zeck, 2011)

3.1.4   Propagation of local field potentials

Local field potentials are dynamic: they expand (**Fig.3.7 c**) or propagate across the retinal surface (**Fig.3.5 b & Fig.3.6 a**) but never collapsed. Occasionally we observed the initiation of two LFPs within the imaged piece of retina. Within one retina consecutive wave-like LFPs propagated in the same direction (**Fig.3.5 b**). Because the propagation of LFPs resembled activity patterns seen in immature retinas, we adopted methodology used to assay the speed of developmental waves (Blankenship et al., 2009.). We consider LFPs averaged over 2 milliseconds of electrical activity. In each such averaged voltage map we identified those sensor areas that measured voltages smaller - 100 µV as a 'region of interest (ROI)'. The next ROI was calculated after a fixed delay Δt (**Fig.3.6 b**). The identified ROIs propagated across the retina with a median velocity of 8 mm/sec (**Fig. 3.6 c;** n=292 waves in 5 retinas; for details of velocity calculation see *see* **sect. 2.8**). The propagation of electrical activity could, in principle, be assessed using the RGC spiking. However, because RGCs started a burst (3 – 10 action potentials) every 100 – 150 ms methodology used in extracellular recordings of developing retinas (Demas et al., 2003), that display much longer inter-burst intervals, failed here.

The analysis of RGC spiking and LFP propagation suggests that RGC depolarisations occur through a local mechanism that spreads laterally across the retina. To identify circuitry involved in the generation and propagation of LFPs and concomitant RGC spiking, we applied pharmacological agents that disrupted either RGC spiking and/or LFPs.
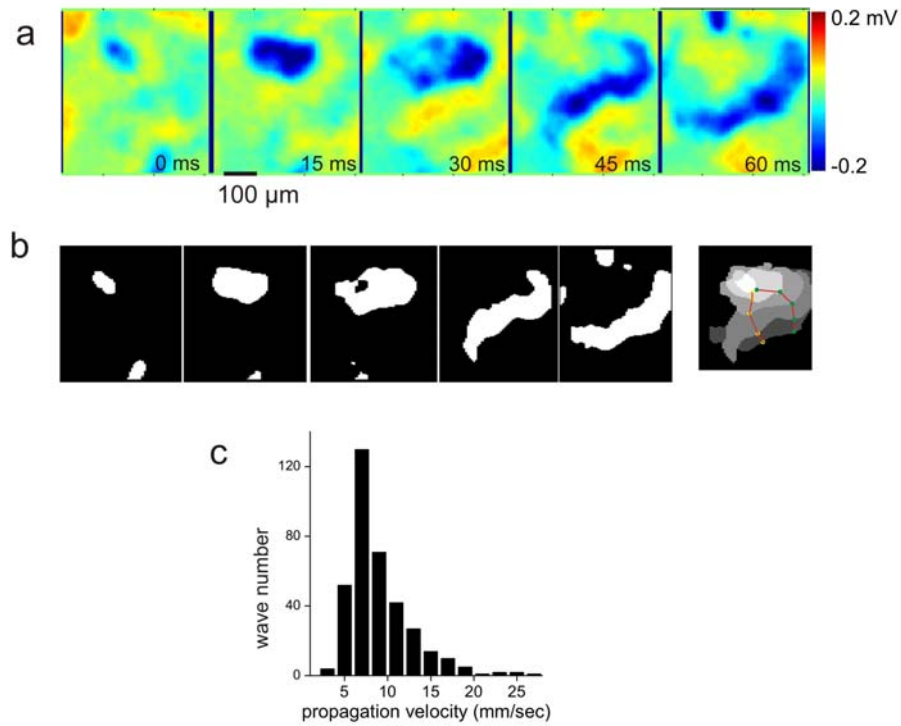
Fig. 3.6: Local field potentials propagate across the retina

(a) Extracellular voltage maps recorded at time intervals of 15 msec. Each image represents the average activity over 2 ms. The activity was recorded in the same retina shown in **Fig. 3b,** but recorded at a later time.
(b) For the estimation of the wave-like LFP propagation velocities (*Methods*), we identified region of interest with voltages more negative than - 100 μV. Each binary image represents the region of interest calculated for each voltage map shown in (**a).**
Right frame: Spatial extension of LFP propagation. Each grayscale represents the region of interest at one of the five time points. Two arbitrary points are shown that were selected to trace back the propagation paths (red).
(c) Histogram of LFP propagation velocities. A total of 292 LFPs within 5 retinas were evaluated. Bin size is 2.5 mm/sec. Median value: 8 mm/sec.
Local field potentials persist when voltage gated sodium channels or inhibitory receptors are blocked. (*adapted from* Menzler & Zeck, 2011)

We first excluded the hypothesis that spontaneous sodium-spikes are responsible for the extracellular LFPs by adding the sodium channel blocker TTX (0.2 μM) to the perfusion solution. Under these conditions we measured LFPs but no RGC spikes (**Fig. 3.7 a**). The sodium channel blocker abolished the RGC firing in all but seven RGCs from a total of 138 identified cells in three retinas. The RGC firing rate dropped to 0.3 Hz (n= 7 RGCs in 3 retinas).
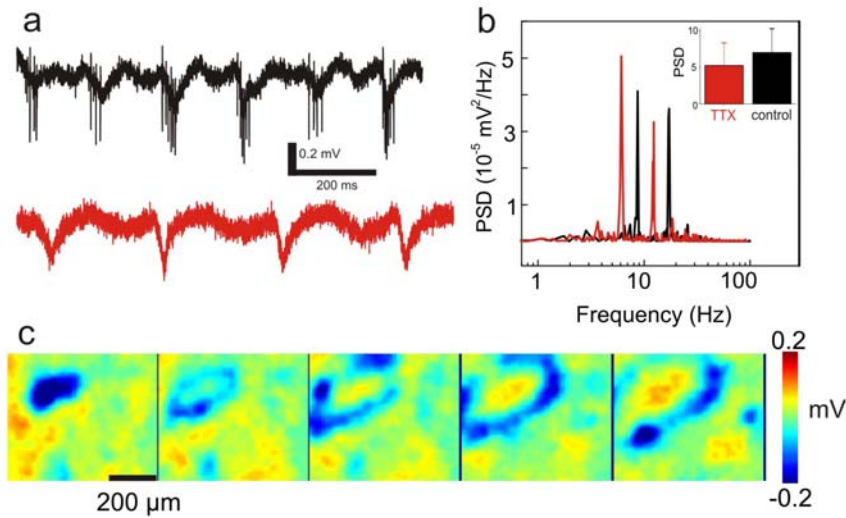
Figure 3.7: Application of the sodium channel blocker TTX abolishes RGC spikes but does not inhibit the initiation and propagation of LFPs.

(a) Extracellular voltage recording on one sensor, showing the RGC spikes and LFPs under control conditions (top trace) and after the application of 0.2 µM TTX (red trace, bottom).
(b) Power spectral density of the traces shown in **(a)** demonstrate that TTX reduces the fundamental LFP frequency. The amplitude of the LFPs, reflected in the power spectral density (PSD), does not change significantly after the application of TTX.
Inset: Average peak power measured on 30 sensors before (black) and after (red) the application of TTX.
(c) Representative electrical images of TTX treated *rd1* retina indicating the LFP expansion. Each frame represents the electrical activity averaged over 2 msec. The time interval between frames is 15 msec. The traces shown in **(a)** were selected from a sensor in the center of the array. (*adapted from* Menzler & Zeck, 2011)

The LFP amplitude measured as the peak of the voltage power spectrum (**Fig.3.7 b)** did not change after application of TTX. We quantified LFP amplitudes on twenty sensors that recorded from the same retina before and after the application of TTX.

The average of the maximum power spectral densities was not different ($p=0.1$) in the two conditions (inset, **Fig. 3.7 b**). Similarly, no visible changes occur in the overall LFP shape (**Fig.3.7 c).** However, the LFP propagation velocity (**Table 2)** decreased to 6.6 ± 2.6 mm/sec (mean ± std, n= 55 waves, statistical significance $p<0.05$)**.** The LFP fundamental frequency decreased from an average of 9 Hz to 6.2 Hz calculated on 16 sensors in the 3 retinas (one trace shown in **Fig 3.7 a**). After washout the rhythmic sodium spikes appeared again in all three retinas tested.

This experiment proves that although sodium-channels shape certain LFP properties, the RGC action potentials do not contribute to LFPs. Thus neurotransmitters acting on nonspecific ion channels may be responsible for the LFP generation.

In a second experiment we investigated the contribution of inhibitory circuits on the generation of LFPs and rhythmic RGC activity. In the *rd1* retina the two inhibitory cell classes are preserved to a very different degree – horizontal cells retract axonal and dendritic processes whereas amacrine cells appear morphologically well preserved (Strettoi and Pignatelli, 2000; Park et al., 2001; Strettoi et al., 2002). Amacrine cells inhibit synaptically connected bipolar cells or RGCs by the release of either GABA or glycine (Wässle, 2004). Horizontal cells modulate photoreceptor output through feedback mechanisms that are still debated (Wässle, 2004).

The application of the combination of glycinergic receptor blocker Strychnine (20 µM) and GABA$_A$ receptor blocker gabazine (40 µM) had the following effects on RGC spiking and LFPs. The average firing rate (**Table 2**) of RGCs cells did not change significantly (p=0.09) in the presence of inhibitory receptor blockers. Blocking inhibitory receptors led to the synchronization of more RGCs (**Fig. 3.8 a,b,c)**. The central peak in the spike CCs occurred with a time lag of less than 5 ms in 43% of the CCs (average over RGCs in 5 retinas) as compared to 23% in untreated retinas (**Fig. 3.4 b**). Within each retina the probability of synchronous RGC activity increased on average two-fold. RGC spike trains and LFP minima correlated with low time lag in the presence of inhibitory receptor blockers, as was observed for the unperturbed state (compare **Fig. 3.8 d, e** and **Fig. 3.5 c, d**). The spatial extent and extracellular amplitude of LFP increased after disinhibition of the retina (**Fig. 3.8 f**). However, we never measured simultaneous low-frequency oscillations covering the whole sensor array (1mm^2) – both, in disinhibited and also in unperturbed *rd1* retinas.The fundamental RGC spiking frequency (**Table 2**), the LFP frequency and the LFP conduction velocities decreased compared to the unperturbed state significantly (6 ± 2 mm/sec, mean ± std, n= 110 waves, p<0.05). The application of each inhibitory blocker alone revealed that strychnine (2 µM, n=2 retinas) had a stronger effect on the LFPs than gabazine (40 µM, n=2 retinas) (**Fig. 3.8 a, d**).
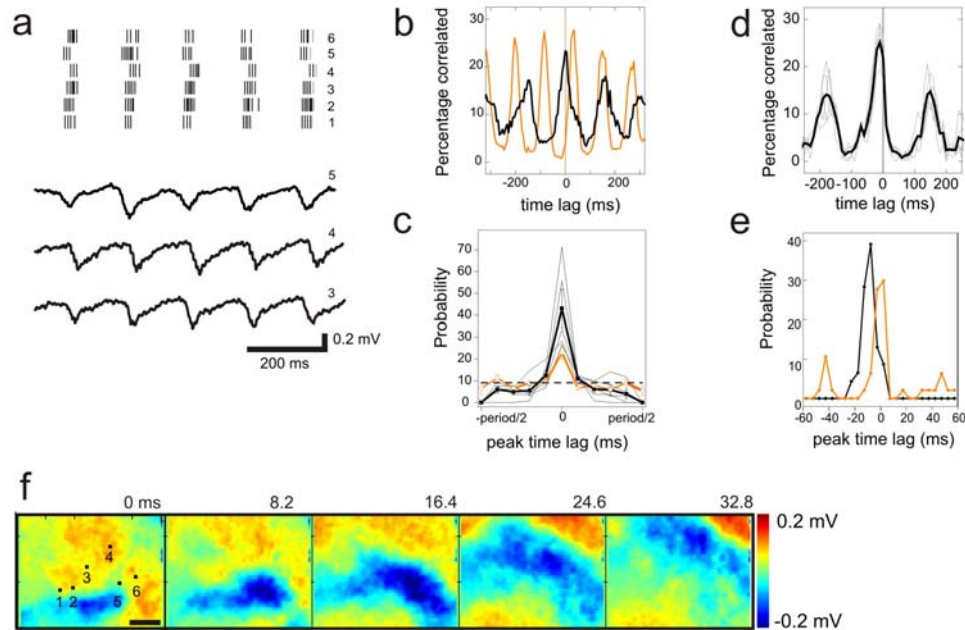
Figure 3.8: Inhibition of glycinergic and GABAergic receptors increases the LFPs and the synchronization among *rd1* RGCs.

(a) *Upper traces:* Spike trains from six RGCs recorded after the application of inhibitory receptor blockers. Each tick marks the occurrence of one spike. The sensor locations are marked in subplot **(f).**
Lower traces: LFPs measured near the spike recording sensors (band-pass of 1 -60 Hz) at three positions (indicated by numbers) on the array.
(b) An example spike-train cross-correlogram (CC) before (orange) and after the application of inhibitory receptor blockers (black trace). The CC peak shifts to zero lag when inhibitory receptors are blocked. The CCs were calculated for the spike trains of cell 3 and 4.
(c) Average probability distribution of minimum time lag of the central CC peak under control conditions (orange, see **Fig 14b**), and with inhibitory receptors blocked (black). The distributions are calculated for the same five retinas (gray) that were evaluated in the untreated retinas (**Fig 14b**). The uniform distribution is shown as a dashed line.
(d) CC calculated between LFP minima and RGC spike trains for the three LFPs and RGCs shown in (a).
(e) Distribution of peak time lags for CCs calculated between RGC spike trains and nearby LFPs before (orange) and after (black) the application of glycinergic and GABAergic receptor blockers. The probability distribution was calculated for RGC-LFP pairs in one retina.
(f) Propagation of the LFPs in the presence of inhibitory receptor blockers. Each frame shows the electrical image averaged over 2 msec (see Methods). Scale bar: 200 μm.
(*adapted from* Menzler & Zeck, 2011)

These results indicate that although inhibitory neurons shape the physical LFP properties, they do not contribute to their generation. The results suggest that in the unperturbed *rd1* retinas, glycinergic and GABAergic inhibition prevents the recruitment of additional excitatory neurons that depolarize the RGCs. The average

LFP amplitude - measured as the peak of the voltage power spectrum – increased significantly (p < 0.001) when glycinergic receptors were blocked (**Fig. 3.9 d**). The LFP amplitude did not increase significantly when only GABA$_A$ receptors were blocked (**Fig. 3.9 a**; p=0.07). Strychnine reduced the fundamental LFP frequency to a larger extends than gabazine (**Fig. 3.9 c, f**). Both substances increased the proportion of positive correlations at zero lag (**Fig. 3.8 b, e**)
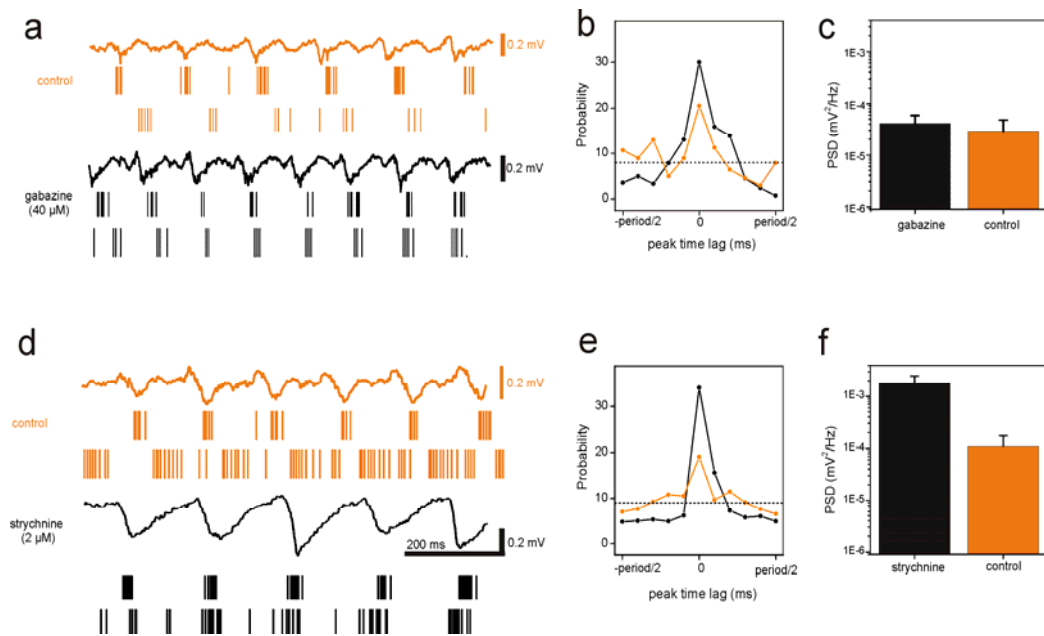
Figure 3.9: Effect of either SR 95531 or strychnine on RGC spiking

(a) Application of the GABA receptor blocker Gabazine alone did not alter the LFP or spiking frequency but induced an increase in synchronicity **(b)**. The amplitude of the LFP was not affected **(c)**. Strychnine altered the fundamental frequency of spiking and the LFP to ∼ 5 Hz **(d)** and increased synchronicity **(e)**. Also the LFP amplitude was increased **(f)**. (*adapted from* Menzler & Zeck, 2011)

3.1.5   Local field potentials require glutamatergic input to RGCs

The excitatory neurotransmitter glutamate is used at several types of synapses in the retina: in the outer retina at the photoreceptor-bipolar cell synapse and in the inner retina at the synapses between bipolar cells, amacrine cells and ganglion cells (Thoreson and Witkovsky, 1999; Wässle, 2004). In the retina glutamate is sensed by ionotrophic (AMPA/kainate and NMDA) receptors and by

metabotrophic receptors. We therefore checked if glutamate induced transmembrane currents are responsible for rhythmic RGC spiking. The application of a ionotrophic glutamate receptor (*iGluR*) blocker cocktail (100 µM DNQX/ 20 µM AP7) led to the disappearance of LFPs (compare **Fig. 3.10 a** and **c**, n = 4 retinas). This change was accompanied by a significant decrease of the RGC firing rate (**Table 2**) and the disappearance of rhythmic spike trains. After the washout of the receptor blockers, the majority of RGCs (80 % in the considered RGC population) recovered their rhythmic activity.
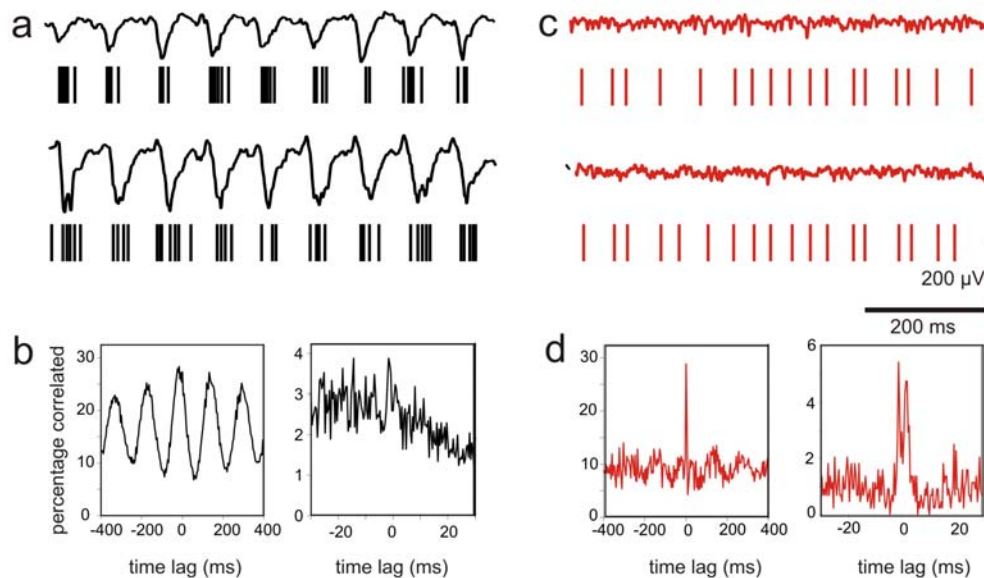
Figure 3.10: Inhibition of ionotrophic glutamate receptors abolishes LFPs and the rhythmic RGC spiking.
(a) Recording of two rhythmic RGCs and low-frequency extracellular voltage changes (band-pass of 1-60 Hz) in the untreated *rd1* retina. The RGC spikes (ticks in second and third row) occur at the minimum of the extracellular voltages recorded on nearby sensors (first and forth row respectively). The RGCs are part of the recording shown in **Fig 12a-d**.
(b) Crosscorrelation (CC) of the two *rd1* RGC spike trains (shown in *a*) reveal the rhythmic activity centered near zero time lag. *Left panel*: CC calculated with a bin width of 4 ms. *Right panel*: CC calculated with a bin width of 0.4 ms
(c) The LFPs and RGC spike trains at the same positions as shown in **(a)** after the application of ionotrophic glutamate receptor blockers (DNQX and AP-7). The low-frequency voltage modulation disappears. The RGC spiking is not rhythmic any more and occurs at a lower rate.
(d) CC of the RGC spike trains shown in **(c)** reveal synchronous activity centered at zero time lag. *Left Panel*: CC calculated with a bin width of 4 ms. *Right panel*: CC calculated with a bin width of 0.4 ms reveals a double-peaked CC characteristic of electrical coupling.
(*adapted from* Menzler & Zeck, 2011)

Why do *rd1* RGCs continue to spike after inhibition of their major presynaptic input? The retinas treated with the *iGluR* blocker cocktail revealed electrically coupled RGCs that are not seen in the unperturbed *rd1* retina. The strong presynaptic input common to neighboring RGCs may obscure the electrical coupling in *rd1* retinas (**Fig. 3.10 b).** Inhibition of the glutamatergic input reveals a sharp peak in the CC at zero time lag (**Fig- 3.10 d),** whereas in the untreated retina the same CC displayed a broad peak (**Fig. 3.10 b**). When computed at high resolution, the peaked CC displayed two sub-peaks around zero lag similar to those seen in unperturbed *rd1* and *wt* retinas (**Fig 3.10 d** and **Fig. 3.3 d).** The maxima for this pair and those of 39 others in 3 retinas were located on average at -1.5 ± 0.3 ms and 1.4 ± 0.3 ms respectively. The average distance between electrically coupled *rd1* RGCs in the presence of *iGluR* blockers is 128 ± 38 μm. The average strength of 0.22 ± 0.06 (bin size 4 ms) is similar to the strength without *iGluR* blockers (p=0.26).

	Spontaneous firing rate (Hz, mean ±std)	Fundamental spiking frequency (Hz, mean ± std)	LFP velocity (mm/sec)
Control wt retina	17 ± 10	-	-
Untreated *rd1* retina	26 ± 13	9.2 ± 1.8	8
TTX treated *rd1*	0.2	5 *	6.6
DNQX treated *rd1*	15.5 ± 4	-	0
Strychnine/ Gabazine treated *rd1*	22 ± 10	6.7 ± 0.8	6
MFA	0.6	0	0
CBX	7 ± 3	0	0

TABLE 2: Properties of retinal ganglion cells and local field potentials in *rd1* retinas.

These results indicate that *rd1* RGCs exhibit non-rhythmic spiking in the presence of *iGluR* blockers that may be attributed to stronger electrical coupling between nearby RGCs (and possibly retinal interneurons) as compared to *wt* RGCs (coupling strength: 0.01).

The application of AMPA/kainate receptor blockers alone (DNQX) had qualitatively similar results as those reported above. In contrast, the application of the NMDA receptor blocker AP-7 (100 μM) alone did not lead to any significant changes in either RGC spiking or LFP properties (n = 2 retinas), indicating that AMPA/kainate receptors are sufficient to mediate the oscillatory behavior. Metabotrophic glutamate receptors of type 6 (mGluR6) are expressed in the *wt* retina at the sign-inverting synapse between photoreceptors and ON bipolar cells (Wässle, 2004). Immunhistochemical evidence suggest a reduced expression of this receptor in *rd1* retinas (Chua et al., 2009) whereas a recent functional study using resensitized cones in *rd1* retinas proves that the ON pathway is still functional (Busskamp et al.). The mGluR6 receptor antagonist AP-4 (50 – 100 μM) had no effect on either the spontaneous RGC activity (n = 2 retinas) or on LFPs (*data not shown*). In summary, this set of experiments indicates that AMPA/kainate receptors on the RGCs elicit membrane currents that are reflected in our recordings as LFPs. In the following a possible mechanism mediating the LFP propagation will be investigated.

3.1.6 Gap junctional coupling is required for the propagation of local field potentials

The median LFP propagation speed of ~ 8 mm/sec is higher than the activity propagation measured for developmental retinal waves. Given that the fastest (stage I) developmental retinal waves are inhibited by gap junction blockers (Syed et al., 2004) we tested if LFP propagation measured here also relies on gap junction coupling. We investigated the effect of two gap junction blockers – carbenoxolone (CBX) and meclofenamic acid (MFA) - on the RGC spiking activity and the occurrence of LFPs. Application of CBX (n = 3 *rd1* retinas) at a concentration of 100 μM for 10minutes abolished the LFPs and the rhythmic RGC spiking in *rd1* retinas (**Fig. 3.11 a**).In the presence of CBX, 50% of the ganglion cells (82 out of 162) maintained an average firing rate of 7 Hz, however the spiking was no longer rhythmic. Washout of CBX (20 -30 minutes) restored the LFPs and the rhythmic RGC spiking activity (**Fig.3.11 a,** right panel**).** However, not all RGCs recorded prior to CBX application were identified after the wash-out. We therefore repeated experiments using the new gap-junction blocker MFA **(**100 μM, Veruki and Hartveit, 2009). The application of MFA (n = 3 *rd1* retinas) minutes completely abolished the LFPs and the RGC spiking in *rd1* retinas within 3 minutes (**Fig.3.11 b**, second panel). Washout of MFA (~ 15 minutes) restored the LFPs and the rhythmic RGC spiking activity (**Fig. 3.11 b).** All RGCs recorded before the application of MFA were again identified after the wash-out of MFA. The percentages of rhythmic RGCs before and after the wash-out of the two gap-junction blockers are summarized in **Fig 3.10 c**. To test if RGCs are capable of spiking in the presence of MFA, we added glutamate (300 μM, n=2 *rd1* retinas) to the perfusion solution. After the application of glutamate, a large number of RGCs (60 out of 90) started to elicit action potentials at an average firing rate of 5 Hz. However, bath-applied glutamate did not restore LFPs and did not elicit rhythmic RGC spiking in the presence of MFA (**Fig. 3.11 b**, third panel).
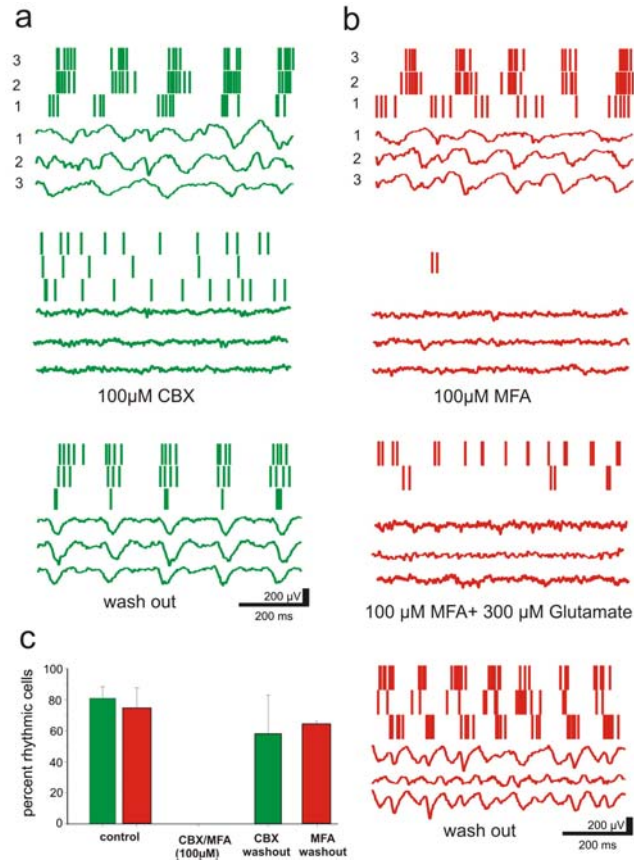
Figure 3.11: Application of gap junction blockers abolishes LFPs and the rhythmic RGC spiking.
 (a) Effect of the gap-junction blocker Carbenoxolone (CBX) on RGC spiking and LFPs.
First panel: Raster plot of three rhythmic *rd1* RGCs and the LFPs measured 32 μm from the soma recordings. Numbers on the left indicate the correspondence between RGCs and LFPs.
Second panel: The application of 100 μM CBX reduced the firing rate in the RGCs, abolished rhythmic spiking and the LFP.
Third panel: wash out of CBX restored rhythmic spiking and the LFP
(b) The gap-junction blocker MFA has similar effects as CBX.
First panel: Control recording of three *rd1* RGCs and nearby LFPs.
Second panel: The application of 100 μM MFA reduced the firing rate in the RGCs, abolished rhythmic spiking and the LFP.
Third panel: Application of glutamate (300 μM) in the presence of MFA (100 μM) recovered non-rhythmic spiking in *rd1* RGCs but not the LFPs.
Fourth panel: Rhythmic RGC spiking and LFPs reappear after the washout of the MFA and glutamate.
(c) In the presence of either CBX or MFA (gray bar) the percentage of rhythmic cells dropped from ~80 % to zero but recovered after wash-out of the drug. After washout of CBX (n=3 retinas) 60 % of RGCs were rhythmic again. After washout of MFA (n = 4 retinas) 64% of the RGCs were rhythmic again. (*adapted from* Menzler & Zeck, 2011)

The spike train autocorrelograms and pairwise CCs did not display any peaks (*data not shown*), indicating that RGCs spike independent. The application of CBX or MFA

(both at 100µM) to *wt* retinas did not change the spontaneous RGC firing rate. We conclude that glutamate release in the presence of functional electrical synapses is required for the aberrant LFPs and concomitant rhythmic RGC spiking. The application of gap-junction blockers carbenoxolone or meclofenamic acid for 10 minutes had no effect on spontaneous activity in *wt* mice (**Fig. 3.12**).
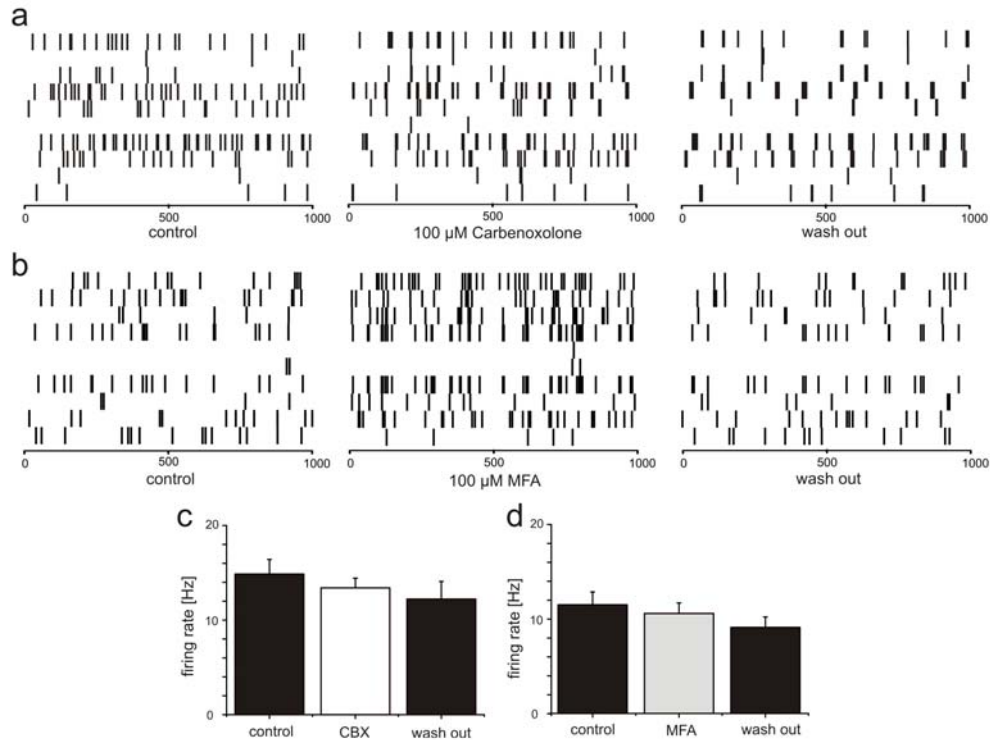
Figure 3.12: Effect of gap junction blocker carbenoxolone and meclofenamic acid on spontaneous activity of *wt* mouse RGCs
In darkness *wt* RGCs spike at a rate of 12-14 Hz **(a &b,** first panel**)**. Perfusion with 100 µM gap junction blocker Carbenoxolone does not change the average firing rate **(a**, middle panel**)**. After wash out , firing rate is similar to control **(a**, right panel**)**. The effect of 100 µM MFA is similar **(b)**, whether during perfusion **(b**, middle panel**)** nor after wash out **(b,** right panel**)** a difference is observed.
The bar plots in **(g)** and **(h)** summarize the effect of both blockers on spontaneous activity. Sample size was n = 82 (2 retinas) for Carbenoxolone and n = 83 cells (2 retinas) for MFA.

3.2 Induction of the rd1 phenotype in healthy mice: the role of the dark current and synaptic inhibition

The results presented in the following section are used in a manuscript "Bleaching of photoreceptors in C57BL/6 retinas induces rhythmic activity that resembles the rd1 phenotype" by Menzler & Zeck. Preparing to submission.

The pharmacological and statistical analysis of *rd1* RGCs suggests that the inhibition in *rd1* retinas is reduced. The blockage of GABAergic and glycinergic synapses located at bipolar-, amacrine- and retinal ganglion cells in *rd1* did not abolish or reduce the rhythmic spiking or the LFP (**Fig. 3.9 a & d**). Reduced inhibition is known to facilitate rhythmic activity in the motor cortex (Castro-Alamancos et al., 2007) and in the hippocampus (Traub et al., 2003).

It is shown in the *rd1* recordings that the rhythmic hyperactivity is generated presynaptic. The only cell type known to excite cells via glutamate release are bipolar cells. The findings in *rd1* here suggests, that bipolar cells start increased glutamate release upon photoreceptor loss and are synchronized via AII amacrine cells (Menzler&Zeck, 2011; Borowska et al., 2011).

In the normal retina, ON- and OFF-bipolar cells receive constant glutamate release in darkness from photoreceptors (see **Introduction).** Bleaching of photoreceptors, i.e. the constant illumination of the photoreceptors, activates the PDE and closes the cGMP gated cation channels in the retina. Bleaching attenuates photoreceptor activity for long intervals even when the actual bleaching is stopped (Fain et al., 2001).

Bleaching mimics the loss of photoreceptors *in nuce*. Decrease of the dark current signals the presence of light to all ON-Bipolar cells. As all RBCs and half of the CBC are of ON polarity, the majority of bipolar cells should increase their glutamate release upon photoreceptor bleaching (Gosh et al., 2003)

In the following I will investigate the effect of bleaching on C57Bl/6 spontaneous activity and the role of inhibitory synaptic signaling.

Multi-transistor-arrays or Multi-electrode-arrays record simultaneously signals from large cell populations. In contrast to patch clamp experiments, it is not possible to determine the cell type by intracellular dye load

In addition to ganglion cells those displaced amacrine cells that generate action potentials will be recorded by the extracellular array (Heflin & Cook, 2007) and

afterwards assigned to an RGC. Amacrine cells display ON- and OFF-responses and therefore the cell class cannot be determined by light response.

We therefore tried to determine RGCs visualizing its axon, using a Spike triggered Average (STA) method from Petrusca et al., 2009 (*see* **sect. 2.10)**.

RGCs have only one axon and all RGC axons run nearly parallel toward the optic disc. Other cell types, e.g. displaced amacrine cells have no axons or posses axonal trees of which axonal action potential do not propagate to the optic nerve but somewhere into the Inner plexiform layer (Majumdar et al. 2009).
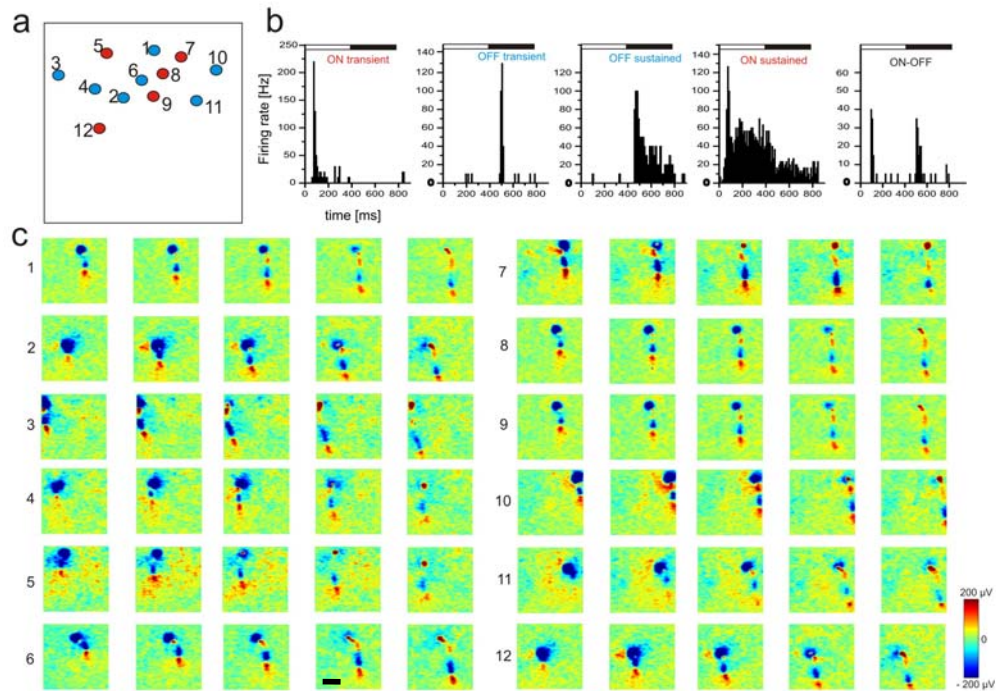
Figure 3.13: Recorded cells were identified as RGCs upon their axon
In **(a)** the location of 12 cells on the array is indicated. Cells were only recorded in the upper half of the array. All cells were either of ON (red) or OFF-type (blue). Five types of light responses were identified in mouse using PSTHs **(b)**. In **(c 1-12)** the propagation of an axonal action potential for the respective cells in **(a)** is shown. For each cell 5 electric images represent the average transistor signal during the first 0.4 ms after a somatic spike. Between two images is a temporal difference of 0.08 ms (at 12 kHz sampling frequency). These cells are also shown in **Fig. 4**. Black bar indicates 200 μm. Voltage values are color coded.

In each sample we identified cells with axons and analyzed this subset of cells separately to detect differences between the complete sample and this sample of 'identified RGCs' . In **Fig. 3.13 a,** a schematic sensor array is shown with RGCs of which an axon was found. The propagation of axonal action potentials from the respective cells are shown in **Fig. 3.13 c**. The propagation direction of all axons found, was coherent.

We further identified 5 types of light responses in the RGC sample (**Fig. 3.13 b**) using peri stimulus time histograms (PSTHs). While cells of either ON- and OFF-type were frequently found, ON-OFF cells were rare.

3.2.1 Constant illumination leads to spontaneous oscillatory activity in C56BL6 RGCs

Spontaneous activity from four C57/Bl6 mouse retinas was recorded for up to three hours after the retina adhered to the MTA chip. For the first forty minutes the retinal activity was recorded in darkness, then light responses were measured for about 20 minutes and afterwards the retina constantly illuminated at intensities of 40 to 80 mW/mm^2, for up to 2 hours**.**

In **Fig. 3.14 a,** the typical maintained activity of C57Bl6 RGCs within one retina recorded in darkness is illustrated.

The average maintained activity in darkness of this sample was with 13 Hz ± 1.3 Hz (n = 139 cells in 3 retinas, mean ± SEM) not different from previously recorded maintained activity in C57Bl6 retinas (n = 430; p = 0.4).

Constant illumination of the retina increases the average spontaneous firing rate (**Fig. 3.14 b**) significantly to 38 Hz ± 3.6 (mean ± SEM; p < 0.01). This induced hyperactivity and concerned cells in both major cell types recorded (ON and OFF RGCs). The ON cell subpopulation spiked with 36 Hz ± 4.8 (n=86) and OFF cells with 40 Hz ± 4.7 (n=43) when exposed to bright light . Both cell types increased their average firing rates.

After a long interval (> 2 hr) of constant illumination, rhythmic spiking was observed in about 50% (**Fig. 3.14 c**, n = 65 cells) of the RGCs. The Autocorrelations of spike trains clearly reveal multiple peaks and thus a rhythmic firing of ~ 5 Hz. The average fundamental frequency calculated for 65 rhythmic cells was 5.1 ± 1 Hz (**Fig. 3.14 h**). ON and OFF RGCs were differently affected by this shift of the activity

pattern: 32 % of ON and 69 % of OFF ganglion cells in three retinas displayed rhythmic bursting. RGCs that did not initiate rhythmic spiking increased the maintained firing rate upon illumination.

A feature of *rd1* RGC spiking is the synchronous rhythmicity measured in many but not all cells (Menzler & Zeck 2011). We cross correlated spike trains of ganglion cells recorded in darkness, during the first half hour of illumination and after rhythmic activity appeared. The cross correlogram (CCs) of two cells shown in the raster plots (**Fig. 3.14a-b**) are illustrated for the different conditions in **Fig. 3.14 d**.
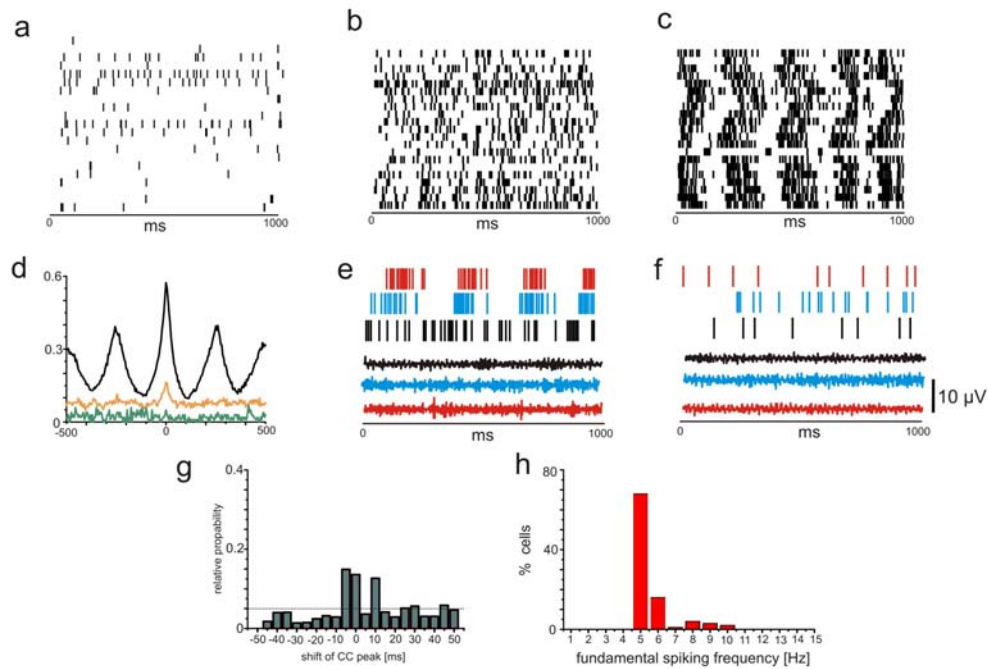
Figure 3.14: Long exposure of the retina to white light induces oscillatory spiking in many retinal ganglion cells
The raster plots show spontaneous activity of C57BL/6 RGCs in darkness **(a),** after 30 min of illumination **(b)** and after 2 hrs of illumination **(c).**
(d) Correlating two cells from **(a)** revealed no positive correlation during darkness (green line), but increasing correlation strength at the beginning of the light stimulation (orange line). Start of rhythmic spiking after 2 hrs caused a strong correlation (black line).
In **(e)** two rhythmic and one not rhythmic cell are shown with respective low-pass filtered voltage traces.
(f) Application of 50 µM DNQX abolishes rhythmic spiking and decreases the firing rate in all three cells.
(g) Phase distribution of CCs between RGCs during rhythmic activity. Most cells have a CC maximum shifted from zero.
(h) Distribution of fundamental frequencies among rhythmic cells. The rhythmic cells showed an average fundamental frequency of 5.1 ±1 Hz (Mean ± SEM)

There was no correlated activity between these two OFF cell, which were 140 μm apart, cells in darkness (**Fig. 3.14 d**; green line). In spike trains recorded during initial illumination about 10% of all cells displayed positive correlations, like the example in **Fig. 3.14 d** (yellow line). When the RGCs started rhythmic firing, positive cross correlations were found between 58 % of the cells, similar to those in **Fig. 3.14 d** (black line).

To test whether these CCs indicate rhythmic excitatory input, the iGluR antagonist DNQX was added to the perfusion.

As illustrated in **Fig. 3.14 f** the block of glutamatergic input stopped the rhythmic activity (**Fig. 3.14 e**) and decreased the firing rate from averagely 30 ± 4 Hz to 15 ± 1 Hz in all RGCs (n = 14 cells). This firing rate is similar to baseline activity in darkness.

No local field potentials were detected under these conditions (**Fig. 3.14 e & f,** low pass filtered voltage traces).

The majority of CCs (90%) was phase-shifted to other ganglion cells. Cells spiking out of phase showed a CC maximum shifted from zero (**Fig. 3.14 g**). The majority of cells in C57Bl/6 retinas seem to receive rhythmic but not synchronous input during constant illumination. In *rd1* retinas, the distribution of phase shifts had a peak at zero. The increased firing rates and the effect of glutamate antagonists point toward enhanced excitatory input.

In this sample we identified 27 cells with axon, 14 were OFF-cells and 10 ON-cells. They had an average firing rate of 8 ± 1 Hz in darkness and the firing rate increased upon illumination to 24 ± 1 Hz. Of these cells 24 initiated rhythmic 5 Hz oscillations. Of the 14 cells perfused with DNQX, eight were found to have an axon. Their average firing rate was reduced from 22 ± 2 Hz to 6 ± 2 Hz by iGluR block..

That not all cells showed rhythmic spiking and that the CCs maxima were shifted, reveals the possibility, that inhibitory synapses suppress rhythmic activity and broad range synchronization. Therefore, additionally to bleaching we applied blockers for GABA and glycin receptors.

3.2.3 Combined antagonization of Glycine and GABA Receptors induces oscillations in C56Bl6 RGCs

In a new set of experiments spontaneous activity was recorded similar to the previous experiments. The retina was constantly illuminated and 30 minutes after start of illumination shortly perfused with a mixture of 5 µM Strychnine and 30 µM SR 95531 to block inhibitory transmission within the retinal patch (*see* **sect. 2.14**). The raster plots in **Fig. 3.15 a** illustrate maintained activity in darkness (14 Hz ± 2.6) and under constant illumination (**Fig. 3.15 b**) Constant illumination increased the mean firing rate of RGCs in this retinal patch to 39Hz ± 2.5 (n = 246 cells in 7 retinas). No rhythmic activity was detected at this early time point.
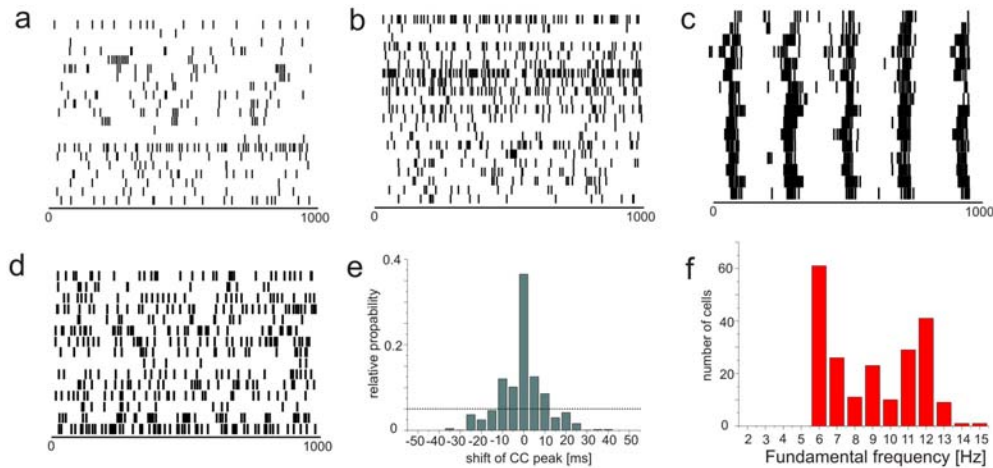
Figure 3.15: Disinhibition of bleached retina initiates synchronous rhythmic activity
Raster plots illustrate spontaneous activity in darkness **(a),** at beginning illumination **(b)** and during perfusion with strychnine and SR95531 **(c)** of selected retinal ganglion cells. After washout of the inhibitory blockers, the rhythmic activity disappeared **(d).** In **(e)** Distribution of the CC maximum lag reveals that a large proportion of the cells is in phase. Dashed line indicates chance level. The fundamental frequency between different retinal samples **(f)** varied from 5 to10 Hz.

Perfusion with the blocker mixture Strychnine and SR 95531 led to oscillatory spiking in 83 % of all cells (**Fig. 3.15 c**). About 53 % of the ON cell population (n = 79 ON cells) and 93% of OFF cells (n = 74 cells) exhibited rhythmic spiking. Inhibitory blockers changed only the spiking pattern and not the firing rate compared to the illumination condition.

Application of either Strychnine or SR 95531 alone did not lead to rhythmic firing.

After wash out of the blocker mixture for more than 10 minutes the rhythmic spiking disappeared (**Fig. 3.15 d**). After wash out, average firing rates were similar to the values before blocker wash in (34±5 Hz).

The fundamental frequency of the spike trains varied between 5 and 10 Hz between retinas (**Fig. 3.15 f**). Cross correlation of spike trains recorded in darkness and during initial bright light illumination revealed no positive correlations, while during perfusion with the blocker mixture strong correlations appeared between 85 % of all cells.

In contrast to spontaneous oscillations the distribution of phase shifts was narrow and 70 % of the CC displayed phase shifts with less than 10 milliseconds (**Fig. 3.15 e**). This indicates synchronous rhythmic input for the majority of the cells, as has been demonstrated for *rd1* RGCs after Strychnine and SR95531 wash in (**Fig. 3.8 c**). Indeed, in addition to the fast extracellular voltage deflections caused by action potentials an additional slow voltage signal was recorded, similar to the LFPs found in *rd1* retinas.

3.2.4 Oscillatory spiking in the disinhibited retina is accompanied by a static LFP

The rhythmic bursting of RGCs during perfusion with inhibition blocker mix was accompanied by oscillatory extracellular voltage changes similar to the Local Field potentials (LFPs) detected in *rd1* mice.
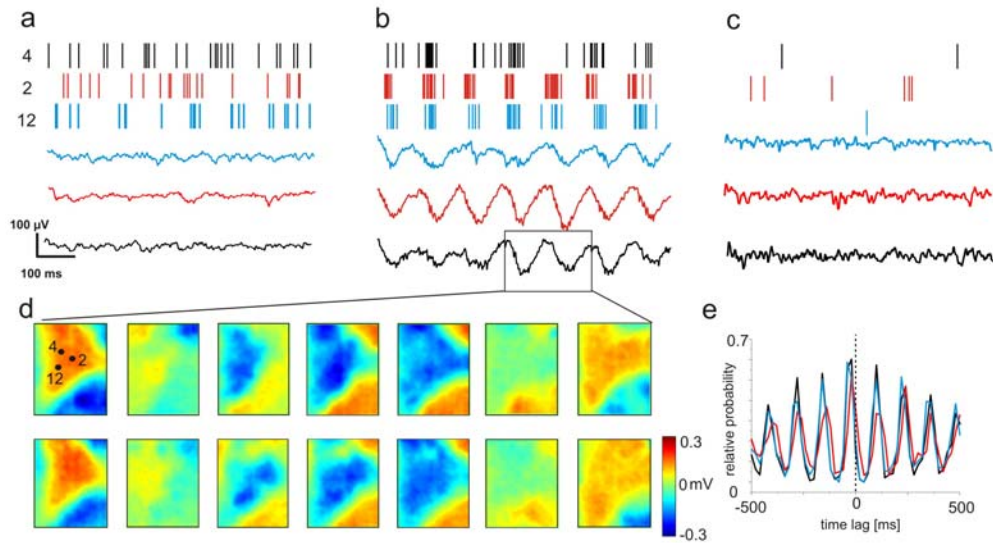
Figure 3.16: Static LFPs emerge during application of strychnine & SR 95531 during illumination
Spiking pattern and corresponding voltage trace of three cells during illumination **(a),** during application of strychnine & SR 95531 **(b)** and during application of inhibitory blocker mix & 50 μM DNQX **(c).** In **(d)** voltage maps show two LFP cycles (total 250 ms). The LFP is initiated at the same position and not propagating. Voltage values are color coded. The rhythmic bursting of the cells and the LFP minima are correlated with little time lag **(e)**.
CCs of recorded RGCs show little time lag, as all cells participated in the same LFP phase.

Spike pattern of three RGCs before and during blocker perfusion are illustrated in **Fig. 3.16 a & b**. The three voltage traces below the raster plots are low pass filtered and show the emergence of a slow voltage deflection concomitant with rhythmic spiking. The RGC spiking is in synchrony to the LFP minimum as indicated by the cross correlation of spikes and LFP minima (**Fig. 3.16 e**).
Spatially, the LFPs covered large areas of the recording array and did not propagate. In **Fig. 3.16 d** the voltage maps illustrate the spatial LFP properties. The cells of panel A-C are indicated by black dots on the voltage map. The voltage map is taken from the retina in **Fig. 3.13** and the three cells correspond to cell 2, 4 and 12..

Though LFPs were static, the location of their origin was variable in time. All rhythmic spiking cells and the LFP were sensitive to glutamate receptor antagonist DNQX (**Fig. 3.16 c**).

DNQX in combination with Strychnine and Gabazine blocked rhythmic activity and LFP generation, the average firing rate was significantly decreased from 36 ± 5 Hz to 12 ± 3 Hz (n= 113 cells, mean $\pm$ SEM; $p < 0.01$) to 12 ± 3 Hz. The average firing rate remained on this level after drug wash out.

We identified 52 cells with axons of which 44 became rhythmic during bleaching and blocker treatment. These cells spiked with 14 ± 1 Hz in darkness and the firing rate increased to 36 ± 3 Hz during illumination. Of the 44 cells initiating rhythmic bursts 28 had a fundamental frequency of 5 Hz while the others obtained frequencies around 10 Hz. Application of DNQX reduced the firing rate in this sample from 36 ± 3 Hz to 13 ± 1 Hz. We found no significant difference in the analysis performed for cells with or without identified axon.

These experiments show that deprivation of the dark current increases RGC firing rates in C57BL/6.

The increased activity results in spontaneous rhythmic spiking and upon blockage of inhibitory synapses, LFP driven, synchronous oscillations appear.

3.3   Pharmacology of wistar RGC spontaneous activity

In addition to mouse models of *rd1,* a variety of rat *rd* models are known (Marc & Jones, 2005). In rat *rd* models, e.g. the P23H-1 rat and the RCS rat, photoreceptors degenerate slow and rhythmic activity was recorded in a subset of RGCs (Kolomiets et al., 2010). But as made evident by recent studies, the electrical phenotype in *rd* rats may not be similar to what was recorded in *rd* mice (Sekirnjak et al., 2011; Kolomiets et al., 2010; Margolis & Detwiler, 2008; Menzler & Zeck, 2011).

Mice and rats investigated in this study displayed differences in maintained activity. In dark adapted rats a higher firing rate for OFF-cells than for ON-cells is observed, that is not detected in mice (**Fig. 3.17**).

Averaged spontaneous activity in mouse ON-cells (n= 256) and OFF-cells (n = 144) was 12 ± 2 Hz (mean ± SEM), which is consistent with published values (Margolis & Detwiler, 2007). In rat RGCs OFF-cells (n = 90) spiked with 16 ± 1 Hz (mean ± SEM) significantly more than ON-cells (n = 130) that showed 5 ± 1 Hz spontaneous activity. The firing rates obtained for dark adapted rats here are similar to a recently published study (Sekirnjak et al., 2011).
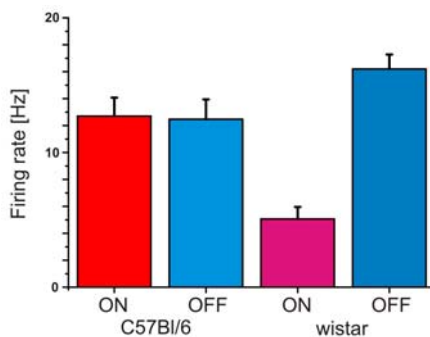
Figure 3.17: ON- and OFF-cell spontaneous activity in mouse and rat RGCs
Bars indicate mean ± SEM, recordings performed in darkness.

To investigate the effect of constant photoreceptor bleaching and the impact of pharmacologic blockers, similar experiments as conducted in mouse, were repeated in rat retina.

I applied constant illumination to wistar retinas, which showed an increase of firing rate (**Fig. 3.18 a)**. In two retinas ON-cells increased their firing rates from 2.4 ±1.6 Hz (n= 16 cells; mean±SEM) to 9 ±4 Hz , while OFF-cells had an elevated firing rate at 17 ± 2 Hz (n=24 cells) compared 10 ± 4 Hz in darkness. The average firing rate for

all cells in the sample (n= 58) changed from 6 ± 2 Hz to 11 ± 1 Hz. The increase was significant (p < 0.05) for all groups. The cells did not initiate spontaneous rhythmic activity.
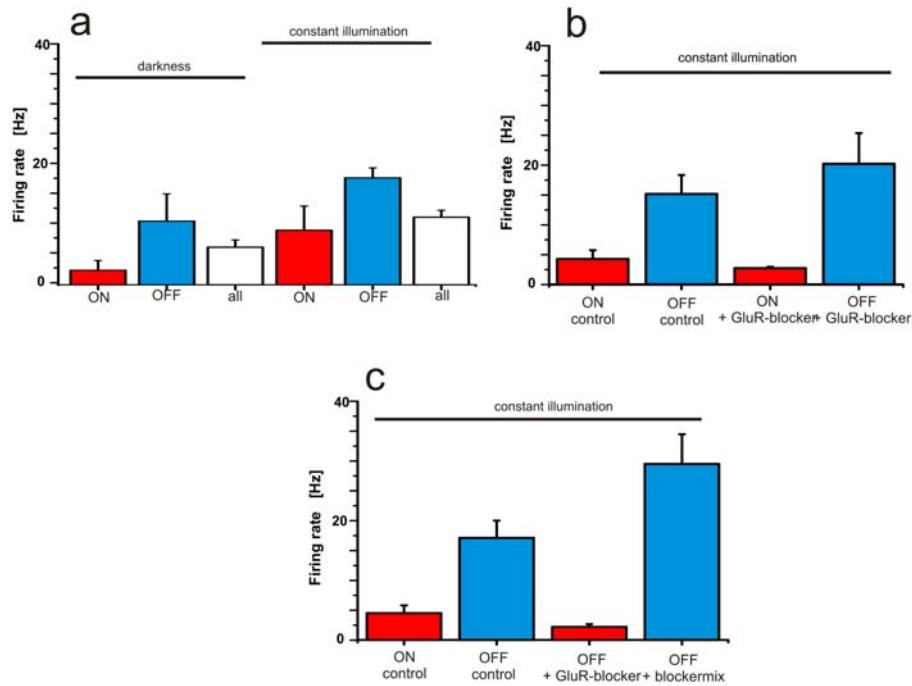
Figure 3.18: The effect of illumination and pharmacologic agents on rat RGC activity

    (a) Constant bleaching of two retinas for ∼ 2 hrs changed the average firing rate of ON- (red), OFF-cells (blue) and of all cells (white) in the sample significantly (p<0.05).

    (b) The GluR blocker only slightly affected the average firing rates. The increase in firing rate for OFF-cells was not significant.

    (c) Perfusion of rat RGCs during illumination with a mixture of GluR blockers, Gabazine (SR 95531) and Strychnine significantly increased the firing rate of OFF-cells, but decreased the firing rate of ON-cells. Bars indicate mean ± SEM.

To test if this elevated activity is due to glutamate release I applied a mixture of 50 μM DNQX, 20 μM AP-4 and 20 μM AP-7 to two retinas under constant illumination. In **Fig. 3.18 b** is shown that glutamate receptor blockers decreased the very low spontaneous activity of ON-cells (4.3 Hz ± 1.5 Hz; n= 27; 2 retinas) in the sample to 2.75 ± 0.25 Hz, while OFF cell maintained activity (15.3 ± 3.2 Hz, n = 20 cells) was increased (20.4 ± 5.2 Hz, p = 0.06), but not significantly.

The GluR blockers had only a small effect, different to what was seen in C57Bl/6 mice.
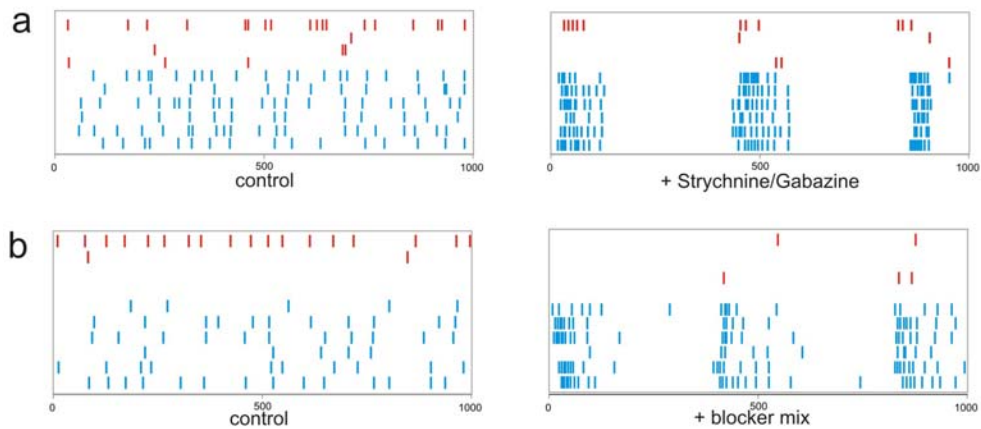
Figure 3.19: Effect of synaptic blockers on wistar RGC maintained activity

(a) During application of 10 μM Strychnine & 30 μM Gabazine one ON-cells (red) and all OFF-cells (blue) initiate a 3 Hz oscillation.

(b) During illumination, the application of a blocker cocktail of 50 μM DNQX, 10 μM Strychnine, 30 μM Gabazine, 20 μM AP-7 and 20 μM AP-4 increased OFF-cells spontaneous firing rate and all OFF-cells initiated a 3 Hz oscillation. ON-cells showed reduced firing rates.

An increase in OFF-cell spontaneous firing was achived by the application of 50 μM DNQX, 10 μM Strychnine, 30 μM Gabazine, 20 μM AP-4 and 20 μM AP-7. The OFF-RGC baseline activity (20.4 ± 5.2 Hz, n = 25 cells, 3 retinas) was increased to 29.7 ± 5 Hz. The effect on OFF-RGCs indicates that the presynaptic input of these cells is inhibitory and its removal increases the spontaneous firing rate. The inhibitor cocktail also affected ON-cells spontaneous firing rate and decreased it from 4.5 ±1.3 Hz (n = 42; 3 retinas) to 2.2 ± 0.4 Hz.

During application of the blocker cocktail, all recorded OFF-cells started rhythmic spiking (**Fig. 3.19 b)** at a fundamental frequency of 3 Hz (n=25). ON-cells showed no patterned activity.

To test if this oscillations appear by loss of inhibition analogue to the findings in mouse (*see* **sect. 3.2.1**) we applied only Strychnine and Gabazine during illumination to one retina (**Fig. 3.19 a**, n = 28 cells).

Gabazine and Strychnine did not change the initial firing rates of OFF-RGCs (from 20 ±4 Hz to 20 ± 7 Hz) and ON RGCs (from 5.7 ± 1.8 Hz to 5.8 ± 2.2 Hz), but induced rhythmic spiking in all OFF-RGCs (n = 9) and in three ON cells (n = 11).

We found no hints for the emergence of a local field potential under this conditions in wistar rats. Bleaching alone had no significant effect on rat RGC spontaneous activity.

Comparing this results with those of the bleaching experiment in mouse is interesting as the rd phenotype in rats and mice are different. In *rd* rats only a subtype of cells show slow oscillations while in *rd1* mice the majority of the population initiates rhythmic spiking.

3.4 Ganglion cell activity after optic nerve lesion

*Some results presented in this section are used for a manuscript "*Impairment of axonal transmission and RGC degeneration in rat and rabbit after optic nerve injury" *by Menzler, Leibig, Zeitler, Lambacher and Zeck. Preparing to submission.*

In traumatic injuries, glaucoma, cancer or some forms of retinitis pigmentosa, degeneration of RGCs occurs, that first affects the morphology of the cells and subsequently leads to apoptosis. Cell degeneration is triggered by direct injury or due to secondary degeneration. In the secondary degeneration, cells degenerate because of changes in their microenvironment, e.g. cones in *rd* degenerate though there is no gene mutation (Levkovich-Verbin et al., 2010; Punzo et al., 2009).

In the following experiments I used rats suffering from direct RGC degeneration due to a surgical lesion of the optic nerve. This animal model is used in glaucoma research, as it resembles the clinical phenotype and shows fast degeneration (Levkovich-Verbin, 2001)

Because of direct lesion of the RGC axons, axonal function should attenuate first.

To asses changes in axonal function I determined the axonal conduction velocity of intra-retinal, not myelinated axons in rats. I take advantage of the STA-analysis presented in prior sections (*see* **sect. 2.10**) and for the first time visualize the propagation of axonal action potentials in rat retinas. STA analysis enables the detection of the propagating action potential over the whole sensor array (1 mm^2) and facilitates the determination of the conduction velocity. This was described previously for rabbits (Zeck et al., 2011), where single axonal APs can be detected without further analysis.

To confirm that changes in axonal conduction velocity are due to axonal injury,

I used two types of surgical lesion: optic nerve crush (ONC) and optic nerve section (ONS). In rats receiving ONS the axon are physically disrupted and axonal endings are open. Therefore these cells can be labeled retrograde to estimate RGC density.

In stained retinas the induced cell loss was confirmed by cell count. Furthermore, in retinas were stained RGCs become sparse I could match the electrical image of spiking cells with the micrographs to identify the cells recorded. If in a region where spikes were recorded a stained cell was detectable, the staining of the cell indicated axonal injury otherwise the dye (Rhodamine-dextrane) couldn't enter the cell.

The retinas with sectioned optic nerve were used as control for the retinas with crushed axons, where I expect to see a similar but maybe slower change of the axonal conduction velocity.

An additional I recorded somatic action potentials. Following a study investigating the effect of axotomy on single RGCs in cats (Takao et al., 2002), one should expect slight changes in the maintained firing rate after two weeks and a change of the average firing rate of the light response. I expected to see differences in the RGC response if a prior change in axonal propagation velocity was detected.

3.4.1 Decrease of RGC density after optic nerve injury

To supervise the effect of optic nerve injury on RGC density eight rat retinas were retrograde stained during eye surgery using Rhodamine-dextrane. This was possible only in rats receiving ONS where the axons were accessible for dyes.

One days after the Rhodamine injection averagely 1208 ± 131 cells per mm^2 (n = 2 retinas) were counted (**Fig. 3.20 a & g**), four days after the cell density decreased slightly to 1090 ± 127 (n = 2 retinas) cells per mm^2. A strong cell density decrease was found in retinal patches prepared eight days after surgery, where the mean cell density was 499 ± 33 cells per mm^2 (**Fig. 3.20 b & e**; n = 3 retinas). In one rat retina analyzed two weeks after staining, we found only 3 cells per mm^2 (**Fig. 3.20 c & f;** n = 1 retina).

Rhodamine dextrane staining does not indicate viability and is also incorporated by glial cells and lysosomes after RGC apoptosis. The cells counted are chosen by the criterion of size and may not reflect the number of functional cells. In **Fig. 3.20 a,** the 5 x magnification of stained cells on an MTA chip illustrates the cell density one day after dye injection. Cells are of round shape and thick axon bundles are visible (**Fig. 3.20 d**).

One week after surgery cell labeling becomes sparse (**Fig. 20 b**) and axon bundle labeling appears thinner. In the 20x magnification (**Fig. 3.20 e**) deformed and apoptotic cells are observed (blue arrows). The RGC degeneration comes to an end after two weeks where only apoptotic bodies are visible (**Fig. 3.20 c & f**).
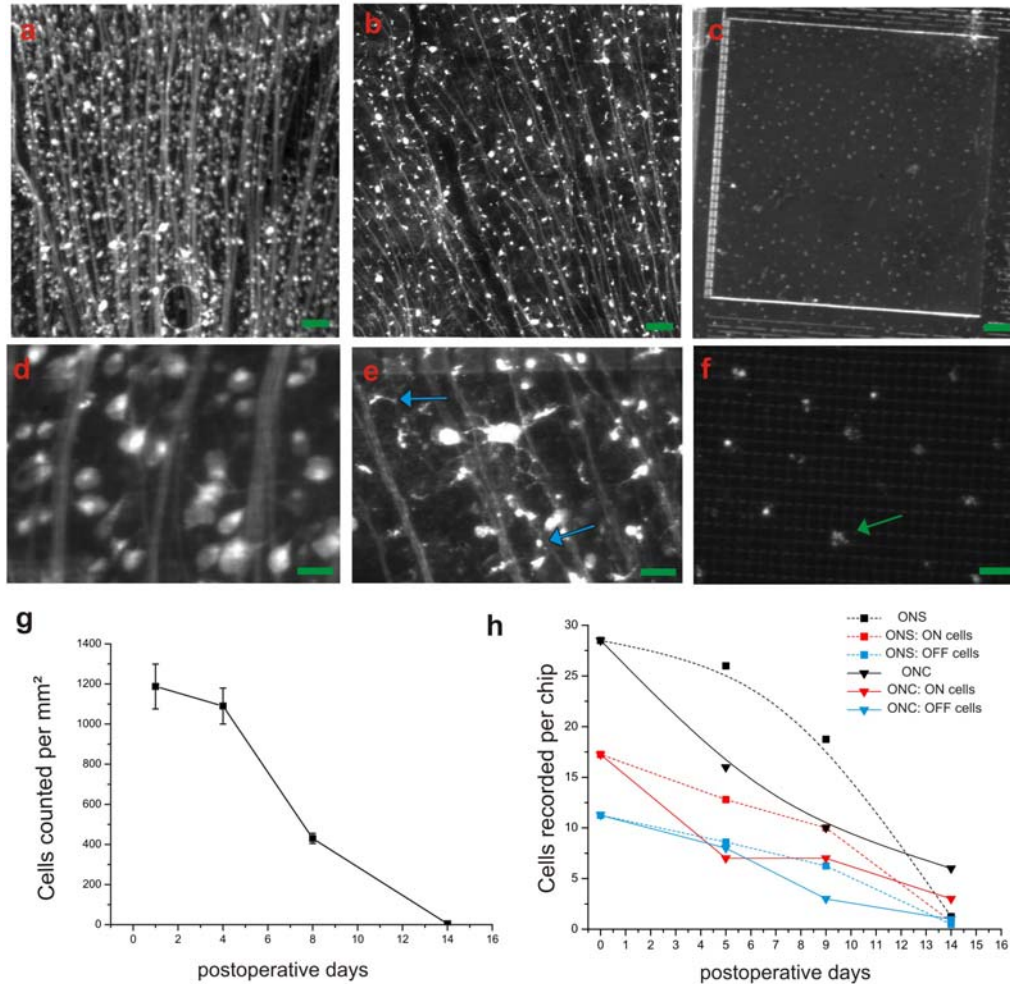
Figure 3.20: Staining of RGCs after ONS indicates cell loss
(a – b) shows retinal patches with stained RGCs on the Neurochip (5x magnification). On this patches 1014 cells **(a)**, 379 **(b)** and 3 **(c)** cells were counted. Green bars indicate 100 μm.
(d - f) pictures are taken from the corresponding patches above with 20x magnification. Green bars indicate 20 μm. In **(d)** axon bundles and normal RGC somas are visible one day after surgery. Through the cell layer the transistor grid is visible. In **(e)** 8 days after surgery apoptotic and deformed cells appear (blue arrows), cell density is decreased and axon bundles are thinned. **(f)** After 14 days only apoptotic bodies are visible (green arrow).
In **(g)** the average cell number counted per mm^2 is plotted against post operative time intervals. Staining was done with ONS animals. Symbols indicate mean ± SEM. Analogue to **(g)** the number of cells recorded per retinal proportion is plotted in **(h)**. ONS is indicates by a square and ONC by a triangle symbol. Colors correspond to ON- (red), OFF- (blue) cells and all cells (black). Symbols indicate mean values.

The time course of degeneration revealed here is consistent with previous findings (Berkelaar et al., 1994) for ONS degeneration though absolute cell numbers found in the literature are higher.

No co-staining was performed to assure retrograde dye load of all cells and the presence of unstained cells can not be excluded. Cells that were not injured and not stained are subject to secondary degeneration (Levkovitch-Verbin et al., 2010) and should not influence the result of this study.

Retinas that underwent optic nerve crush were not stained. Therefore the ONS retinas served as control to monitor effects of axon damage. Quantifying the cells recorded per retinal patch, a decline in cell number is seen in animals receiving ONC that is analogue to ONS (**Fig. 3.19 h**). The relation of recorded cells and de facto cells in a retinal proportion depends on various factors (Lambacher et al., 2011) and therefore this statistic only indicates a trend. For ONS and ONC the number of recorded cells declines in time and gives an important hint, that the optic nerve injuries performed here lead to RGC loss.

3.4.2   Axonal conduction velocity in rat retinas following optic nerve injury

Electrical activity propagates along the axon of the retinal ganglion cell. To assess functional changes in retinal axons, we measured intra-retinal propagation velocities at different time intervals following optic nerve injury in rats: after four, eight and fourteen days. In rat retinas only proximal axons and no axons of passage were detected. **Fig. 3.21 a** illustrates the action potential propagation of a control rat RGC that is qualitatively similar to those seen in the rabbit retina (Zeck et al., 2011). In control rat retinas (**Fig. 3.21 b**) we measured an average conduction velocity of 1155 ± 101 μm/ms (n = 24 axons; mean± std).

A significant decrease in propagation velocity was detected as early as the first recording interval, at day four. At this time point RGC density is still similar to control (Berkelaar et al., 1994; Kanamori et al, 2009; **Fig. 3.20 g**). Four days after ONS only a few axons (n= 5) were detected, that had a propagation velocity of 892 ± 151 μm/ms (mean ± std). In retinas eight days after ONS more axons were detected (n =31) that had an average conduction velocity of 815 ± 97 μm/ms (n = 31). The decay in axonal conduction is significant for day eight in retinas with sectioned optic nerve (p < 0.01) compared to control, but not compared to day four after ONS. After fourteen days, neither cells nor axons were detected in ONS rats.

RGCs that received ONC showed a similar decrease in axonal conduction velocity. Within four days it decreased to 918 ± 136 µm/s (n = 17), which is significantly lower than control velocity (p < 0.05). At day eight the velocity decreased slightly further and was 829 ± 151 µm/ms (n = 10, after ONC). Fourteen days after ONC still four axons were detected that propagated at an average velocity of 754 ± 68 µm/ms. Across the operated groups, differences were not significant (p > 0.08).
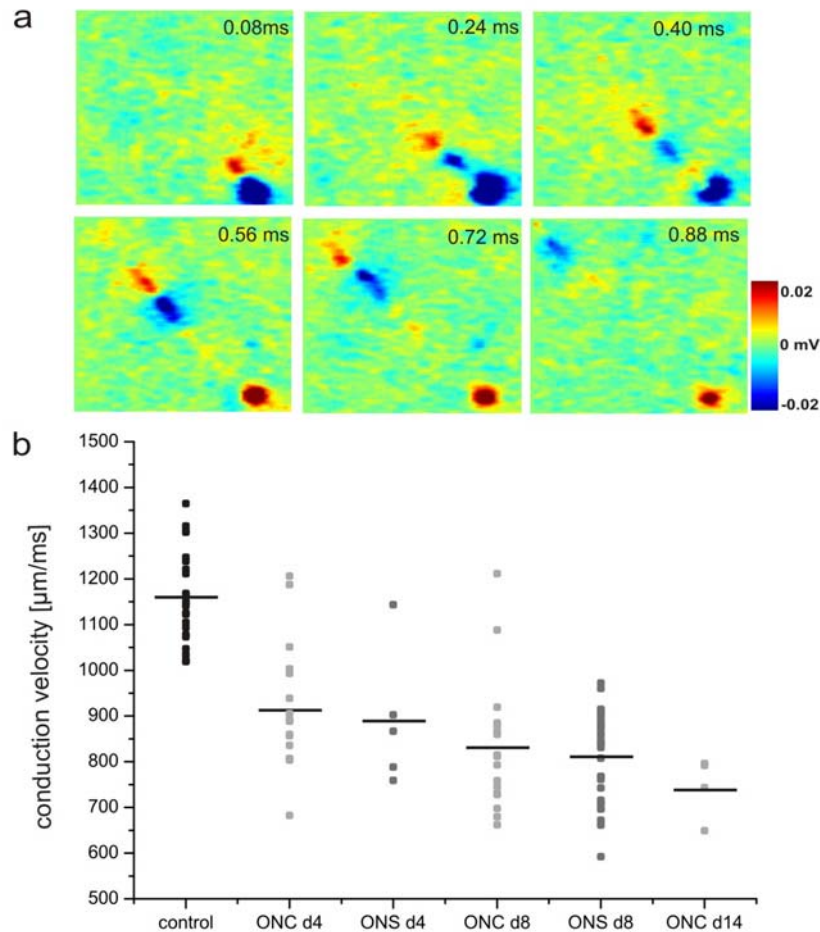
Figure 3.21: Intraretinal axonal velocity in rat retinas after optic nerve injury.
(a) A sequence of six consecutive electrical images illustrates the propagation of an axonal action potential across the sensor array. The electrical images constitute the 'spike triggered averages' (see Materials and Methods). The bar indicates 300 µm.
(b) Average conduction velocities of intraretinal axons in rat following optic nerve crush or optic nerve section. Symbols indicate values of single averaged action potentials, horizontal bar indicates the mean value.
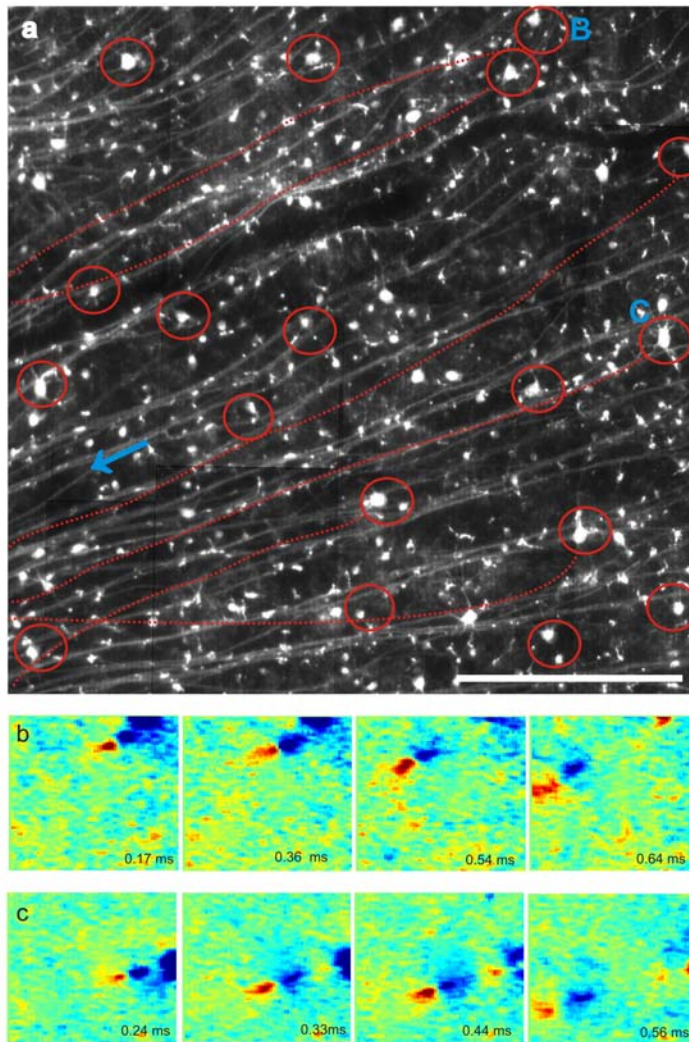
Figure 3.22: Match of electrical and fluorescence image of cells with identified axon
In **(a)** a retina eight days after surgery is shown, that was stained with rhodamine dextrane. The picture shows the array surface. Red circles indicate the areas where somatic spikes were recorded, in most of the circles only one stained cell is present. We suppose this cells to be those recorded from. The dotted red line indicates the path of the axonal AP over the array. The direction of the optic disc is indicated by a blue arrow. For the cells labeled with and C the electrical image of the propagation of an axonal action potential is shown in **(b)** and **(c)**. The axonal APs travel towards the optic disk. The white bar indicates 300 μm.

The decline in axonal propagation velocity at day four prior to massive cell loss suggests that it is among the first events after optic nerve injury. We further tested if it precedes degenerative changes of RGC electrical activity.

In rats that received ONS and retrograde labeling we were able to match the cells we recorded with fluorescence micrographs at day eight. At this post-operative time-point RGC density significantly declined. In **Fig. 3.22 a,** a labeled retina eight days

after ONS is shown. The red circles indicate areas where somatic spikes were recorded and in most areas only one stained cell is visible. If an axon was detected, the propagation path is indicated as red dotted line. To my knowledge this is the first time a fluorescent image of a ganglion cell and a corresponding recording of axonal AP propagation could be matched. Two example axonal action potentials are shown below (**Fig. 3.22 b),** they propagate in the same direction, towards the optic disc (blue arrow).

3.4.3 Maintained ganglion cell activity in retinas following optic nerve crush or optic nerve section

Axonal injury leads to degeneration of RGCs in rat retina. To investigate if changes in somatic activity are induced by optic nerve lesion, I evaluated RGC activity recorded within the same ex vivo retinas as reported above.

Spontaneous activity was recorded over a period of 30 min, beginning 15 min after the retinal proportion was adhered to the MTA-chip.

The maintained activity of 14 rat RGCs is shown in **Fig. 3.23 a**. ON and OFF rat RGCs differed with respect to their spontaneous firing rates. The first seven rows depict OFF RGCs, the remaining seven rows show ON cell activity from one retina. A qualitative inspection of the raster plot after optic nerve injury suggests that spontaneous activity decreases especially in OFF-cells (**Fig. 3. 23 b**).
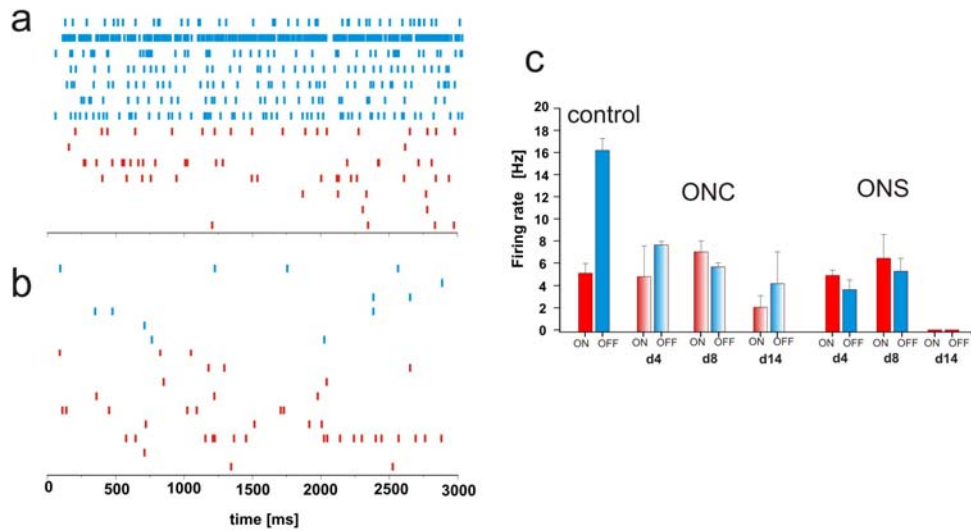
Figure 3.23: Changes in spontaneous activity of rat RGCs due to optic nerve lesion
In **(a)** three seconds of spontaneous activity recorded in a control retina in darkness are shown, The first seven rows show OFF-cells (blue), the last seven ON-cells (red). OFF-cells are more active than ON-cells. The effect of optic nerve lesion on spontaneous activity is illustrated in **(b)** where the first seven rows show OFF-cell activity (blue) while the other rows ON-cells (red) of a retina recorded eight days after ONS. ON-cells seem to be more active than OFF-cells.
The change in spontaneous activity is quantified in **(c)** for ON- and OFF-cells. In control retinas OFF-cells exhibit a significantly higher firing rate than ON-cells. This difference is not detectable after ONC or ONS at all recorded time points. Bars indicate mean ± SEM.

Control RGCs showed an average spontaneous discharge rate of 14.7 ± 1.3 Hz (n = 246 cells). The OFF (**Fig. 3.23 c**) RGC firing rate (16 .6 Hz ± 2 Hz, n = 90) is significantly (p= 0.002) higher than the ON RGC firing rate (5.6 Hz ± 1.1 Hz, n= 130).

	POD 0 Firing rate [Hz]	4 Firing rate [Hz]	8 Firing rate [Hz]	14 Firing rate [Hz]
ON-cells control	5.6 ± 1.1 (130)	-	-	-
OFF-cells control	17.6 ± 1.0 (90)	-	-	-
OFF- cells ONS	-	3.6 ± 0.9 (43)*	5.2 ± 0.4 (50)*	-
ON-cells ONS	-	4.8 ± 0.5 (64)	6.4 ± 1.2 (80)	-
OFF-cells ONC	-	7.6 ± 0.3 (25)*	5.5 ± 0.4 (20)*	4.5 ± 2.8 (9)*
ON-cells ONC	-	4.7 ± 2.7 (21)	7 ± 1 (37)	2 ± 1 (13)*

Table 3: Maintained firing rates in rat RGCs after optic nerve lesion
Firing rates indicate mean ± SEM; number of cells in brackets, asterisks indicate significant (p< 0.05) change compared to control

Following ONC or ONS the average firing rate of OFF-cells is decreased at all recording time points (**Table 3**). At the first recording time point the maintained activity of OFF-cells is 80% and 60% reduced compared to control for ONS and ONC respectively. After eight days the level of OFF-spontaneous activity is similar for both groups at around 5 Hz and is not changed one week later at postoperative day 14 for ONC RGCs. After ONS no spontaneous active cells were detected at day 14.

In contrast, ON-cell activity is unaffected until post-operative day 14, when after ONS no spontaneous active cells were detected and after ONC the average ON-cell firing rate was significantly reduced from 5.6 ± 1.1 Hz in the control to 2 ± 1 H. Only OFF-cell maintained activity is decreased within the first two weeks after optic nerve lesion, more severe after ONS. Interestingly, changes in maintained activity of *rd* rats were also reported for OFF-cells only (Sekirnjak et al., 2011).

3.4.4 RGC response to light flashes

Light increment or decrement triggers responses of most RGCs. The concept of ON and OFF cells is well established and aberrations from normal response should indicate degenerative change.
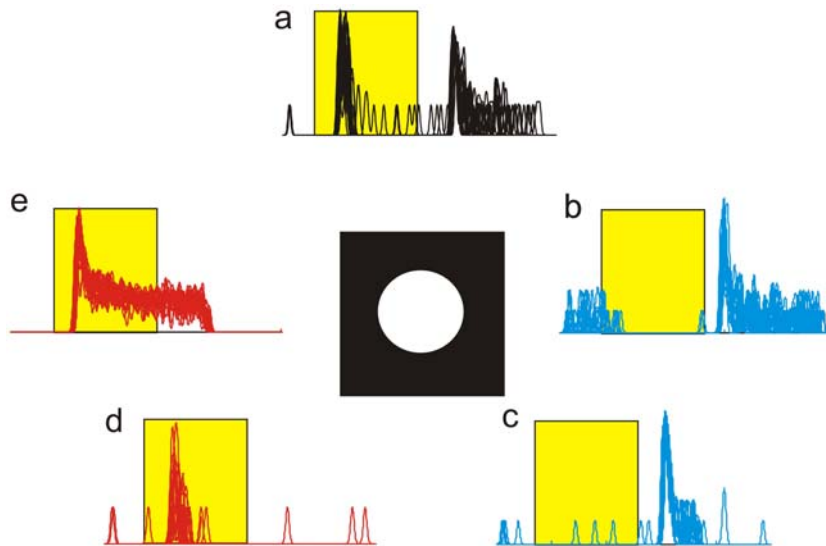
Figure 3.24: Different types of light responses found in wistar RGCs

The majority of RGCs that respond to light can be assigned to five types or classes based on their spiking pattern. The Peri-Stimulus-Time-Histogram (PSTH) in **(a)** shows a cell with ON-OFF-response characteristic. In **(b)** a OFF-sustained cell is shown. The PSTHs in **(c)** and **(d)** are typical for an OFF-transient and an ON-transient cell respectively. In **(e)** a ON-sustained cell is depicted. Relative proportions of this cell types found in the samples of control and operated cells are listed in **Table 3**.

To evoke activity in the majority of ON RGCs in a retinal portion, I flashed bright stimuli (spot size > 1 mm diameter, 400 ms duration, 96% contrast) onto a dark background. OFF RGCs were stimulated with the inverse stimulus (*see* **sect.2.13**) . Before and after each light flash, retinas were adapted to the stimulus background for 10 sec. The experiment was repeated for each retina 10 times. The types of light responses found in the rat retina are summarized in **Fig. 3.24**.

In **Table 4** the relative proportion of the cell types found in the respective samples are listed. As the majority of cells recorded showed ON-sustained and OFF-sustained responses, theses cells were merged with the transient types in the following to one sample.

	Cells N =	ON transient %	ON sustained %	OFF transient %	OFF sustained %	ON-OFF %	Not classified %
Control	256	1	53	1	39	3	4
ONS 4d	131	0	57	0	33	2	10
ONC 4d	73	2	39	0	24	0	35
ONS 8d	129	0	48	4	32	0	16
ONC 8d	52	2	53	0	23	0	22
ONS 14d	5	0	80	0	0	0	20
ONC 14 d	25	0	55	2	22	0	21

Table 4: Proportion of cell-types found in the respective samples

	POD 0 Latency [ms]	4 Latency [ms]	8 Latency [ms]	14 Latency [ms]
ON-cells control	66 ± 1.8 (138)	-	-	-
OFF-cells control	56 ± 1.4 (90)	-	-	-
OFF- cells ONS	-	68 ± 1.8 (43)*	86 ± 4.3 (50)*	-
ON-cells ONS	-	66 ± 2 (64)	80 ± 1.9 (80)*	-
OFF-cells ONC	-	77 ± 1.7 (25)*	82 ± 3.1 (20)*	-
ON-cells ONC	-	70 ± 3 (21)	75 ± 1.3 (37)*	-

Table 5: Changes in response latency after optic nerve lesion
Latency values indicate mean ± SEM; number of cells in brackets, asterisks indicate significant ($p < 0.05$) difference compared to control

	POD 0 Firing rate [Hz]	4 Firing rate [Hz]	8 Firing rate [Hz]	14 Firing rate [Hz]
ON-cells control	45 ± 1.2 (138)	-	-	-
OFF-cells control	38 ± 1.3 (90)	-	-	-
OFF- cells ONS	-	21 ± 1.4 (43)*	17 ± 1 (50)*	-
ON-cells ONS	-	27 ± 2.1 (64)*	20 ± 0.7 (80)*	-
OFF-cells ONC	-	17 ± 1 (25)*	24 ± 2 (20)*	-
ON-cells ONC	-	21 ± 2 (21)*	20 ± 0.7 (37)*	-

Table 6: Firing rates of light response in rat RGCs after optic nerve lesion
Firing rates indicate mean ± SEM; number of cells in brackets, asterisks indicate significant ($p < 0.05$) change compared to control

Examples for the light responses of control and operated rat RGCs are shown in **Fig. 3.25 a**. From the RGC response, we calculated the response latency as the time delay between stimulus onset and the first spike of the light response.

After four days the OFF-response latency was significantly affected in both treated groups and increased for over 10msec from 56 ± 1.4 msec to 68 ± 1.8msec (ONS) and 77 ± 1.7 msec (ONC). Eight days after the operation the OFF-response latency increased further to over 80 msec (**Table 5**). For ON-cells the first significant increase was detected eight days after surgery in both groups, where the response latency increased from 66 ± 1.8 Hz in controls to 80 ± 1.9 msec (ONS) and 75 ± 1.3 (ONC) msec (**Table5**).
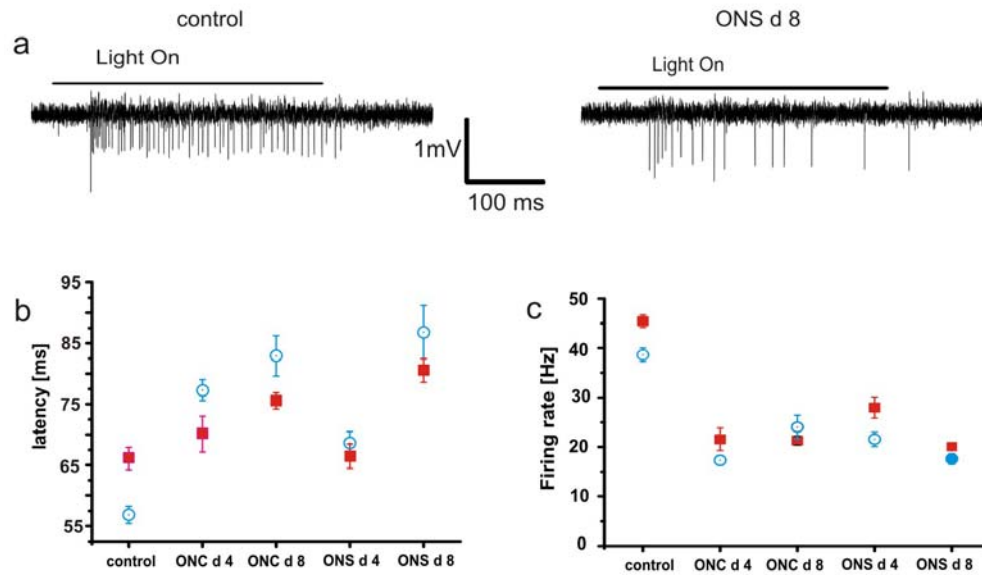
Figure 3.25: Changes in latency and firing rate after optic nerve lesion
In **(a)** raw traces of light responses of a control On-sustained cell (left) and an ON-sustained cell eight days after ONS are shown. The cell from the operated retina exhibits reduced spiking intensity. The increase in response latency for ON- and OFF-cells is summarized in **(b)**. ON-cells (red squares) in control animals have a higher latency than OFF-cells (blue circles). For both cell types the latency is increased either after ONC or ONS. Only retinas recorded four days after ONS showed no latency increase for ON-cells. Latency increase seems to accumulate by time.
The decrease in firing rate is summarized in **(c)**. After four days the firing rate decrease for about 50 % in both surgical conditions and remain on this level later on.

While the changes in maintained activity and light response delay affected ON-cells later than OFF-cells, the firing rates of the light response decreased at the same time

for both cell types. The average firing rate for both cell types decreased for about 50% within the first four postoperative days and remained on this level at day eight.

3.4.5 Rat RGC response to moving gratings

Response latencies of ON-cells were unchanged four days after surgery, but OFF-cell latency was affected at the earliest recoding time point. Changes in latency may reflect altered dendritic input, as shrinkage of the dendritic tree is reported to be an early event after optic nerve injury (Leung et al., 2011; Thanos, 1988).

Full field flashes may therefore not be appropriate stimuli to detect fine changes in dendritic structure.

I tested the response of RGC to grating stimuli with varying spatial frequency. The resolution of spatial frequencies is closely related to dendritic tree diameter (Wässle & Boycott, 1991).

The raster plot in **Fig. 3.26 a** illustrates the typical response of eight control RGCs (4 ON- and 4 OFF-cells) to gratings with 0.05 cycles/degree (top), 0.1 c/d (middle) and 0.2 c/d (bottom) spatial frequencies. In **Fig. 3.26 b** the response of eight RGCs from a retina after ONS is shown for the same stimulus parameters.

The response amplitude was quantified as the first harmonic of the Fourier transformed spike train (Pu et al., 2006). Responses were normalized to the control (**Fig. 3.26 c**).

Control RGCs had significantly ($p < 0.05$; n = 79) higher response amplitudes for gratings with 0.05 c/d, 0.1 c/d and 0.2 c/d spatial frequency than all operated animals (**Fig. 3.26 c**).

In animals treated with ONS (**Fig. 3.26 c**, red lines) the response amplitude four days after surgery (n = 28) was significantly ($p < 0.01$) decreased for 0.05, 0.1 and 0.02 c/d compared to control and to animals four days after ONC. Eight days after ONS (n = 57) the response decreased significantly further ($p < 0.01$) compared to control and to all other groups.

RGCs from animals four days after ONC (n = 33) performed significantly ($p < 0.05$) better in grating discrimination than animals eight days after ONC (n = 38, **Fig. 3.25 c;** blue lines), but both groups showed significantly reduced responses with respect to control ($p < 0.05$). We found no difference between ON- and OFF-cells here.
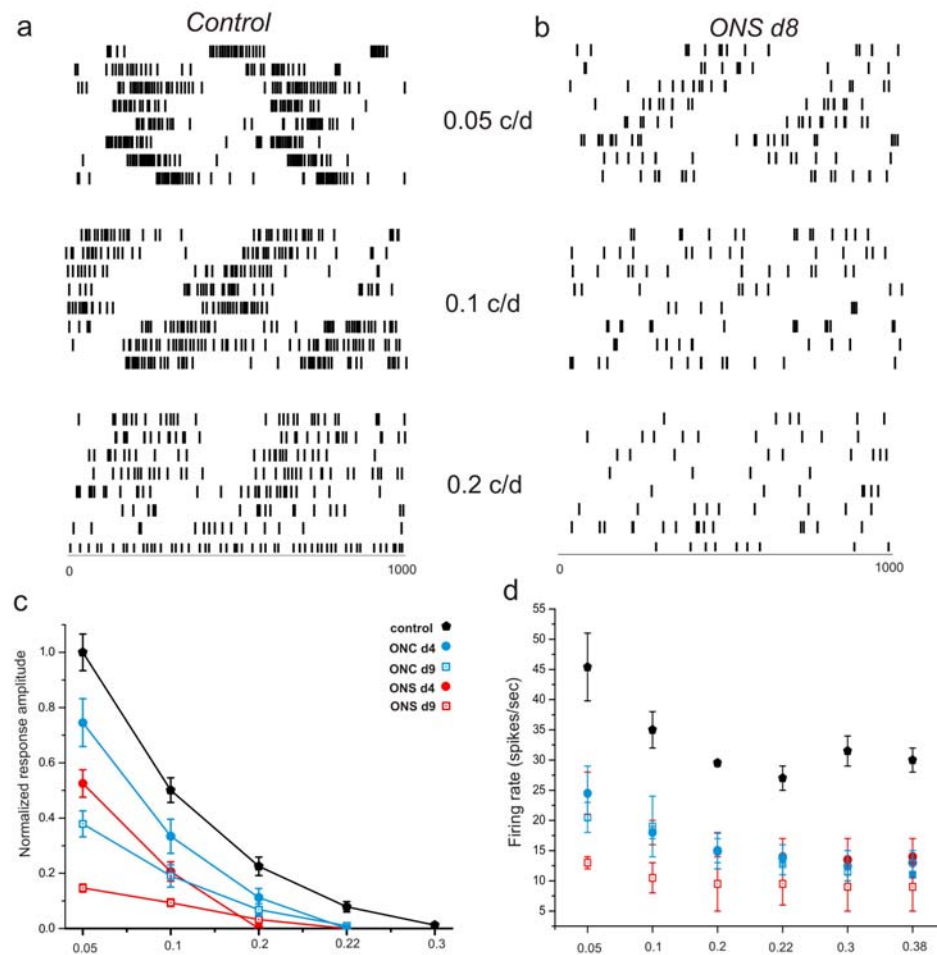
Figure 3.26: Rat RGC response to moving gratings of varying spatial frequency.
Grating stimuli were presented to the retinas with spatial frequencies from 0.05 c/d to 0.38 c/d at a temporal Frequency of 2 Hz.
(**A** & **B)** Raster plots illustrate the typical response to gratings with 0.05 c/d, 0.1 c/d and 0.2 c/d spatial frequency of eight control RGCs (A) and eight RGCs eight days after ONS (B).
(**C**) Summarizes the RGC response based on the average amplitude of the first harmonic of the Fourier transformed spike train: While control RGC discriminate bars up to 0.2 c/d, operated animals show a depressed response.
The mean firing rates of operated animals are 50 % of control values as summarized in (**D**), but were above maintained activity. The firing rate decreased with increasing spatial frequency in all groups. Symbols indicate mean ± SEM.The change in firing rates is similar to the experiments with light flash stimulation. We found no significant differences between ON- and OFF-cells. These experiments indicate that individual RGCs decrease their ability to encode moving grating stimuli after optic nerve injuries.

Changes with respect to the average firing rate (**Fig. 3.26 a, b, d**) were similar to those observed in full field flash experiments. .

As illustrated in **Fig. 3.26 d** control RGCs (black circles) exhibited an initial average firing rate of 45 Hz ±7 Hz (mean ± SEM) when a grating of 0.05 c/d was presented at constant temporal frequency. Firing rate then decreased with increasing spatial frequency but never fell below 25 Hz. Average firing rates of operated RGCs were typically around 25 Hz for 0.05 c/d spatial frequency and below for increasing spatial frequencies. ONS treated rats after eight days after surgery exhibited firing rates below 15 Hz for all spatial frequencies. We could not detect differences for ON- and OFF-cells.

Cells tested here, were a subset of the cells which were analyzed for changes in latency. The results indicate that RGC visual acuity is severely impaired four days after optic nerve lesion and this suggests changes of the dendritic input.

3.5 Correlated activity of rat RGCs

In retinas after Optic nerve section and retrograde staining it is possible to assign recorded activity to individual cells. The micrograph in **Fig. 3.27 a** shows stained RGCs eight days after ONS. Red circles indicate the areas where transistors recorded action potentials and the cells within this area are supposed to be their origin. The two cells in **Fig. 3.27 a** marked 'A' and 'B' had a positive correlation of their spike trains that is depicted in **Fig. 3.27 b**. The cells were spaced 150 μm.
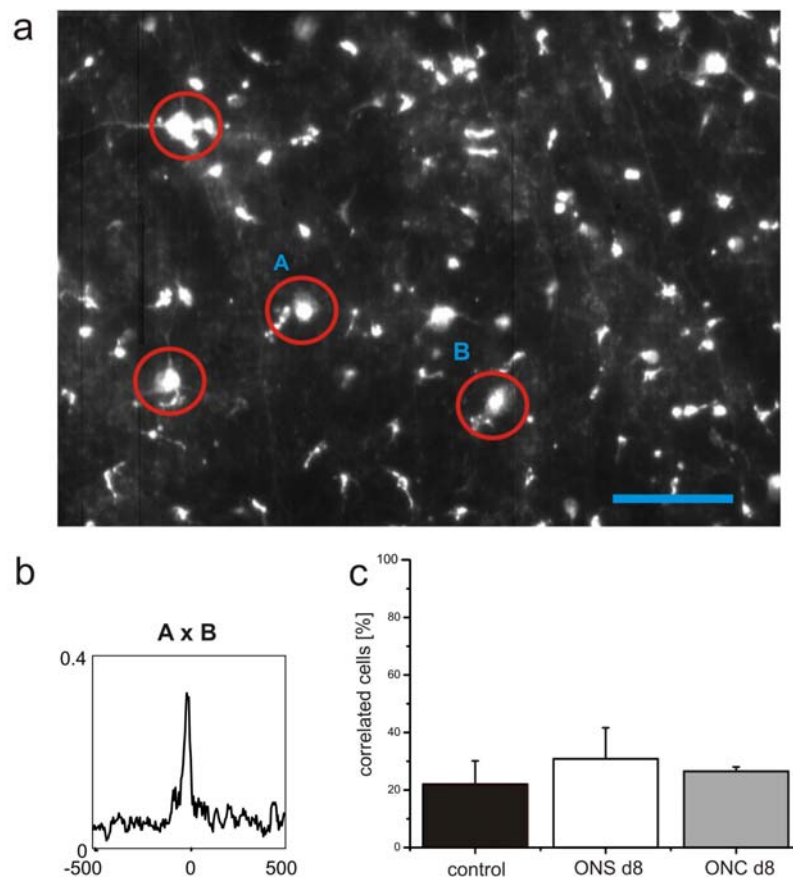
Figure 3.2 : Correlated firing of control and operated rat RGCs
In **(a)** four cells from which action potentials were recorded are indicated by red circles. Scale bar indicates 100 μm. For the cells marked 'A' and 'B' the CC is shown in **(b)**. In graph **(c)** the proportion of correlated cells is summarized for control (black) and operated retinas (white, eight days after ONS; grey, eight days after ONC). Bars indicate Mean ± SEM.

In wistar rats correlations between spontaneously firing RGCs are frequently detected and occur between 20 % of the RGCs (**Fig. 3.27c**). Interestingly we found no substantial change after optic nerve injury.

Though cell loss and decrease of spontaneous firing rate still a similar proportion of cells displays correlated firing eight days after surgery. The majority of correlated firing cells were OFF-RGCs. Double peak CCs indicating gap junctions were rarely found between wistar RGCs.

4. Discussion

4.1 A small brain

The retina is a part of the brain. Like all neocortical structures, the retina has a layered and not a nuclear organization, where cells of similar function cluster. Therefore the retina has been considered as the best accessible part of the brain.

The retina is not just a detector of stimulus energy like the ear, where the hair cells encode the degree of deflection of their cilia and signal it to the cochlear nucleus.

In the retina even the detector cells, the photoreceptors, do not just encode stimulus energy but are specialized to optimize the received information. Therefore the retina can not be compared to a *camera obscura* that transforms photon energy into changes of chemical structure which then are signalled to the brain.

The retina provides a range of adaption, filter and detection mechanisms to reduce the amount of information signalled to the brain and increase the significance of the information (Gollisch & Meister, 2010, Wässle, 2004; Borst & Euler, 2011).

4.2 Spontaneous activity

Regarding to a simple scheme of telecommunication an encoder and a decoder are connected by a channel (Shannon, 1954). To optimize the transmitted information, encoding and transmission should avoid noise that increases the ambiguousness of the information.

The spontaneous activity of RGC constitutes such noise.

The presence of this activity increases sensory threshold, because an information has to exceed the background of the system (Kuffler, 1957; Ala-Laurila, 2011). Thus, spontaneous activity at the first sight is obstructive for signal detection.

Therefore it was undertaken to identify the source of spontaneous discharges in the retina. In principle, two concepts exist about the origin of maintained activity in the retina: Stochastic events in photoreceptors that modulate the dark current and induce activity in the postsynaptic cells (Kuffler et al., 1957; Rodieck et al. 1965; Birge & Barlow, 1995; Ala-Laurila et al., 2011) or the existence of pacemaker cells (Feigenspan et al., 1998; Margolis & Detwiler 2007; Petite-Jaques et al., 2005).

The recordings presented here suggest that spontaneous activity in the *rd1* retina is generated independently from photoreceptor noise, but in the healthy retina photoreceptor noise contributes to spontaneous activity (Ala-Laurila et al., 2011). The

participation of pace maker cells in the generation of retinal maintained activity is also supported by the finding that the spontaneous activity of OFF-cells in mouse retina is not decreased by synaptic blockers (Margolis & Detwiler, 2007) and that amacrine cells display spontaneous oscillations of their membrane potential (Petite-Jaques). That RGCs themselves are pace makers contrasts with the finding, that spontaneous activity in *rd1* mice can be completely abolished by synaptic blockers (Margolis & Detwiler, 2008; Menzler & Zeck, 2011). Similar results were obtained in rats (Sekirnjak, 2011), indicating that the pace maker must be presynaptic to RGCs. An interesting feature of spontaneous activity is the effect of light and darkness on spontaneous activity.
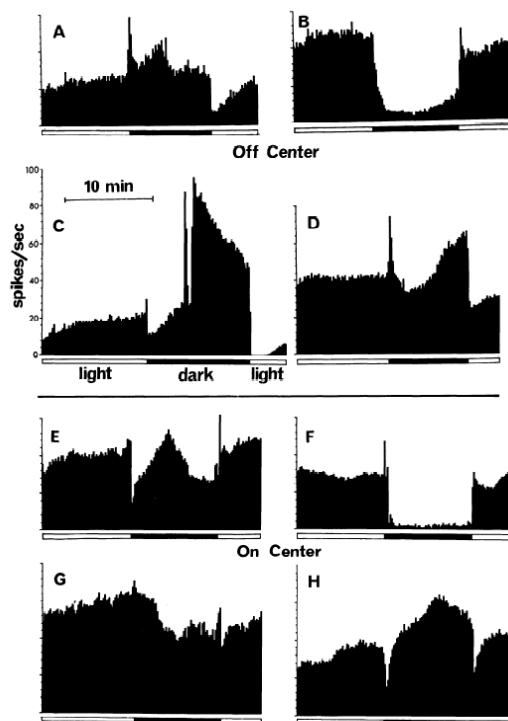
Figure 4.1: Variation of spontaneous firing rates of four OFF- (top) and four ON-cells (bottom) in constant darkness or illumination (from Rodieck, 1967). ON- or OFF-cell polarity of cat RGCs in vivo seems not to account for the activity variation in both conditions.

The ON- and OFF- pathways in the retina are well known, but allow no prediction about the firing rate of the respective cell in darkness or light (Rodieck, 1967, **Figure 4.1**). This observation suggests that the generation of spontaneous activity may

recruit other pathways additional to those that create the functional response (Ala-Laurila, 2011).

Though spontaneous activity is present in the retina, the significance of the phenomenon is not clear.

Spontaneous activity is ubiquitously found in the CNS and often occurs in form of oscillations (Singer., 1993; Timofeev & Bazhenov 2005). The best example is neuronal activity in sleep, where the brain is completely deafferented, but not inactive (Steriade, 1993). In the brain, noise feed recurrent networks and depending on their connectivity, oscillations of a variety of frequencies occur (Buszaki, 2006). In the brain, spontaneous oscillations serve for a number of functions in the adult and developing brain and support especially synaptic plasticity (Steriade & Timofeev, 2003)

In retinal development this role of oscillating activity also comes into play.

Patterned spontaneous activity is observed in retinal cells prior to eye opening and propagates in a wave like manner over the retina.

Such retinal waves help to establish and eliminate synaptic contacts, form topic maps and organize synaptic target areas, e.g. ocular dominance columns (Wong, 1999; Sengpiel & Kind, 2002).

In the fetus, maturing RGCs start concerted electrical activity (stage I waves) that is necessary to develop synaptic contact to the LGN (Penn et al., 1988; Syed et al. 2004). In newborn animals prior to eye opening the retinal waves propagate via chemical synapses and two periods can be characterized by the neurotransmitter antagonists that block wave generation (Firth et al., 2005; Blankenship & Feller 2010). In the early period retinal waves rely on cholinergic synapses (stage II waves). Acetylcholine is an excitatory neurotransmitter released by starburst ACs.

At a later period the generation of retinal waves switches to glutamatergic transmission (stage III waves), probably around the time bipolar cells form functional synapses with RGCs and ACs.

The correlated activity exhibited in retinal waves during development is not restricted to the retina, but drives similar rhythmic activity in the visual cortex and in the superior colliculus (Hanganu et al., 2006).

After eye opening the rhythmic and synchronized activity disappears and the spontaneous activity recorded in the mature retina is left over.

In the retina after eye opening, synapses are of course changed by experience. But in principle, synapse formation in the retina is completed before. The adult retina for sure is capable of local plasticity, but it can be argued that its need for plasticity is lower than in higher brain areas.

However, the retina shows oscillating activity during development, that enables synapse formation. The recordings concerning rd1 retinas and bleached C57Bl/6 retinas presented here, suggest that in degenerative states this activity patterns reappear and that furthermore in the adult retina this activity is suppressed.

Comparing the spontaneous activity recorded here with retinal waves, a common feature is that in both cases the retinal circuits lack input from the photoreceptors. This suggests not only that the rhythmic retinal activity is suppressed by active photoreceptors, but also underlines that the rhythmic activity is generated upstream to RGCs, as it is in postnatal retinal waves.

An interesting feature of retinal physiology found here is the difference of maintained activity in ON- and OFF-cells of the rat, which is not lost under illumination.

The rat OFF-RGCs are especially sensitive to retinal degeneration as shown for *rd* (Sekirnjak et al., 2011) and for glaucomatous degeneration here. In the case that photoreceptors are intact and RGCs degenerate, like in glaucoma, no rhythmic activity was detected in upstream cells.

Therefore the loss of a cell class is not the trigger for rhythmic activity, but the deprivation of sensory input.

4.3 Phenomenology of the rhythmic RGC activity and LFPs in the *rd1* retina

In the present study maintained activity was recorded in normal C57Bl/6 mice and two mouse strains with photoreceptor loss caused by a mutation in the PDE6b gene (C3H and FVB strains).

In this study rhythmic activity was recorded in the majority of RGCs investigated. Rhythmic RGC activity has been found in three morphologically identified *rd1* RGCs (Margolis et al., 2008) and at much longer time-scales in rod-degenerated rat RGCs (Kolomiets et al.,2010; Sauve et al., 2001; Marc et al., 2003; Sekirnjak et al., 2009). It is therefore tempting to speculate that photoreceptor degeneration induces pathologic rhythmic activity in the human disease of *retinitis pigmentosa*.

Photoreceptor degenerated retinas retain functional synaptic connections with higher visual centres in mice (Thyagarajan et al.,2010; Bi et al., 2006; Lagali et al., 2008; Lin et al., 2008) and humans (Chen et al., 2006; Zrenner et al., 2010). An early study in anaesthetized *rd1* mice reports rhythmic activity in neurons of the superior colliculus (Drager and Hubel, 1978) that are postsynaptic to RGCs. Correlated RGC activity in restricted retinal areas driven by extended LFPs (**Fig. 3.5 b**, **Fig. 3.6, Fig.3.7**) may thus give rise to photopsias reported by *RP* patients. A high percentage of *RP* patients describe the sensation of phosphenes or some forms of flashes (Heckenlively et al., 1988; Bittner et al., 2009). It's hypothesized that phosphenes occur from the high percentage of synchronous RGC spikes (**Fig. 3.4**) that may lead to elevated activity in higher visual areas (Drager and Hubel, 1978).

Maturation of neuronal circuits is characterized by spontaneous synchronized activity that propagates across extended neural circuits (Wong, 1999; Blankenship et al., 2009). A characteristic feature of developing retinas is concerted RGC activity, reflected as calcium waves or RGC population bursts (Wong, 1999; Blankenship et al., 2009). In developmental waves and in *rd1* retinas (**Fig. 3.5**) consecutive population bursts are initiated in close proximity. However, in developing retinas the inter-burst intervals (seconds - minutes) are much longer as compared to the degenerated *rd1* retinas (~100-150msec).

In *rd1* retinas, LFPs expanded and propagated across the retinal ganglion cell layer, depolarizing the RGCs in the corresponding areas. The propagation velocity (8 mm/sec) is by an order of magnitude higher than the velocities measured across developmental retinal waves in different species (0.1 - 1.5 mm/sec) (Wong, 1999).The fastest developmental waves (stage I) were abolished by gap junction blockers (Syed et al., 2004) as were the wave-like LFPs in this study. Slower waves (stage III) are suggested to rely on glutamate spill over (Blankenship et al., 2009). This mechanism appears unlikely here. The application of AMPA/kainate antagonists did not block stage III waves, indicating that extrasynaptic glutamate receptors are involved. In the *rd1* retinas, LFPs are abolished by AMPA/kainate antagonists.

4.4 Mechanisms underlying the rhythmic RGC activity and the propagating local field potentials

RGCs rhythmic activity could originate within the cells themselves or could be driven by presynaptic input. A previous patch-clamp study established that three identified RGC subtypes are driven by rhythmic presynaptic input (Margolis et al., 2008). Our data are consistent with this result. Rhythmic spiking ceases after the application of *iGlu* receptors antagonists that suppress excitatory presynaptic input to RGCs (**Fig. 3.10**). We therefore infer that RGCs do not act as pacemakers in the *rd1* retina. In the adult *rd1* retina, glutamate is released by bipolar cells, as the majority of photoreceptors are lost. The pharmacological experiments (**Fig. 3.8, Fig. 3.9 & Fig 3.10**) demonstrate that *rd1* RGCs receive an excitatory rhythmic driving force that is absent in *wt* retinas. This driving force is modulated but does not rely on inhibitory neurotransmitters.

How does the rhythmic activity propagate across the retina? We discussed that glutamate spill-over is unlikely to mediate the activity propagation in *rd1* retinas. Our results suggest that gap junctions are involved (**Fig 3.11**). Electrical coupling is abundant in the retina (for review see Sohl et al., 2005; Bloomfield and Volgyi, 2009) and has been reported between all major neuronal classes. Our recordings demonstrate that the coupling strength between *rd1* RGCs is twice as large as that in *wt* retinas (**Fig. 3.3**). Strong electrical RGC coupling persists when *iGlu* receptors and thus LFPs are blocked (**Fig 3.10**). However, the propagation of membrane depolarisations through strong electrical RGC synapses appears unlikely. The majority of rhythmic RGCs are out of phase (**Fig.3.4**) and do not display electrical coupling (**Fig 3.3c).** Photoreceptors largely disappeared in the adult *rd1* retina (Lin et al., 2009). Horizontal cells are electrically coupled in *wt* retinas (Hombach et al., 2004; Bloomfield and Volgyi, 2009) but their coverage diminishes during degeneration (Strettoi and Pignatelli, 2000). Among the amacrine cells, one of the most abundant cell types is the glycinergic AII cell (Wässle, 2004). Strychnine strongly modulates the LFPs in *rd1* retinas (Suppl.Fig.2) suggesting the contribution of glycinergic cells. AII cells are electrically coupled to ON bipolar cells (Strettoi et al., 1992; Feigenspan et al., 2001) and to neighbouring AIIs (Veruki and Hartveit, 2002). Signal transmission between electrically coupled neurons and specifically between AII amacrine cells exhibit low-pass filter characteristics (Veruki and Hartveit, 2002). Lower coupling strength between AII cells results in higher phase

shift between paired voltage traces (Veruki et al., 2008). The almost random distribution of CC phase lags between rhythmic RGCs (**Fig. 3.4**) may be attributed to variable gap junction coupling between AII cells or between AII and bipolar cells. Indirect evidence reporting the accumulation of glycine in bipolar cells of rod degenerated rat retinas suggests increased gap junction permeability between bipolar and AII amacrine cells (Fletcher, 2000). Furthermore, TTX inhibits voltage-gated sodium channels in AII cells and slows down the output of the AII network (Tian et al.,2010). This could explain the decreased LFP propagation velocity in TTX treated *rd1* retinas (**Table 2**).

We therefore suggest the transmission of excitation from rhythmic bipolar cells through a network of electrically coupled amacrine cells.

Consistent with this conclusion, a recent patch-clamp study reported rhythmic activity in rd mouse cone bipolar cells, that is independent of chemical synaptic input and must rely on electrical coupling with amacrine cells (Borowska et al., 2011).

4.5 Induction of the rd1 mouse phenotype in C57Bl/6 mice

The recordings of *rd1* RGCs and pharmacologic experiments conducted here showed that only glutamate antagonists and gap junction blockers affect the spiking pattern in *rd1* mice. Constant wash in of Strychnine and SR 95531 had no effect on RGC spiking and the LFP in *rd1*.

It is known, that in the *rd1* mouse the process of neural remodeling is delayed and not observed before PND 600 (Marc & Jones 2005). From the morphologic changes reported is unknown how and if they affect the physiology of cells downstream of photoreceptors and horizontal cells (see **Introduction**). The most obvious change in the rd1 mouse is the loss of photoreceptors and concomitantly the loss of the dark current. The permanent release of glutamate in darkness silences ON-BCs, while the stop of glutamate release activates them.

As other profound structural changes are absent in this animal model, I suggest that

A prevention of dark current mediated glutamate release for a long time triggers a *rd1* activity in healthy mouse retinas.

This idea, that *rd1* acts similar to a strong light stimulus, was first formulated as "equivalent light hypothesis" (Fain & Lissmann, 1993), which was aimed to

understand photoreceptor degeneration itself, but can be transferred to the downstream neurons also.

In the present experiments constant illumination or bleaching increased the firing rate and initiated oscillating spiking in about half of the cells, mainly OFF-cells (**Fig. 3.14**). Constant illumination constantly activates the PDE and prevents glutamate release (Fain et al. 2001).

Long term illumination elevates the spontaneous firing rate in ON-RGCs which must be due to elevated release of glutamate from ON-BCs.

ON-BCs are known to cross inhibit OFF-BCs and OFF-RGCs (Liang & Freed, 2010) and experiments using L-AP4 in light adapted retinas show, that pharmacologic "decoupling" of ON-BCs from photoreceptors increases the activity of OFF-RGCs (Müller et al., 1988) in cats.

The rhythmic spiking in RGCs here relies on glutamatergic input, thereby the oscillation have to be generated by BCs or ACs. How could the loss of the dark current trigger rhythmic activity ?

One possibility is that ON-BCs start a rhythmic release of glutamate as it was found in ON-CBCs in rd1 mice (Borowska et al., 2011). In our *wt* data only a minority of ON-RGCs gathered rhythmic spiking during illumination.

This may indicate that either the ON-BCs do not rhythmically release glutamate or that they are rhythmic, but lack synchrony. In the latter case the single rhythmic EPSPs at the dendrites of RGCs will be averaged out.

Rhythmic activity in OFF-cells may be due to pace maker properties in OFF-cells (Margolis et al., 2007), which initiated a stable 5 Hz oscillation upon bleaching. However, the rhythm may also originate from rhythmic wide-field amacrine cells (Petite-Jaques et al., 2005).

In additional experiments where Strychnine and SR 95531 were applied during illumination, we were able to demonstrate, that inhibitory synapses are not involved in the initiation of rhythmic activity (**Fig. 3.15**). Therefore a participation of amacrine cells, which release only inhibitory neurotransmitter, via chemical synapses, can be excluded. The exact mechanism for the generation of rhythmic spiking for ON- and OFF-cell has to be elucidated in future studies.

During blockage of inhibitory synapses, the emergence of a static Local Field potential and the high degree of synchronization between the cells, which was not present during spontaneous illumination, demonstrate, that loss of dark current with concomitant loss of inhibition are the conditions to enable rhythmic

hyperactivity (**Fig. 3.16**). The variance of the fundamental frequencies observed in the experiments using Strychnine and SR 95531 during illumination may be due to variation in local blocker concentrations. I suggest that loss of inhibition trigger the bipolar cells and that the LFP reflects the activation of large BC populations at once. After loss of inhibitory signaling the source of rhythmic excitation must be the membrane properties of bipolar cells and perhaps gap junctions are involved.

Bipolar cells have fast and slow transmitter vesicle reservoir at their synaptic knobs And maybe the rhythmic activity reflects the kinetic of depletion and restoration of the glutamate transmitter reservoir (Petite-Jaques & Bloomfield, 2008).

4.6 Pharmacology of rat RGC activity in during bleaching

Wistar rat RGCs responded slightly different to the procedure before tested in mice. The RGCs spontaneous firing rates was sensitive to bleaching, but no rhythmic activity appeared.

Application of neurotransmitter antagonists for GABAergic, glycinergic and glutamatergic synapses changed the RGC maintained activity, but rather increased than abolished maintained activity in OFF-cells.

A recent study (Margolis & Detwiler, 2007) suggests that OFF-RGCs display pacemaker properties and their maintained firing is insensitive to synaptic blockers. However, while the blockers used here did also not abolish OFF-RGC activity (**Fig. 3.17**), a study in P23H rats reported a decrease of RGC firing rates after wash in of synaptic blockers (Sekirnjak et al., 2011) for a longer time (> 10 minutes), at higher concentrations and additionally used a blocker for ACh-receptors.

It is known that starburst amacrine cells release ACh and also during this study Curare was used to block cholinergic activity in the retina (not shown). But it was found here that ACh receptor antagonists work only in high concentrations and not reliably.

That the blockage of inhibitory synapses induces oscillatory spiking is consistent with my findings in mouse, though wistar RGCs display a lower fundamental frequency (**Fig. 3.18**) at ~ 3 Hz.

The results in rat and mouse demonstrate that the retina is capable of regaining of rhythmic activity, by simple deafferentation and decrease of inhibitory synapse strength.

Retinal wave like activity is therefore blocked in the retina after eye opening by activation of the photoreceptors and inhibitory synaptic signaling.

4.7 RGC degeneration after axonal injury

RGCs are directly affected in a variety of retinal diseases e.g. glaucoma and some forms of retinal degeneration in animal models (in P23H and RCS rats; Sekirnjak et al. 20111)..

In the present study changes in retinal ganglion cell physiology were investigated in rats after optic nerve injury.

Significant changes in intra-retinal axonal conduction velocity were measured at postoperative day four in rats, but did not change significantly further. The mean intra-retinal velocity in operated retinas remained at approximately 71% of the control value (**Fig. 3.21**).

Additionally OFF-RGCs in operated rat retina showed significantly decreased spontaneous activity (**Fig. 3.23**).

 For all five functional cell types identified in rat retina (**Fig. 3.24** and **Table 3**) the average firing rate of the light response decreased after the operation while the response latency increased (**Tables 4 & 5**).

Evaluation of the spatial resolution of surviving RGCs using grating stimuli with increasing spatial frequency showed that RGCs of most operated animals were not longer able to discriminate bars of 0.1 cycles/degree. Again, operated animals showed a decreased firing rate during these experiments (**Fig. 3.26**)

4.8 Changes of intra-retinal axon function after injury

In rats the mean axon density does not decrease within the first four days following optic nerve crush but a reduction within 14 days was reported (Kanamori et al., 2010, Mey &Thanos, 1993). As the loss of single intra-retinal axons is difficult to determine the decrease of labeled retinal ganglion cells has been used to infer axon loss. A variety of intra-axonal changes have been reported in axons following optic nerve injury. These changes include axonal deformations (Allcutt et al. 1984, Germain et al. 2007) and various cytological alterations (Barron et al.,1986). In DBA mice, axonal atrophy is reported to precede RGC degeneration (Jakobs et al., 2005). However, it is unclear if the axon diameter decreases early (within two weeks)

following ONC (Misantone et al. 1984). In axotomized kitten, axon diameter is only slightly changed (Watanabe & Fukuda, 2002). Additionally, a recent study demonstrates that, injured axon are rapidly defragmented after lesion, too fast to assume a prior shrinkage (Knoferle et al., 2010).

According to classical cable theory (Hodgkin, 1954) the conduction velocity of unmyelinated axons depends on axon diameter and intra-retinal resistivity.

In axotomized RGCs, it was shown that sealing of the axonal stump by internal vesicles is critical for axonal survival (Tuck & Cavalli, 2010). The seal constituted by the vesicles is important to maintain the electrical functions of the axon (Fishman & Bittner, 2003; Eddleman et al., 2000; Zelena et al., 1968; Godell et al. 1997).

Sealing maintains the electrical function of the axon, otherwise vesicle traffic could increase the axon's inner resistivity.

Here, I recorded a significant decrease in axonal propagation velocity prior to massive cell loss (**Fig. 3.21**). This suggests that morphologic features like axon diameter are not yet altered.

I suggest, that the significant but not large reduction in axon conduction velocity is due to an increase of the inner axonal resistance and less to shrinkage of axon diameter. The axon therefore maintains much of its electrical functionality until complete collapse.

Impairment of axonal conduction should precede loss of somatic function. Recordings with rabbits in our lab that received optic nerve crush, demonstrated reduced axonal propagation velocity after one week when the cell responses were not altered (*experiments done by* Christian Leibig).

In rat recordings, the earliest recording time point (d4) was either too late to detect differences between axonal and somatic degeneration or both events occur concomitant. I conclude that both events are in close temporal proximity and that the time, axonal malfunction precedes somatic degenerative changes must be very short.

4.9 Changes of retinal ganglion cell function after injury

The somata and dendrites of retinal ganglion cells are affected by optic nerve injuries. The RGC density decreases (Berkelaar et al., 1994), soma and dendrites of the surviving RGCs shrink soon after injury (Leung et al., 2011, Thanos, 1988).

Shrinking dendritic area should cause decreased synaptic input and leads to altered light responses of surviving cells. Operated OFF-cells showed a significant decrease of response latency after four days post-operative, while ON-cells were unaffected until day eight (**Table 5**). The average firing rate was decreased for both cell types at four days post-operative (**Table 6**).

In a study using axotomized cats (Takao et al., 2002) was shown that the surviving RGCs maintain their response properties (X- and Y-cells), but some cells show decreased firing rates. It was therefore suggested that RGC membrane properties change and excitability is lowered.

The integrity of synaptic input was tested here using gratings of increasing spatial frequency. This stimulus is more sensitive, as the spatial resolution of RGCs depends on denritic tree diameter. For both groups the spatial resolution is clearly decreased At four days after surgery (**Fig. 3.26)**, indicating changes in dendrite structure.

In OFF cells all properties examined here, maintained firing rate, response latency response firing rate are decreased at the earliest time point, while in ON-cells initially only the light response showed a decreased firing rate.

For both cell types the conduction velocity as well as the visual acuity was decreased as early as four days after surgery.

The assignment of the observed changes to compartments is speculative. The pharmacologic analysis of rat RGCs suggest that OFF-cells may exhibit pace maker properties and that the decrease in maintained firing rate can be due to altered membrane properties as suggested for axotomized cats (Takao et al., 2002).

But response latencies for ON-cells are significantly changed until a change in maintained activity is detected. Also the average light evoked firing rate is altered prior to any change in spontaneous spiking. Therefor spontaneous spiking in ON-RGCs may also only partially rely on presynaptic input.

Beside the difficulties that are related to the unknown origin of maintained activity, changes in light responsiveness seem to be related to changes in synaptic input for both cell types.

4.10 The challenge of neuronal degeneration

Like all tissues neuronal structures are subject to acquired and inherited diseases as well as to contingent injuries. Cells of similar function exist in million copies in each tissue and the mass compensates the loss or malfunction of single elements or small populations, while the immune system prevents a spreading of the disease.

When larger proportions of cells are affected, the organ or tissue needs medical treatment. The aim of treatment is the maintenance by application of inhibiting and/or promoting substances that rebalance the tissues condition. In cases where this is unsuccessful, modern medicine tries to replace the organ either by prosthesis or a donated organ.

These methods are well established for a lot of organs, heart, kidney and liver can be replaced which is not possible with the brain and this not only for surgical reasons.

The brain has a complex internal structure and surgery revealed that interruption of neuronal circuits fundamentally changes personality and furthermore, neuronal function. Intervention into neuronal structures in human calls therefore for caution and attention. Different is the situation with the PNS, where medical problems focus on axonal integrity and growth promotion. Though this implies less structural and ethical complexities, the regeneration of peripheral nerves is still puzzling.

Nevertheless the palette of neurological and psychiatric diseases is long and treatments are necessary.

Manipulation of retinal tissue has not so many ethical implications as in the brain, but faces similar practical problems. Therefore a lot of treatment strategies designed and evaluated in the retina may later be applied to cortical sites.

In principle, retinal defects can be treated by the application of neuroprotective or growth promoting substances, surgery, stem cell therapy (MacLaren et al. 2006), optogenetics (Busskamp et al., 2011) and prostheses.

Recent studies using optogenetic tools showed that responsiveness of retinal channels in *rd1* can be restored, but the behavioural experiments undertaken do not answer the question if complete vision is restored (Thyagarajan et al., 2010; Busskamp et al. 2010).

It was shown here by bleaching experiments that aberrant activity in *rd1* retinas is mainly due to deafferentation and may be silenced as sensory input enters into the circuit.

In glaucoma, the growth promoting effect of cristallins on injured axons provides a new perspective for treatments (Fischer et al., 2008). Otherwise in surgery the use of nerve grafts becomes common, that allows axons to regenerate and grow into their target region (Myoshi et al., 2010), but its use is by now restricted to the PNS.

The most advanced treatment approach for injured sensory neurons that is currently in clinical trial phase, are neuro-prostheses, in the case of the retina, the retina prosthesis.

Prostheses are external devices that can be removed easier than stem cells or genes delivered to target cells. That made them more appealing on the ethical level. On the other hand it's difficult to bring electronics in close contact with the correct targets and tune the device to either receive or deliver signals properly.

The development of semiconductor technology makes the devices smaller and as it is seen by the MTA-chip used here, transistors are small enough to come in contact with just one cell that they can stimulate or read out (Fromherz, 2002). Actually a stimulation chip, implanted into the eye of patients with retinitis pigmentosa, is in clinical trial and so far enables the patient's simple vision (Zrenner et al., 2011).

Such smart devices could also bridge the gap between eye and brain when the optic nerve is degenerated and are useful to treat a variety of neurologic diseases.

REFERENCES

Allcutt, D., Berry, M., & Sievers, J. (1984). A qualitative comparison of the reactions of retinal ganglion cell axons to optic nerve crush in neonatal and adult mice. Brain Research,318 (2), 231-240.

Almasieh M, Zhou Y, Kelly ME, Casanova C, Di Polo A (2010) Structural and functional neuroprotection in glaucoma: role of galantamine-mediated activation of muscarinic acetylcholine receptors. Cell Death Dis e27

Ala-Laurila P, Greschner M, Chichilnisky EJ, Rieke F (2011) Cone photoreceptor contributions to noise and correlations in the retinal output. Nat Neuroscience 4(10):1309-16

Baltan, S., Inman, D.M., Danilov, C.A., Morrison, R.S., Calkins, D.J., & Horner, P.J. (2010). Metabolic Vulnerability Disposes Retinal Ganglion Cell Axons to Dysfunction in a Model of Glaucomatous Degeneration. J. Neurosci., 30 (16), 5644-5652.

Barron, K.D., Dentinger, M.P., Krohel, G., Easton, S.K., & Mankes, R. (1986).Qualitative and quantitative ultrastructural observations on retinal ganglion cell layer of rat retina after intraorbital optic nerve crush. J. Neurocytology, 15 (3): 345-362.

Berkelaar, M., Clarke, D.B., Wang, Y.C., Bray, G.M., & Aguayo, A.J. (1994). Axotomy results in delayed death and apoptosis of retinal ganglion cells in adult rats. J.Neurosci., 14 (7), 4368-4374.

Bi AD, Cui JJ, Ma YP, Olshevskaya E, Pu ML, Dizhoor AM, Pan ZH (2006) Ectopic expression of a microbial-type rhodopsin restores visual responses in mice with photoreceptor degeneration. Neuron 50:23-33.

Bittner AK, Diener-West M, Dagnelie G (2009) A survey of photopsias in self-reported Retinitis Pigmentosa. Retina 29:1513-1521.

Bird AC (1995) Retinal photoreceptor dystrophies. Am J Ophthal 119, 543-562

Birge RR, Barlow (1995) On the molecular origins of thermal noise in vertebrate and invertebrate photoreceptors.Biophys Chem 55(1-2):115-26

Blankenship AG, Feller MB (2010) Mechanisms underlying spontaneous patterned activity in developing neural circuits. Nat Rev Neurosci 11:18-29.

Blankenship AG, Ford KJ, Johnson J, Seal RP, Edwards RH, Copenhagen DR, Feller MB (2009) Synaptic and Extrasynaptic Factors Governing Glutamatergic Retinal Waves. Neuron 62:230-241.

Bloomfield SA, Volgyi B (2009) The diverse functional roles and regulation of neuronal gap junctions in the retina. Nat Rev Neurosci 10:495-506.

Breuer, O., Lawhorn, C., Miller, T., Smith, D. M., & Brown, L. L. (2005). Functional architecture of the mammalian striatum: mouse vascular and striosome organization and their anatomic relationships. Neuroscience letters, 385(3), 198-203

Bolz, J., Rosner, G., & Wassle, H. (1982). Response latency of brisk-sustained (X) and brisktransient (Y) cells in the cat retina. J. Physiol., 328 171-190.

Borowska T, Trenholm S, Awatramani GB (2011) An intrinsic neural oscillator in the degenerating mouse retina. J Neurosci 31(13):5000-12

Borst A , Euler T (2011) Seeing things in motion: Models, Circuits and Mechanisms. Neuron 71 (6) 974-994

Brivanlou, I. H., Warland, D. K., & Meister, M. (1998). Mechanisms of concerted firing among retinal ganglion cells. Neuron, 20(3), 527-39.

Busskamp V, Duebel J, Balya D, Fradot M, Viney TJ, Siegert S, Groner AC, Cabuy E, Forster V, Seeliger M, Biel M, Humphries P, Paques M, Mohand-Said S, Trono D, Deisseroth K, Sahel JA, Picaud S, Roska B (2010) Genetic Reactivation of Cone Photoreceptors Restores Visual Responses in Retinitis Pigmentosa. Science 329:413-417.

Busskamp V, Picaud S, Sahel JA, Roska B (2011) Optogenetic therapy for retinitis pigmentosa. Gene Ther., epub ahead of print

Buszaki G (2006) Rhythms of the brain.Oxford University Press

Calvet, M. C. (1974). Patterns of spontaneous electrical activity in tissue cultures of mammalian cerebral cortex vs. cerebellum. Brain research, 69(2), 281-95.

Carter-Dawson, L. D., & LaVail, M. M. (1979). Rods and cones in the mouse retina. II. Autoradiographic analysis of cell generation using tritiated thymidine. The Journal of comparative neurology, 188(2), 263-72.

Carlen PL, Skinner F, Zhang L, Naus C, Kushnir M, Velazquez JLP (2000) The role of gap junctions in seizures. Brain Research Reviews 32:235-241.

Castro-Alamancos MA, Rigas P, Tawara-Hirata Y (2007) Resonance (similar to 10 Hz) of excitatory networks in motor cortex: effects of voltage-dependent ion channel blockers. J. Physiol. 578:173-191.

Chang B, Hawes NL, Hurd RE, Davisson MT, Nusinowitz S, Heckenlively JR (2002) Retinal degeneration mutants in the mouse. Vision Res. 42:517-525.

Chen S-J, Mahadevappa M, Roizenblatt R, Weiland J, Humayun M (2006) Neural responses elicited by electrical stimulation of the retina. Trans Am Ophthalmol Soc 104:252-59

Chua J, Fletcher EL, Kalloniatis M (2009) Functional Remodeling of Glutamate Receptors by Inner Retinal Neurons Occurs From an Early Stage of Retinal Degeneration. J. Comp. Neurol. 514:473-491.

Coleman, M. (2005). Axon degeneration mechanisms: Commonality amid diversity. Nature Reviews Neuroscience, 6 (11), 889-898.

Colicos, M, Firth, S. I., Bosze, J., Goldstein, J., & Feller, M. B. (2004). Emergence of realistic retinal networks in culture promoted by the superior colliculus. Devl neurosci, 26(5-6), 406-16.

Creutzfeldt, O., & Sakmann, B. (1969). Neurophysiology of vision. Ann. Rev. Physiol, 31, 499-544.

Daw NR, Jensen RJ, Brunken, WJ (1990) Rod pathways in mammalian retinae. Trends Neurosci Mar;13(3):110-5

Demas J, Eglen SJ, Wong ROL (2003) Developmental loss of synchronous spontaneous activity in the mouse retina is independent of visual experience. J.Neurosci. 23:2851-2860.

Drager UC, Hubel DH (1978) Studies of visual function and its decay in mice with hereditary retinal degeneration. J.Comp.Neurol.180:85-114.

Drager UC, Olsen JF (1981) Ganglion-cell distribution in the retina of the mouse. Inv. Ophthalmology & Visual Sci. 20:285-293.

Dreosti E, Esposti F, Baden T, Lagnado L (2011) In vivo evidence that retinal bipolar cells generate spikes modulated by light. Nat Neurosci 14(8):951-2

Dudek FE, Yasumura T, Rash JE (1998) 'Non-synaptic' mechanicsms in seizures and epileptogenesis. Cell Biology Intern. 22:793-805.

Dyer MA, Cepko CL (2001)Regulating oproliferation during retinal development. Nat Rev Neurosci. 1 May;2(5):333-42

Eversmann B, Jenkner M, Hofmann F, Paulus C, Brederlow R, Holzapfl B, Fromherz P, Merz M, Brenner M, Schreiter M, Gabl R, Plehnert K, Steinhauser M, Eckstein G, Schmitt-Landsiedel D, Thewes R (2003) A 128x128 CMOS biosensor array for extracellular recording of neural activity. IEEE J. Solid-State Circuits 38:2306-2317.

Euler T, Wässle H (2004) Immunocytochemical identification of bipolar cells in the rat retina. J Comp Neurol 361(3) 461-478

Fain GL, Lissman JE (1993) Photoreceptor degeneration in vitamin A deprivation and retinitis pigmentosa: the equivalent light hypothesis. Exp Eye Res 57(3):335-40

Fain GL, Mathews HR, Cornwall MC, Koutalos Y (2001) Adaption in vertebrate photoreceptors.Physiol Rev 81(1):117-151

Fariss RN, Li ZY, Milam AH (2000) Abnormalities in rod photoreceptors, amacrine cells, and horizontal cells in human retinas with retinitis pigmentosa. Am. J. Ophthalmology 129:215-223.

Feigenspan A, Gustincich S, Bean BP, Raviola E (1998) Spontaneous activity of solitary dopaminergic cells of the retina. J. Neurosci. 18:6776-6789.

Feigenspan A, Teubner B, Willecke K, Weiler R (2001) Expression of neuronal connexin36 in AII amacrine cells of the mammalian retina. J. Neurosci. 21:230-239.

Fletcher EL (2000) Alterations in neurochemistry during retinal degeneration. Microscopy Res. & Tech. 50:89-102.

Flint AC, Connors BW (1996) Two types of network oscillations in neocortex mediated by distinct glutamate receptor subtypes and neuronal populations. J.Neurophysiol. 75:951-956.

Firth, S. I., Wang, C.-T., & Feller, M. B. (2005). Retinal waves: mechanisms and function in visual system development. Cell calcium, 37(5), 425-32.

Fischer, D., Hauk, T. G., Müller, A., & Thanos, Solon. (2008). Crystallins of the beta/gamma-superfamily mimic the effects of lens injury and promote axon regeneration. Molecular and cellular neurosciences, 37(3), 471-9.

Franze, K., Grosche, J., Skatchkov, S. N., Schinkinger, S., Foja, C., Schild, D., et al. (2007). Muller cells are living optical fibers in the vertebrate retina. Proceedings of the National Academy of Sciences of the United States of America, 104(20), 8287-92.

References

Gao J, Schwartz G, Berry MJ, Holmes P (2009) An oscillatory circuit underlying the detection of disruptions in temporally-periodic patterns. Network 20:106-135.

Germain, F., Calvo, M., & de la Villa, P. (2004). Rabbit retinal ganglion cell survival after optic nerve section and its effect on the inner plexiform layer. Exp Eye Res, 78(1), 95-102.

Germain, F., Fernandez, E., & de la Villa, P. (2003). Morphometrical analysis of dendritic arborization in axotomized retinal ganglion cells. Europ. J. Neurosci., 18 (5), 1103-1109.

Germain, F., Fernandez, E., & La Villa, P.D. (2007). Morphological signs of apoptosis in axotomized ganglion cells of the rabbit retina. Neuroscience, 144 (3), 898-910.

Goddel CM, Smyers ME, Eddleman CS, Ballinger ML, Fishman HM, Bittner GD (1997) Calpain promotes the sealing of severed giant axons. PNAS 94(9):4751-6

Goldblum, D., & Mittag, T. (2002). Prospects for relevant glaucoma models with retinal ganglion cell damage in the rodent eye. Vision Research, 42 (4), 471-478.

Gosh KK, Bujan S, Haverkamp S, FEigenspan A, Wässle H (2003) Types of bipolar cells in the mouse retina. J Comp Neurol 26: 70-82

Grafstein .B, Murray M, Ingoglia NA (1972) Protein syntheisi and axonal transport in retinal ganglion cells of mice lacking photoreceptors . Brain Research 44: 37.

Gray CM, Maldonado PM, Wilson M, McNaughton B (1995) Tetrodes markedly improve the reliability and yield of multiple single-unit isolation from multi-unit recordings in cat striate cortex. J Neurosci Methods 63(1-2):43-54

Griffin, W.; Glass, D., & George, B. (1995). Axotomy-Induced Axonal Degeneration is mediated by calcium influx Influx through Ion-Specific Channels. J Neurosci 15(10), 6445-52 .

Heckenlively JR, Yoser SL, Friedman LH, Oversier JJ (1988) CLINICAL FINDINGS AND COMMON SYMPTOMS IN RETINITIS PIGMENTOSA. Am. J. Ophthalmology 105:504-511.

Hanganu, I. L., Ben-Ari, Y., & Khazipov, R. (2006). Retinal waves trigger spindle bursts in the neonatal rat visual cortex. The Journal of neuroscience 26(25), 6728-36.

Heflin SJ, Cook PB (2007) Narrow and wide field amacrine cells fire action potentials in response to depolarization and light stimulation. Vis Neurosci 24(2):197-206

Heiduschka, P., & Thanos, S. (2000). Restoration of the retinofugal pathway. Progress in retinal and eye research, 19(5), 577-606.

Heiduschka, P., Julien, S., Schuettauf, F., & Schnichels, S. (2010). Loss of retinal function in aged DBA/2J mice - New insights into retinal neurodegeneration. Experimental Eye Research, 91 (5), 779-783.32

Hellström M, Harvey AR (1998) Retinal ganglion cell gene therapy and visual system repair. Curr Gene Ther 11(2):116-31

Hombach S, Janssen-Bienhold U, Sohl G, Schubert T, Bussow H, Ott T, Weiler R, Willecke K (2004) Functional expression of connexin57 in horizontal cells of the mouse retina. Europ. J. Neurosci. 19:2633-2640.

References

Hodgkin, A.L. (1954). A note on conduction velocity. J.Physiol. 125 (1), 221-224.

Hodgkin Al, Huxley AF (1952) Propagation of electrical signals along giant nerve fibers. Proc R Soc Lond B Biol Sci 140(899):177-83.

Hu EH, Bloomfield SA (2003) Gap junctional coupling underlies the short-latency spike synchrony of retinal alpha ganglion cells. J. Neurosci. 23:6768-6777.

Hughes, A. Wässle H (1979). An estimate of image quality in the rat eye. IOVS, 18 (8), 878-81..

Humayun MS, Prince M, de Juan E, Barron Y, Moskowitz M, Klock IB, Milam AH (1999) Morphometric analysis of the extramacular retina from postmortem eyes with retinitis pigmentosa. Investigative Ophthalmology & Visual Science 40:143-148.

Jakobs, T.C., Libby, R.T., Ben, Y.X., John, S.W.M., & Masland, R.H. (2005). Retinal ganglion cell degeneration is topological but not cell type specific in DBA/2J mice. Journal Cell Biol,171 (2), 313-325.

Jiménez, a J., García-Fernández, J. M., González, B., & Foster, R. G. (1996). The spatio-temporal pattern of photoreceptor degeneration in the aged rd/rd mouse retina. Cell and tissue research, 284(2), 193-202.

Jones, B. W., & Marc, R. E. (2005). Retinal remodeling during retinal degeneration. Experimental eye research, 81(2), 123-37.

Kanamori, A., Catrinescu, M.-M., Traistaru, M., Beaubien, R., & Levin, L.A. (2010). In VivoImaging of Retinal Ganglion Cell Axons within the Nerve Fiber Layer. Investigative Ophthalmology & Visual Science, 51 (4), 2011-2018.

Keeler, C. E. (1924). The Inheritance of a Retinal Abnormality in White Mice. Proceedings of the National Academy of Sciences of the United States of America, 10(7), 329-33.

Kermer, P., Klocker, N., Weishaupt, J.H., & Bahr, M. (2001). Transection of the optic nerve inrats: studying neuronal death and survival in vivo. Brain Research Protocols, 7 (3), 255-260.

Klocker, N., Zerfowski, M., Gellrich, N.C., & Bahr, M. (2001). Morphological and functional analysis of an incomplete CNS fiber tract lesion: Graded crush of the rat optic nerve. J.Neurosci. Methods, 110 (1-2), 147-153.

Knoferle, J., Koch, J.C., Ostendorf, T., Michel, U., Planchamp, V., Vutova, P., Tonges, L.,Stadelmann, C., Bruck, W., Bahr, M., & Lingor, P. (2010). Mechanisms of acute axonal degeneration in the optic nerve in vivo. Proc. Nat. Acad. Sci., 107 (13), 6064

Kolb H, Gouras P (1974) ELECTRON-MICROSCOPIC OBSERVATIONS OF HUMAN RETINITIS PIGMENTOSA, DOMINANTLY INHERITED. Investigative Ophthalmology 13:487-498.

Kolb H, Nelson R, Fernandez E, Brian R (2011): Webvision - The organization of the Retina and Visual System. http://webvision.med.utah.edu/

Kolomiets B, Dubus E, Simonutti M, Rosolen S, Sahel JA, Picaud S Late histological and functional changes in the P23H rat retina after photoreceptor loss. Neurobiology of Disease 38:47-58.

Korsching, S. (1993). The neurotrophic factor concept: a reexamination. The Journal of neuroscience : the official journal of the Society for Neuroscience, 13(7), 2739-48.

Kurokawa, T., Katai, N., Kikuchi, T., Shibuki, H., Kuroiwa, S., Arai, J., (1999). Apoptotic Photoreceptors of Royal College of Surgeons Rats. Investigative Ophthalmology, 40(8), 1802-1886.

Krishnamoorthy, R. R., Agarwal, P., Prasanna, G., Vopat, K., Lambert, W., Sheedlo, H. J., et al. (2001). Characterization of a transformed rat retinal ganglion cell line. Brain research. Molecular brain research, 86(1-2), 1-12.

Kuffler, S.W., Fitzhugh, R., & Barlow, H.B. (1957). Maintained activity in the cat's retina inlight and darkness. J. Gen Physiol, 40 (5), 683-702.

Kuffler SW (1953) Discharge patterns and functional organization of the mammalian retina. J Neurophysiol Jan;16(1):37-68

Lagali PS, Balya D, Awatramani GB, Munch TA, Kim DS, Busskamp V, Cepko CL, Roska B (2008) Light-activated channels targeted to ON bipolar cells restore visual function in retinal degeneration. Nature Neurosci. 11:667-675.

Lambacher A, Jenkner M, Merz M, Eversmann B, Kaul RA, Hofmann F, Thewes R, Fromherz P (2004) Electrical imaging of neuronal activity by multi-transistor-array (MTA) recording at 7.8 µm resolution. Applied Physics A 79:1607-1611.

Lambacher A, Vitzthum V,Zeitler R, Eickenscheidt M, Eversmann B, Thewes R, Fromherz P (2010) Identifying Firing Mammalian Neurons in Networks with High-Resolution Multi-Transistor Array (MTA) Applied Physics A, in press

Levkovitch-Verbin, H. (2004). Animal models of optic nerve diseases. Eye (London, England), 18(11), 1066-74.

Levkovitch-Verbin, Hani, Dardik, R., Vander, S., & Melamed, S. (2010). Mechanism of retinal ganglion cells death in secondary degeneration of the optic nerve. Experimental eye research, 91(2), 127-34.

Leung, C.K.-s., Weinreb, R.N., Li, Z.W., Liu, S., Lindsey, J.D., Choi, N., Liu, L., Cheung,C.Y.-l., Ye, C., Qiu, K., Chen, L.J., Yung, W.H., Crowston, J.G., Pu, M., So, K.F., Pang, C.P., & Lam, D.S.C. (2011). Long-Term In Vivo Imaging and Measurement of Dendritic Shrinkage of Retinal Ganglion Cells. Investigative Ophthalmology & Visual Science, 52 (3), 1539-1547.

Liang Z, Freed MA (2010) The ON Pathway Rectifies the OFF Pathway of the Mammalian Retina. J Neurosci 30(16): 5533-5543

Lin B, Masland RH, Strettoi E (2009) Remodeling of cone photoreceptor cells after rod degeneration in rd mice. Exp. Eye Res. 88:589-599.

Lin B, Koizumi A, Tanaka N, Panda S, Masland RH (2008) Restoration of visual function in retinal degeneration mice by ectopic expression of melanopsin. Proceedings of the National Academy of Sciences of the United States of America 105:16009-16014.

Masland RH (2001) Neuronal diversity in the retina. Curr Opin Biol 11(4):431-6

MacLaren, R. E., Pearson, R., MacNeil, a, Douglas, R. H., Salt, T. E., Akimoto, M.(2006). Retinal repair by transplantation of photoreceptor precursors. Nature, 444(7116), 203-7.

Majumdar S, Weiss J, Wässle H (2009) Glycinergic input of widefield, displaced amacrine cells of the mouse retina. J Physiol;587(Pt 15):3831-49

Marc RE, Jones BW, Watt CB, Strettoi E (2003) Neural remodeling in retinal degeneration. Progress in Retinal and Eye Research 22:607-655.

Marc RE, Jones BW (2005) Retinal remodelling during retinal degeneration. Exp Eye Res 81(2):123-37

Marc RE, Jones BW, Watt CB, Vasquez-Chona F,Vaughan DK, Organisciak CT (2008) Extreme remodelling triggered by light damage. Mol Vis 14:782-806

Margolis DJ, Newkirk G, Euler T, Detwiler PB (2008) Functional stability of retinal ganglion cells after degeneration-induced changes in synaptic input. J. Neurosci. 28:6526-6536.

Margolis, D.J., & Detwiler, P.B. (2007). Different mechanisms generate maintained activity in ON and OFF retinal ganglion cells. J. Neurosci., 27 (22), 5994-6005.

Mastronarde DN (1989) Correlated firing of retinal ganglion cells. Trends in Neurosci. 12:75-80.

Mazzoni, A., Broccard, F. D., Garcia-Perez, E., Bonifazi, P., Ruaro, M. E., & Torre, V. (2007). On the dynamics of the spontaneous activity in neuronal networks. PloS one, 2(5).

Mazzoni F, Novelli E, Strettoi E (2008) Retinal Ganglion Cells Survive and Maintain Normal Dendritic Morphology in a Mouse Model of Inherited Photoreceptor Degeneration. J. Neurosci. 28:14282-14292.

Menzler, J., & Zeck, G. (2011). Network Oscillations in Rod-Degenerated Mouse Retinas. J. Neurosci., 31 (6), 2280-2291.

Mey, J., & Thanos, S. (1993). Intravitreal injections of neurotrophic factors support the survival of axotomized retinal ganglion cells in adult rats in vivo. Brain research, 602 (2), 304-317.33

Misantone, L.J., Gershenbaum, M., & Murray, M. (1984). Viability of retinal ganglion Cells after optic nerve crush in adult rats. J.Neurocyt., 13 (3), 449-466.

Moore, S., & Thanos, S. (1996). Differential increases in rat retinal ganglion cell size with various methodMüller F, Wässle H, Voigt T (1988) Pharmacological modulation of the rod pathway in the cat retina. J Neurophysiol 59(6):1657-72

Nelson, R., Famiglietti, E. V., & Kolb, H. (1978). Intracellular staining reveals different levels of stratification for on- and off-center ganglion cells in cat retina. Journal of neurophysiology, 41(2), 472-83.

Park SJ, Kim IB, Choi KR, Moon JI, Oh SJ, Chung JW, Chun MH (2001) Reorganization of horizontal cell processes in the developing FVB/N mouse retina. Cell and Tissue Res. 306:341-346.

Penn, a a. (1998). Competition in Retinogeniculate Patterning Driven by Spontaneous Activity. Science, 279(5359), 2108-2112.

Petit-Jacques J, Volgyi B, Rudy B, Bloomfield S (2005) Spontaneous oscillatory activity of starburst amacrine cells in the mouse retina. J.Neurophysiol. 94:1770-1780.

Petrusca, D., Grivich, M.I., Sher, A., Field, G.D., Gauthier, J.L., Greschner, M., Shlens, J., Chichilnisky, E.J., & Litke, A.M. (2007). Identification and characterization of a Y-likeprimate retinal ganglion cell type. J. Neurosci., 27, 11019-11027.

Pinto DJ, Patrick SL, Huang WC, Connors BW (2005) Initiation, propagation, and termination of epileptiform activity in rodent neocortex in vitro involve distinct mechanisms. J.Neurosci. 25:8131-8140.

Plonsey R, Barr RC (2008) Bioelectricity. A quantitavie approach. Springer 2008

Protti DA, Flores-Herr N, von Gersdorff H (2000) Light evokes Ca2+ spikes in the axon terminal of a retinal bipolar cell. Neuron 25:215-227.

Pu M, Xu L,Zhang H (2006) Visual response properties of retinal ganglion cells in the royal college of surgeons dystrophic rat .IOVS 47(8):3579-85

Punzo, C., Kornacker, K., & Cepko, C. L. (2009). Stimulation of the insulin/mTOR pathway delays cone death in a mouse model of retinitis pigmentosa. Nature neuroscience, 12(1), 44-52.

Puthussery T, Taylor RW (2010) Functional Changes in Inner Retinal Neurons in Animal Models of Photoreceptor Degeneration. Adv Exp Med Biol 664(5) 525-532

Quigley, H. (2011). Glaucoma. Lancet, 377(9774), 1367-77.

Raff, M.C., Whitmore, A.V., & Finn, J.T. (2002). Neuroscience - Axonal self-destruction and neurodegeneration. Science, 296 (5569), 868-871.

Rodieck, R. W. (1967). Maintained activity of cat Retinal Ganglion cells. J Neurophysiol. 1967 Sep;30(5):1043-71

Rodieck R. W, (1998) First steps in seeing. Sinauer Publishing

Rufer M, Wirth SB, Hofer A, Dermietzel R, Pastor A, Kettenmann H, Unsicker K (1996) Regulation of connexin-43, GFAP, and FGF-2 is not accompanied by changes in astroglial coupling in MPTP-lesioned, FGF-2-treated Parkinsonian mice. J. Neurosci. Res. 46:606-617.

Ryu S, Ye J, Goo Y (2010) Temporal Response Properties of Retinal Ganglion Cells in rd1 Mice Evoked by Amplitude-Modulated Electrical Pulse Trains. IOVS in press.

Sakmann, B. (1969). Neurophysiology of vision. Annu Rev Physiol. 1969;31:499-544

Santos A, Humayun MS, deJuan E, Greenburg RJ, Marsh MJ, Klock IB, Milam AH (1997) Preservation of the inner retina in retinitis pigmentosa - A morphometric analysis. Archives of Ophthalmology 115:511-515.

Sanyal S, Bal AK (1973) Comparative light and electron-microscopic study of retinal histogenesis in normal and rd mutant mice. Zeitschrift Anatomie & Entwicklungsgeschichte 142:219-238.

Satoh, H., Kaneda, M., & Kaneko, a. (2001). Intracellular chloride concentration is higher in rod bipolar cells than in cone bipolar cells of the mouse retina. Neuroscience letters, 310(2-3), 161-4.

Sekirnjak C, Hulse C, Jepson LH, Hottowy P, Sher A, Dabrowski W, Litke AM, Chichilnisky EJ (2009) Loss of Responses to Visual But Not Electrical Stimulation in Ganglion Cells of Rats With Severe Photoreceptor Degeneration. J. Neurophysiol. 102:3260-3269.

Sengpiel, F., & Kind, P. C. (2002). The Role of Activity in Development of the Visual System Neuronal activity is important for both the initial. Science, 12(02), 818-826.

Shannon CE (1948) A Mathematical Theory of Information. Bell system Technical Journal 27, pp. 379–423

Sharpe LP, Stockmann A (1999) The importance of seeing nothing. Rod pathways in the retina. Trend Neurosci Nov;22(11):497-504

Sinha SR, Saggau P (2001) Imaging of 4-AP-induced, GABA(A)-dependent spontaneous synchronized activity mediated by the hippocampal interneuron network. J.Neurophysiol. 86:381-391.

Singer W (1993) Synchronization of cortical activity and its putative role in information processing and learning. Ann Rev Physiol55:349-74

Sohl G, Maxeiner S, Willecke K (2005) Expression and functions of neuronal gap junctions. Nat Rev Neurosci 6:191-200.

Sowka, J. (2005). New thoughts on normal tension glaucoma. Optometry (St. Louis, Mo.), 76(10), 600-8.

Stasheff SF (2008) Emergence of sustained spontaneous hyperactivity and temporary preservation of OFF responses in ganglion cells of the retinal degeneration (rd1) mouse. J.Neurophysiol. 99:1408-1421.

Steriade M, McCormick DA, Sejnowski TJ (1993) Thalamocortical oscillations in the sleeping and aroused brain. Science 262:679-85

Steriade M, Timofeev I (2003) Neuronal plasticity in thalamocortical networks during sleep and waking oscillations. Neuron 37:563-576

Stone JL, Barlow WE, Humayun MS, Dejuan E, Milam AH (1992) Morphometric analysis of macular photoreceptors and ganglion-cells in retinas with retinitis pigmentosa. Archives of Ophthalmology 110:1634-1639.

Strettoi E, Pignatelli V (2000) Modifications of retinal neurons in a mouse model of retinitis pigmentosa. PNAS 97:11020-11025.

Strettoi E, Raviola E, Dacheux RF (1992) Synaptic connections of the narrow-field, bistratified rod amacrine cell (AII) in the rabbit retina. J. Comp. Neurol. 325:152-168.

Strettoi E, Porciatti V, Falsini B, Pignatelli V, Rossi C (2002) Morphological and functional abnormalities in the inner retina of the rd/rd mouse. J. Neurosci. 22:5492-5504.

Strettoi E, Pignatelli V, Rossi C, Porciatti V, Falsini B (2003) Remodeling of second-order neurons in the retina of rd/rd mutant mice. Vision Research 43:867-877.

Syed MM, Lee S, Zheng JJ, Zhou ZJ (2004) Stage-dependent dynamics and modulation of spontaneous waves in the developing rabbit retina. J Physiology 560:533-549

References

Takao, M., Miyoshi, T., Watanabe, M., & Fukuda, Y. (2002). Changes in visual response properties of cat retinal ganglion cells within two weeks after axotomy. Experimental Neurology, 177 (1), 171-182

Tasman W, Jaeger E A (Eds) Duane's Ophthalmology. Lipincott Williams & Wilkins 2005

Thanos, S. (1988). Alterations in the morphology of ganglion cell dendrites in the adult Rat retina after optic nerve section and grafting of peripheral nerve segments. Cell and Tissue Research 254 (3), 599-609.

Tsukamoto, Y., Morigiwa, K., Ueda, M., & Sterling, P. (2001). Microcircuits for night vision in mouse retina. J Neurosci 21(21), 8616-23.

Taketo M, Schroeder AC, Mobraaten LE, Gunning KB, Hanten G, Fox RR, Roderick TH, Stewart CL, Lilly F, Hansen CT, Overbeek PA (1991) FVB/N - an inbred mouse strain preferable for transgenic analyses. Proceedings of the National Academy of Sciences of the United States of America 88:2065-2069.

Thoreson WB, Witkovsky P (1999) Glutamate receptors and circuits in the vertebrate retina. Progress Retinal & Eye Res. 18:765-810.

Thyagarajan S, van Wyk M, Lehmann K, Lowel S, Feng GP, Wässle H (2010) Visual Function in Mice with Photoreceptor Degeneration and Transgenic Expression of Channelrhodopsin 2 in Ganglion Cells. J. Neurosci. 30:8745-8758.

Timofeev I, Bazhenov M (2005) Mechanisms and biological role of thalamocortical oscillations. Trends Chronobiol Res

Tuck E, Cavalli V (2010) Roles of membrane trafficking in nerve repair and regeneration. CIB 3(3):209-14.

Uhhaas PJ, Singer W (2006) Neural synchrony in brain disorders: Relevance for cognitive dysfunctions and pathophysiology. Neuron 52:155-168.

Veruki ML, Hartveit E (2002) All (rod) amacrine cells form a network of electrically coupled Interneurons in the mammalian retina. Neuron 33:935-946.

Veruki ML, Hartveit E (2009) Meclofenamic Acid Blocks Electrical Synapses of Retinal AII Amacrine and ON-Cone Bipolar Cells. J.Neurophysiol. 101:2339-2347.

Veruki ML, Oltedal L, Hartveit E (2008) Electrical Synapses Between AII Amacrine Cells: Dynamic Range and Functional Consequences of Variation in Junctional Conductance. J.Neurophysiol. 100:3305-3322

Villegas-Perez MP, Lawrence M, Vidal-Sanz M, LaVeil MM, Lund RD (1998) Ganglion cell loss in RCS rat retina: a result of compression of axons by contracting intraretinal vessels linked to the pigment epithelium. J Comp Neurol 392(1):58-77

Volgyi B, Chheda S, Bloomfield SA (2009) Tracer Coupling Patterns of the Ganglion Cell Subtypes in the Mouse Retina. Journal of Comparative Neurology 512:664-687.

Wang S, Villegas-Perez MC, Visal-Sanz M, Lund R (2000) Progressive optic axon dystrophy and vacuslar changes in rd mice. IOVS 41(2):537-45

Wässle H (2004) Parallel processing in the mammalian retina. Nat Rev Neurosci 5:747-757.

Wässle H, Boycott BB (1991) Functional architecture of the mammalian retina. Physiol Rev Apr;71(2):447-80

References

Wässle H (1996) Paralell processing in the mammalian retina. Nat Rev Neurosci, 5(10) 757-57

Watanabe, M., & Fukuda, Y. (2002). Survival and axonal regeneration of retinal ganglion cells in adult cats. Progr.Retinal and Eye Research, 21 (6), 529-553. Weber AJ, Kaufmann EL, Hubbard WC (1998) Morphology of single ganglion cells in the glaucomatous primate retina: IOVS 39(12):2304-20

Whitmore, A.V., Libby, R.T., & John, S.W.M. (2005). Glaucoma: Thinking in new ways a role for autonomous axonal self-destruction and other compartmentalised processes Prog. Retinal and Eye Research, 24 (6), 639-662.

Wiesel, T; Brown K (1956). Analysis of receptice fields in the cat's retina. Ann N Y Acad Sci. 1959 Nov 12;74(2):405-6.

Wong ROL (1999) Retinal waves and visual system development. Ann. Rev. Neurosci. 22:29-47.

Ying, X., Zhang, J., Wang, Yanhua, Wu, N., Wang, Yi, & Yew, D. T. (2008). Alpha-crystallin protected axons from optic nerve degeneration after crushing in rats. Journal of molecular neuroscience, 35(3), 253-8.

Ye JH, Goo YS (2007) The slow wave component of retinal activity in rd/rd mice recorded with a multi-electrode array. Physiol. Measurement 28:1079-1088.

Zeck GM, Masland RH (2007) Spike train signatures of retinal ganglion cell types. Eur J Neurosci 26:367-380.

Zeck, G., Lambacher, A., & Fromherz, P. (2011). Axonal transmission in the retina. Plos One, 6 (6), e20810.

Zelena J, Lubinska L, Gutman E (1968) Accumulation of organelles at the ends of interrupted axons. Z Zellforsch Mikroskop Anat 91(2):200-19.

Zrenner E, Wilke R, Bartz-Schmidt KU, Gekeler F, Besch D, Benav H, Bruckmann A, Porubska K, Kusnyerik A, Sachs H, Peters T, Wilhelm B, Greppmaier U, Harscher A, Kibbel S, Wrobel W, Stett A (2009) Subretinal Microelectrode Arrays Allow Blind Retinitis Pigmentosa Patients to Recognize Letters and Combine them to Words. Proceedings Intern. Conf. Biomed. Engineering and Informatics, Vols 1-4:1049-1052.

Curriculum vitae

Johann Jacob Wilhelm Friedrich Georg Hermann MENZLER

Birth: the 23rd of august 1978

Education

Since 2011   Postdoctoral position at the Department of Protein Science
                  Head: Prof. Marius Ueffing , Helmholtz Center Munich

2008-2011   PhD thesis about "Discharge patterns of RGC in animal models of
                  Degenerative retinal diseases" at the Department of Systems and
                  Computational Neurobiology , MPI for Neurobiologie,Martinsried.
                  Supervisor: Dr. Günther Zeck.

2007   Diploma thesis in Biology about "Chloride channels in human
                  granulosa cells" at the Institute for Anatomy and Cellbiology Am
                  Biederstein, Munich. Supervisor: Dr. Lars Kunz.

2005   M.A. in philosophy about "Hegels concept of experience in the
                  Phenomenology of the mind"at the Munich School of Philosophy SJ.

Publications

Menzler, J., & Zeck, G. (2011). Network Oscillations in Rod-Degenerated Mouse
        Retinas. J.Neurosci., 31 (6), 2280-2291

Acknowledgements

Ehrenwörtliche Versicherung

Ich versichere hiermit ehrenwörtlich, dass die vorgelegte Dissertation von mir selbstständig und ohne unerlaubte Hilfe angefertigt ist.

München, den ------------------------   ----------------------------------
                                                                 Jacob Menzler

Erklärung

Hiermit erkläre ich, dass ich mich anderweitig einer Doktorprüfung ohne Erfolg nicht unterzogen habe.

München, den ------------------------   ----------------------------------
                                                                 Jacob Menzler